This technical report has been reviewed and is approved for publication.

CHRISTOPHER JEKELI
Contract Manager

THOMAS P. ROONEY, Chief
Geodesy & Gravity Branch

FOR THE COMMANDER

DONALD H. ECKHARDT, Director
Earth Sciences Division

This report has been reviewed by the ESD Public Affairs Office (PA) and is releasable to the National Technical Information Service (NTIS).

Qualified requestors may obtain additional copies from the Defense Technical Information Center. All others should apply to the National Technical Information Service.

If your address has changed, or if you wish to be removed from the mailing list, or if the addressee is no longer employed by your organization, please notify AFGL/DAA, Hanscom AFB, MA 01731-5000. This will assist us in maintaining a current mailing list.

Do not return copies of this report unless contractual obligations or notices on a specific document requires that it be returned.

AFGL-TR-88-0114

GRAVITY FIELD APPROXIMATION USING THE PREDICTORS OF BJERHAMMAR AND HARDY

GEORGE J. PRIOVOLOS

DEPARTMENT OF GEODETIC SCIENCE AND SURVEYING
THE OHIO STATE UNIVERSITY
COLUMBUS, OHIO 43210

MARCH 1988

SCIENTIFIC REPORT NO. 3

APPROVED FOR PUBLIC RELEASE; DISTRIBUTION UNLIMITED

AIR FORCE GEOPHYSICS LABORATORY
AIR FORCE SYSTEMS COMMAND
UNITED STATES AIR FORCE
HANSCOM AIR FORCE BASE, MASSACHUSETTS 01731

Unclassified

SECURITY CLASSIFICATION OF THIS PAGE

AD-A200 622

REPORT DOCUMENTATION PAGE

Form Approved OMB No. 0704-0188

1a. REPORT SECURITY CLASSIFICATION Unclassified	1b. RESTRICTIVE MARKINGS
2a. SECURITY CLASSIFICATION AUTHORITY	3. DISTRIBUTION/AVAILABILITY OF REPORT Approved for public release; distribution Unlimited
2b. DECLASSIFICATION/DOWNGRADING SCHEDULE	
4. PERFORMING ORGANIZATION REPORT NUMBER(S) OSU/DGSS Report No. 387	5. MONITORING ORGANIZATION REPORT NUMBER(S) AFGL-TR-88-0114
6a. NAME OF PERFORMING ORGANIZATION Department of Geodetic Science and Surveying; 6b. OFFICE SYMBOL (If applicable)	7a. NAME OF MONITORING ORGANIZATION Air Force Geophysics Laboratory
6c. ADDRESS (City, State, and ZIP Code) The Ohio State University Columbus, Ohio 43210	7b. ADDRESS (City, State, and ZIP Code) Hanscom AFB Massachusetts 01731
8a. NAME OF FUNDING/SPONSORING ORGANIZATION Air Force Geophysics Laboratory; 8b. OFFICE SYMBOL (If applicable) AFGL	9. PROCUREMENT INSTRUMENT IDENTIFICATION NUMBER F 19628-86-K-0016
8c. ADDRESS (City, State, and ZIP Code) Air Force Systems Command Hanscom AFB, Massachusetts 01731	10. SOURCE OF FUNDING NUMBERS: PROGRAM ELEMENT NO. 62101F; PROJECT NO. 7600; TASK NO. 03; WORK UNIT ACCESSION NO. AQ

11. TITLE (Include Security Classification)

Gravity Field Approximation Using the Predictors of Bjerhammar and Hardy

12. PERSONAL AUTHOR(S)

George J. Priovolos

13a. TYPE OF REPORT	13b. TIME COVERED	14. DATE OF REPORT (Year, Month, Day)	15. PAGE COUNT
Scientific No. 3	FROM ____ TO ____	1988 March	144

16. SUPPLEMENTARY NOTATION

17. COSATI CODES			18. SUBJECT TERMS (Continue on reverse if necessary and identify by block number)
FIELD	GROUP	SUB-GROUP	Geodesy; Gravity; Prediction

19. ABSTRACT (Continue on reverse if necessary and identify by block number)

Gravity field approximation using the predictors of Bjerhammar and Hardy is investigated. In the Bjerhammar method, a finite number of observations is given and it is required to compute a disturbing potential which is harmonic down to a sphere fully internal to the Earth, regular at infinity and it satisfies all the observations. In the Hardy method, a particular family of density anomaly functions is selected which, together with its normal derivatives, vanishes at the boundary. The resulting disturbing potential is non-singular at points that induce potential.

Both methods can use any linear functional of the disturbing potential as observation and/or quantity to be predicted. Both predictors were tested with the White Sands test data. Reference field and residual terrain model effects were removed from the observations and they were restored at the control stations after the predictions were performed.

The best gravity anomaly predictions with both methods were performed with only

20. DISTRIBUTION/AVAILABILITY OF ABSTRACT ☐ UNCLASSIFIED/UNLIMITED ☐ SAME AS RPT. ☐ DTIC USERS	21. ABSTRACT SECURITY CLASSIFICATION Unclassified
22a. NAME OF RESPONSIBLE INDIVIDUAL Christopher Jekeli	22b. TELEPHONE (Include Area Code); 22c. OFFICE SYMBOL AFGL/LWG

DD Form 1473, JUN 86 Previous editions are obsolete. SECURITY CLASSIFICATION OF THIS PAGE

Unclassified

Delta g

Δg observations and the downward continuation onto the nadir points of the observations. The resulting RMS differences of control minus predicted quantities were in the order of 3 to 4 mgals. The best vertical deflection predictions with both methods were performed from a combination of Δg and (ξ,η) data and the downward continuation onto a grid on the geosphere. The resulting RMS differences were smaller than 1". It should be noted that, from gravity observations alone, the Bjerhammar method predicted (ξ,η) to 1" or better, whereas the Hardy method could not do any better than 2.5".

The most important overall result of this work is that when reference field and residual terrain model effects are taken into account, there are at least five methods that can predict (ξ,η) from Δg to the sub-second level, even in mountainous areas. Furthermore, the improvement of the predictions should not be anticipated from a theoretical breakthrough but from data type and coverage improvement. (Geodesy; jhd)

xi, eta

Delta g

FOREWORD

This report was prepared by George J. Priovolos, Graduate Research Associate, Department of Geodetic Science and Surveying, under the supervision of Professor Richard H. Rapp. This study was supported by Air Force Geophysics Laboratory Contract No. F19628-86-K-0016, The Ohio State University Research Foundation Project No. 718188. This contract was administered by The Air Force Geophysics Laboratory, Hanscom Air Force Base, Massachusetts, with Dr. Christopher Jekeli, Scientific Program Officer.

This report was also submitted to the Graduate School of The Ohio State University in partial fulfillment of the requirements for the degree Doctor of Philosophy.

TABLE OF CONTENTS

LIST OF TABLES

LIST OF FIGURES

CHAPTER I

INTRODUCTION

Many important problems of physical geodesy are being solved by integrals extended over the entire Earth. Some examples are Stokes' and Vening-Meinesz' formulae [Heiskanen and Moritz, 1967] and Molodenskii's solution of the boundary value problem of physical geodesy [Moritz, 1980]. The solution of these problems is formulated assuming that gravity is known everywhere on the Earth's surface. However, this is hardly ever the case. Therefore, there is a well justified need for gravity interpolation and extrapolation.

The scope of this study is to investigate two deterministic methods for gravity field approximation. The predictors are deterministic in the sense that no stochastic properties of the gravity field are involved. On the other hand, one feature of both methods is that any linear functional of the disturbing potential can be used as observable and/or quantity to be predicted.

The first method was proposed by Bjerhammar [1964]. He assumed that observations are given at a finite number of stations. The disturbing potential is assumed harmonic (i.e., it satisfies Laplace's equation) down to a sphere fully internal to the Earth. The gravity anomalies at the surface of the internal sphere are solved for by a downward continuation process and then they are used to perform predictions by an upward continuation integral. This formulation and solution of the discrete geodetic boundary value problem is treated in Chapter 2.

Secondly, Hardy's biharmonic potential technique is considered. According to this approach the disturbing potential can be shown to satisfy the biharmonic equation. The biharmonic sources that generate the disturbing potential can be estimated based on observations and then they can be used to predict gravity related quantities. The derivation of the alternate integral for the disturbing potential, the biharmonic equation and its solutions in terms of spherical harmonics, as well as expressions of the gravity anomalies and the deflections of the vertical in terms of the biharmonic sources are given in Chapter 3.

Chapter 4 includes a detailed description of the terrain and the data coverage as well as data reduction computations for the White Sands Test Area in New Mexico. The White Sands test data were used to test both predictors.

This work is continued with a detailed account of the tests performed with both methods. Variations of the methods are tested and the results are discussed and summarized. A comparison is attempted with the results of the four methods tested at the same area [Kearsley et al., 1985]. The aforementioned tests are given in Chapter 5.

Finally, a summary of this investigation together with the conclusions drawn and recommendations for future work is given in Chapter 6.

CHAPTER II

THE BJERHAMMAR PROBLEM

2.1 Introduction

An explicit solution to the geodetic boundary value problem was published by George Gabriel Stokes in 1849 [Heiskanen and Moritz, 1967, p. 94]. The underlying assumptions of his solution are that the mathematical figure of the Earth (the geoid) is approximated by a sphere; there are no masses outside the geoid; and that gravity is known everywhere on the geoid. However, gravity is measured on the surface of the Earth, and the application of Stokes' formula requires on one hand the reduction of measured gravity down to the geoid and on the other hand the absense of masses above the geoid [ibid, p. 126]. In order to solve these two problems gravity reductions must be used. These gravity reductions not only require an assumption for the density of the external masses [Bjerhammar, 1964, p. 9], they also introduce a change of the geoid, the indirect effect [Heiskanen and Moritz, 1967, p. 141]. Molodenskii in 1945 stated that the geoid cannot be determined without knowledge of the mass distribution outside it [Bjerhammar, 1963, p. 3].

Malkin in 1939 redefined the principal problem of physical geodesy so that the physical surface of the Earth became the unknown [ibid, p. 9].

In 1948, Molodenskii presented the solution to the problem of determining the physical surface of the Earth from gravity measurements [Moritz, 1980, p. 330], [Bjerhammar, 1964, p. 3]. The problem is non-linear and the notion of the telluroid is introduced for its Taylor linearization [Moritz, 1980, p. 337]. Molodenskii's solution, Brovar's solution and a solution by analytical continuation are given by Moritz, [1980, pp. 354-388]. Bjerhammar [1963, p. 7] gave credit to Molodenskii for his elegant solution for the distrubing potential but he also realized that the problem of Molodenskii is continuous [Bjerhammar, 1975, p. 185], [Bjerhammar, 1964, p. 3] and the observations are only made at discrete points.

As a result, Bjerhammar defined the discrete geodetic boundary value problem as follows [Bjerhammar, 1975, p. 185], [Bjerhammar, 1964, p. 14], [Bjerhammar, 1963, p. 17], [Moritz, 1980, p. 95], [Bjerhammar, 1986, p. 1]: A finite number of gravity data is given for a non-spherical surface and it is required to find such a solution (gravity field) that the boundary values for the gravity data are satisfied at all given points. The discrete boundary value problem avoids the singularities of downward continuation [Moritz, 1980, p. 95] and has no need for uniform approximation theorems (such as Runge's or Keldych-Lavrentieff's) [Bjerhammar, 1973, p. 480]. Stokes solved the geodetic boundary value problem assuming continuous data coverage on the boundary. An error is introduced in the actual implementation of his solution because an integral is being approximated by a finite sum. On the other hand, Bjerhammar realized the fact that there is only a finite amount of data and consequently he formulated the discrete geodetic boundary value problem.

2.2 Formulation of the Problem

2.2.1 Definitions

This study will follow well established geodetic practices in which the geodetic boundary value problem is independent of time and the space outside the boundary is empty [Moritz, 1980, p. 330]. This is to say that the atmospheric and the tidal effects have been taken into account by corrections to the observed gravity [ibid, pp. 425, 330], [Sanso', 1981, p. 13]. The Earth is assumed to be a rigid body which rotates with constant angular velocity around a fixed axis which passes through its center of mass [Moritz, 1980, pp. 330, 447], [Sanso', 1981, p. 13]. An Earth-fixed rectangular Cartesian coordinate system is defined such that the origin is at the center of mass of the Earth. Its z axis coincides with the Earth's mean axis of rotation, the xz plane coincides with the mean Greenwich meridian plane and the y axis is perpendicular to the xz plane such that the system is right-handed [Moritz, 1980, p. 2]. Therefore, the figure and gravity field of the Earth as well as the coordinate system are assumed to be constant in time [ibid, p. 477].

Let W be the actual gravity potential of the Earth and let U be a normal gravity potential which is an analytic approximation to W; U is usually taken as the potential of an equipotential ellipsoid [Moritz, 1980, p. 337]. Let us also denote by $\vec{g}$ the actual gravity vector and by $\vec{\gamma}$ the normal gravity vector. They are defined as follows [ibid, p. 337]:

$$\vec{g} = \mathrm{grad}W, \tag{2-1}$$

$$\vec{\gamma} = \mathrm{grad}U. \tag{2-2}$$

A point P of the geoid is projected onto the point Q of the ellipsoid by means of the ellipsoidal normal (Figure 1). The gravity anomaly vector $\Delta\vec{g}$ is defined as the difference [Heiskanen and Moritz, 1967, p. 83],

$$\Delta\vec{g} = \vec{g}_P - \vec{\gamma}_Q$$

where $\vec{g}_P$ is the actual gravity vector at P and $\vec{\gamma}_Q$ the normal gravity vector at Q. The difference in magnitude

$$\Delta g = g_P - \gamma_Q \tag{2-3}$$

is the gravity anomaly [ibid, p. 83].

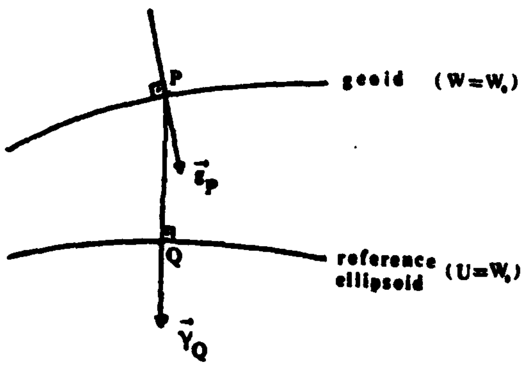

Figure 1. Definition of the gravity anomaly.

The disturbing or anomalous potential T is defined as [Moritz, 1980, p. 12]

$$T = W - U. \tag{2-4}$$

The fundamental equation of physical geodesy, neglecting

$$\frac{\partial W}{\partial h} - \frac{\partial W}{\partial H} + O(e^4)$$

which is smaller than 0.5 mgal [Cruz, 1985], is [Heiskanen and Moritz, 1967, pp. 86, 91]

$$\frac{\partial T}{\partial h} - \frac{1}{\gamma}\cdot\frac{\partial T}{\partial h}\cdot T + \Delta g = 0. \tag{2-5}$$

Introducing the usual spherical approximation, i.e., the tolerance of a relative error in the order of 3×10^{-3} in equations relating quantities of the anomalous field, one can write [Heiskanen and Moritz, 1967, pp. 87–88], [Bjerhammar, 1986, p. 5]:

$$\gamma \cong \frac{GM}{r^2} \;;\; \frac{\partial}{\partial h} \cong \frac{\partial}{\partial r} \;, \tag{2-6}$$

and therefore

$$-\frac{1}{\gamma}\cdot\frac{\partial\gamma}{\partial h} = -\frac{1}{\gamma}\cdot\frac{\partial\gamma}{\partial r} = -\frac{1}{\gamma}\cdot\frac{\partial}{\partial r}\left(\frac{GM}{r^2}\right) = -\frac{r^2}{GM}\cdot\left(\frac{-2GM}{r^3}\right) = \frac{2}{r} \text{ and } \frac{\partial T}{\partial h} = \frac{\partial T}{\partial r} \,.$$

Substituting in (2-5) one gets

$$\frac{\partial T}{\partial r} + \frac{2T}{r} + \Delta g = 0. \tag{2-7}$$

2.2.2 Pizzetti's Formula

Let us now introduce a sphere σ fully internal to the Earth, of radius r_0 and with its center at the center of mass of the Earth. This sphere is hereafter called the Bjerhammar sphere, the internal sphere, or the geosphere.

The aim is to solve the discrete boundary value problem, i.e., given a finite number of observed gravity data, to find a solution (disturbing potential) with the following properties [Bjerhammar, 1986, p. 8]:

(a) T is harmonic outside σ,
(b) T is regular at infinity, i.e., $\lim_{r\to\infty}(T\cdot r)$ = constant, and
(c) All observations are satisfied.

If one assumes no masses outside the sphere σ and denote the gravity anomalies on σ by Δg^* then the disturbing potential T is given by Pizzetti's formula [Heiskanen and Moritz, 1967, p. 93], [Bjerhammar, 1986, p. 7]:

$$T(r, \phi, \lambda) = \frac{r_0}{4\pi}\iint_\sigma S(r, \omega)\Delta g^* d\sigma \tag{2-8}$$

where [Heiskanen and Moritz, 1967, p. 93]

$$S(r, \omega) = \frac{2r_0}{\ell} + \frac{r_0}{r} - \frac{3r_0\ell}{r^2} - \frac{r_0^2}{r^2}\cos\omega\left(5 + 3\ln\frac{r - r_0\cos\omega + \ell}{2r}\right) \tag{2-9}$$

with $\cos\omega = \sin\phi\sin\phi_i + \cos\phi\cos\phi_i\cos(\lambda-\lambda_i)$ (2-10)

and $\ell^2 = r^2 + r_0^2 - 2r_0 r\cos\omega;$ (2-11) also, ϕ, λ are the geodetic latitude and longitude respectively and r is the geocentric distance of the point at which T is computed and ϕ_i, λ_i are the geodetic latitude and longitude respectively of the infinitesimal surface element $d\sigma$.

Let $\bar{x} = [\phi \ \lambda]^T$. Let us also define the evaluation [Moritz, 1980, pp. 37, 200] or Dirac "delta" functional δ [Bjerhammar, 1986, p. 14] by the following relation (σ is the geosphere, R is the set of real numbers and f is some function on σ):

$$f \in \sigma \xrightarrow{\delta} R: \quad \frac{1}{4\pi} \iint_{\sigma} f(\bar{x})\delta(\bar{x} - \bar{x}_i)d\sigma = f(\bar{x}_i) \tag{2-12}$$

The Δg^{x} in equation (2-8) is rewritten as [Bjerhammar, 1986, p. 14]:

$$\Delta g^{x}(\bar{x}) = \sum_{i=1}^{n} \Delta g^{*}(\bar{x}_i)\delta(\bar{x}-\bar{x}_i) \tag{2-13}$$

The $\Delta g^{*}(\bar{x}_i)$ values are a set of fictitious anomalies that generate the observations at the given points [Sjöberg, 1978, p.2], [Katsambalos, 1981, p.58]. The basic postulate of the Dirac Impulse method is that $\Delta g^{*}(\bar{x}) = 0$ everywhere on the geosphere with the exception of n points associated to the given observations [Bjerhammar, 1986, p.14]. Equation (2-13) is the mathematical formulation of the basic postulate.

Substituting (2-13) in (2-8) one obtains

$$\begin{aligned} T(r, \bar{x}) &= \frac{r_0}{4\pi} \iint_{\sigma} S(r, \bar{x}, \bar{x}_M) \ \Delta g^{x}(\bar{x}_M)d\sigma_M = \\ &= \frac{r_0}{4\pi} \iint_{\sigma} S(r, \bar{x}, \bar{x}_M) \cdot \sum_{i=1}^{n} \Delta g^{*}(\bar{x}_i)\delta(\bar{x}_M-\bar{x}_i)d\sigma_M = \\ &= r_0 \sum_{i=1}^{n} \Delta g^{*}(\bar{x}_i) \cdot \frac{1}{4\pi} \iint_{\sigma} S(r, \bar{x}, \bar{x}_M) \cdot \delta(\bar{x}_M-\bar{x}_i)d\sigma_M \end{aligned}$$

which by (2-12) yields (the subscript M in the above derivation was merely introduced to denote the moving point M on the sphere):

$$T(r,\phi,\lambda) = r_0 \sum_{i=1}^{n} \Delta g^{*}(\phi_i, \lambda_i) \cdot S(r,\phi,\lambda,\phi_i,\lambda_i) \tag{2-14}$$

Introducing t and d by

$$t = \frac{r_0}{r} \tag{2-15}$$

$$d = \{1 + t^2 - 2t\cos\omega\}^{1/2} \tag{2-16}$$

one gets from (2-11)

$$\ell = rd \tag{2-17}$$

Letting

$$u = \frac{1}{2}(1 - t\cos\omega + d) \tag{2-18}$$

the generalized Stokes' function $S(r, \omega)$ in (2-9) becomes

$$S(r, \omega) = t(1 - 3d + \frac{2}{d} - t\cos\omega(5 + 3\ln u)) \tag{2-19}$$

Therefore, (2-14) becomes

$$T(r,\phi,\lambda) = r_0 t \sum_{i=1}^{n}(1 - 3d + \frac{2}{d} - t\cos\omega(5 + 3\ln u))\Delta g_i^* \tag{2-20}$$

2.2.3 Gravity anomalies and vertical deflections in terms of Dirac anomalies

All the quantities related to the *disturbing* potential, i.e., all its linear functionals such as gravity anomalies or vertical deflections can be evaluated by applying the pertinent linear operators to T in (2-20).

(a) Gravity Anomalies:

From (2-7) one sees that $\Delta g = LT$, where

$$L = -\frac{\partial}{\partial r} - \frac{2}{r}$$

In order to compute $\frac{\partial T}{\partial r}$, the following derivatives are needed

$$\frac{\partial d}{\partial t} = \frac{t-\cos\omega}{d} \tag{2-21}$$

$$\frac{\partial u}{\partial t} = \frac{1}{2}\left(\frac{t-\cos\omega}{d} - \cos\omega\right) \tag{2-22}$$

Rewriting (2-20) as $T(r, \phi, \lambda) = r_0 \sum_{i=1}^{n} b_i \Delta g_i^*$, with

$$b_i = t - 3dt + \frac{2t}{d} - 5t^2\cos\omega - 3t^2\cos\omega\ell nu \tag{2-23}$$

one has $\frac{\partial T}{\partial r} = r_o \sum_{i=1}^{n} \frac{\partial b_i}{\partial r} \Delta g_i^*$. (2-24)

Now, $\frac{\partial b_i}{\partial r} = \frac{\partial b_i}{\partial t}\frac{\partial t}{\partial r}$, (2-25)

and $\frac{\partial t}{\partial r} = -\frac{t}{r}$.

Thus,

$$\Delta g = -\frac{\partial T}{\partial r} - \frac{2T}{r} = -r_o \sum_{i=1}^{n} \frac{\partial b_i}{\partial t}\frac{\partial t}{\partial r}\Delta g_i^* - \frac{r_o}{r}\sum_{i=1}^{n} 2b_i\Delta g_i^* =$$

$$= -r_o \sum_{i=1}^{n} \frac{\partial b_i}{\partial t}\left(-\frac{t}{r}\right)\Delta g_i^* - 2t\sum_{i=1}^{n} b_i\Delta g_i^*$$

or,

$$\Delta g = -t^2 \sum_{i=1}^{n} M_i\Delta g_i^* \tag{2-27}$$

where $M_i = \frac{2b_i}{t} - \frac{\partial b_i}{\partial t}$

The M_i coefficients can be further reduced (see Appendix A.1) to yield

$$M_i = 1 + \frac{t^2-1}{d^3} + 3t\cos\omega$$

so that (2-27) becomes

$$\Delta g = -t^2 \sum_{i=1}^{n}\left(1 + \frac{t^2-1}{d^3} + 3t\cos\omega\right)\Delta g_i^*$$

or, rearranging terms

$$\Delta g = \sum_{i=1}^{n}\left(\frac{t^2(1-t^2)}{d^3} - 3t^3\cos\omega - t^2\right)\Delta g_i^* \tag{2-28}$$

which is of course the same equation Bjerhammar came up with by discretizing Poisson's equation [Bjerhammar, 1986, p.8],[Bjerhammar, 1964, p.20].

(b) Deflections of the vertical:

The vertical deflections north (ξ) and east (η) are given by Heiskanen and Moritz [1967, p.235]:

$$\xi = -\frac{1}{\gamma}\delta_\phi ; \quad \eta = -\frac{1}{\gamma}\delta_\lambda ,$$

where [ibid, p.233]

$$\delta_\phi = \frac{1}{r}\frac{\partial T}{\partial \phi} ; \quad \delta_\lambda = \frac{1}{r\cos\phi}\frac{\partial T}{\partial \lambda}$$

or, upon substitution

$$\left\{\begin{array}{l} \xi = -\dfrac{1}{\gamma r}\dfrac{\partial T}{\partial \phi} \\ \eta = -\dfrac{1}{\gamma r\cos\phi}\dfrac{\partial T}{\partial \lambda} \end{array}\right\} \tag{2-29}$$

On the other hand

$$\frac{\partial T}{\partial \phi} = \frac{\partial T}{\partial \omega}\frac{\partial \omega}{\partial \phi} \text{ and } \frac{\partial T}{\partial \lambda} = \frac{\partial T}{\partial \omega}\frac{\partial \omega}{\partial \lambda}$$

and [ibid, p.234]

$$\frac{\partial \omega}{\partial \phi} = -\cos\alpha \text{ and } \frac{\partial \omega}{\partial \lambda} = -\cos\phi\sin\alpha$$

therefore

$$\begin{Bmatrix} \xi \\ \eta \end{Bmatrix} = \begin{Bmatrix} \cos\alpha \\ \sin\alpha \end{Bmatrix} \frac{1}{\gamma r}\frac{\partial T}{\partial \omega} \tag{2-30}$$

Now $\frac{\partial T}{\partial \omega} = r_o t \sum_{i=1}^{n} A_i \Delta g_i^*$, with $A_i = \frac{\partial}{\partial \omega}\left[1 - 3d + \frac{2}{d} - 5t\cos\omega - 3t\cos\omega \ell nu\right]$

The A_i derivatives can be evaluated (see Appendix A.2) to yield

$$A_i = t\sin\omega \left[8 - \frac{2}{d^3} - \frac{3(d+1)^2}{2ud} + 3\ell nu\right]$$

thus

$$\frac{\partial T}{\partial \omega} = r_o t^2 \sum_{i=1}^{n} \left[8 - \frac{2}{d^3} - \frac{3(d+1)^2}{2ud} + 3\ell nu\right]\sin\omega \Delta g_i^* \tag{2-31}$$

Substitution of (2-31) in (2-30) yields

$$\begin{Bmatrix} \xi \\ \eta \end{Bmatrix} = \frac{t^2}{\gamma}\sum_{i=1}^{n} \left[8 - \frac{2}{d^3} - \frac{3(d+1)^2}{2ud} + 3\ell nu\right]\sin\omega \begin{Bmatrix} \cos\alpha \\ \sin\alpha \end{Bmatrix}\Delta g_i^* \tag{2-32}$$

Finally, using Heiskanen and Moritz [1967, p.113]

$$\begin{Bmatrix} \sin\omega\cos\alpha = \cos\phi\sin\phi_i - \sin\phi\cos\phi_i\cos(\lambda_i-\lambda) \\ \sin\omega\sin\alpha = \cos\phi_i\sin(\lambda_i-\lambda) \end{Bmatrix} \tag{2-33}$$

one gets

$$\begin{Bmatrix} \xi \\ \eta \end{Bmatrix} = \frac{t^3}{\gamma}\sum_{i=1}^{n}\left(8 - \frac{2}{d^3} - \frac{3(d+1)^2}{2ud} + 3\ell nu\right)\begin{Bmatrix} \cos\phi\sin\phi_i - \sin\phi\cos\phi_i\cos(\lambda_i-\lambda) \\ \cos\phi_i\sin(\lambda_i-\lambda) \end{Bmatrix}\Delta g_i^* \tag{2-34}$$

Equations (2-28) and (2-34) can be used both to compute Δg_i^* from observations and to predict Δg, ξ, η.

2.2.4 A truncated sum

Given a continuous function $f(x)$ and a constant x_0, one can form a sequence $f_n = f(nx_0)$, $n \in N$. This operation is called sampling and x_0 is called the sampling interval. Conversely, given a sequence f_n, one can construct a continuous function $f(x)$, by an operation called pulsing and defined as

$$f(x) = \sum_{n=0}^{\infty} f_n\delta(x - nx_0) = \sum_{n=0}^{\infty} f(nx_0)\delta(x - nx_0)$$

where δ is the Dirac delta functional. The aforementioned operations are well established in the analysis of Linear Systems and can be found in many electrical or mechanical engineering texts such as Brown [1961, p. 176], Aseltine [1958, p. 247] and Tretter [1976, p. 85].

Equation (2-13) is the two-dimensional analog of the above equation defining pulsing. The only difference is that pulsing as defined above is the superposition of an infinite number of impulses whereas (2-13) represents a finite sum.

Bjerhammar realized that in applications one has only a finite number of data, and therefore one can only solve for a finite number of impluses. Consequently he truncated the sum in (2-13) at some integer number n equal to the number of observations.

However, only an infinite number of Δg^* values is able to recontruct the original signal (recall that in order to recover T one needs an infinite number of harmonics). Therefore, the gravity related quantities predicted from n Δg^* values will naturally not include the contribution of the truncated terms beyond n. This is to say that equations such as (2-20), (2-28) and (2-34) can only be considered as approximations.

2.3 Symmetric Kernel Approach

In the original approach the Dirac Impulses were located on the surface of the sphere σ. In the symmetric kernel approach the Dirac Impulses are located at positions (Figure 2) with geocentric radii inversely proportional to the geocentric radii of the observations, i.e. the Dirac Impulse corresponding to the observation at r_i is located at r_{oi}, where [Bjerhammar, 1986, p. 48]

$$r_{oi} = \frac{r_o^2}{r_i} \tag{2-35}$$

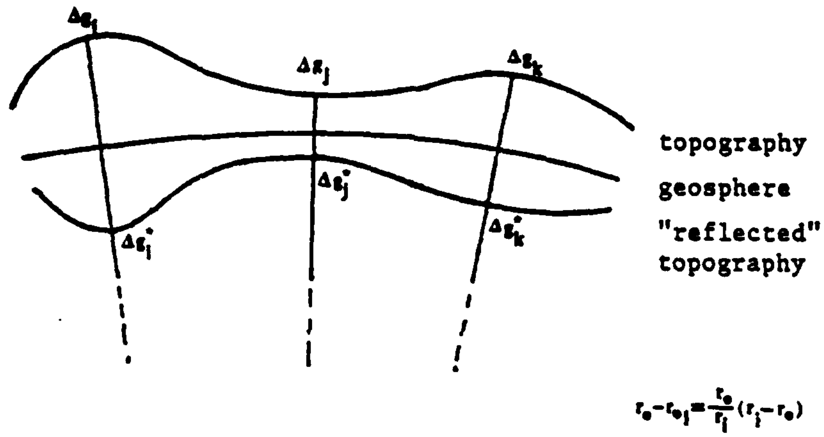

Figure 2. Symmetric Kernel Approach.

Every observation will be associated with a Dirac Impulse at r_{oi}. Considering n observations one will have to consider n Dirac Impulses located, in principal, at n different geospheres. The disturbing potential associated with the i-th Impulse will be given by (see equation (2-14))

$$T_i(r, \phi, \lambda) = r_{oi} S(r, \phi, \lambda, \phi_i, \lambda_i) \Delta g_i^* \tag{2-36}$$

and $\Delta T_i = 0$ at $r > r_{oi}$. The total potential will be

$$T(r, \phi, \lambda) = \sum_{i=1}^{n} r_{oi} S(r, \phi, \lambda, \phi_i, \lambda_i) \Delta g_i^* \tag{2-37}$$

by the superposition principle of the potential [Heiskanen and Moritz, 1967, p.2]

and $\Delta T = 0$ at $r > \max(r_{o1}, \ldots, r_{on}) = \dfrac{r_0^2}{\min(r_1, \ldots, r_n)}$

Introducing t by $t = \dfrac{r_{oi}}{r}$ and d by (2-16) one has

$$t = \frac{r_{oi}}{r} = \frac{r_0^2}{rr_i} \tag{2-38}$$

and

$$S(r, \omega) = t(1 - 3d + \frac{2}{d} - t\cos\omega(5 + 3\ell nu)) \tag{2-39}$$

Therefore (2-37) becomes

$$T(r,\phi,\lambda) = \sum_{i=1}^{n} r_{oi}t(1 - 3d + \frac{2}{d} - t\cos\omega(5 + 3\ell nu))\Delta g_i^* \tag{2-40}$$

Similarly as in the original approach one derives

$$\Delta g = \sum_{i=1}^{n}\left\{\frac{t^2(1-t^2)}{d^3} - 3t^3\cos\omega - t^2\right\}\Delta g_i^* \tag{2-41}$$

$$\left\{\begin{matrix}\xi\\ \eta\end{matrix}\right\} = \frac{1}{\gamma}\sum_{i=1}^{n} t^3\left(8 - \frac{2}{d^3} - \frac{3(d+1)^2}{2ud} + 3\ell nu\right)\left\{\begin{matrix}\cos\phi\sin\phi_i - \sin\phi\cos\phi_i\cos(\lambda_i - \lambda)\\ \cos\phi_i\sin(\lambda_i - \lambda)\end{matrix}\right\}\Delta g_i^* \tag{2-42}$$

2.4 The Linear System

If one assumes n observations comprising the vector ℓ then the linear system is

$$\ell = G\Delta g^* \tag{2-43}$$

In general the vector of the Dirac Impulses Δg^* will be of dimension m. The elements of G can be taken from (2-28) or (2-34) for Δg or ξ, η observations in the original approach and from (2-41), (2-42) for the same type of observations in the symmetric kernel approach. Note that G is of full row rank as long as there are no two observations ℓ_i, ℓ_j of the same type (e.g., Δg or ξ) with $r_i = r_j$.

There are three distinct possibilities:

(i) Exact solution ($m = n$):

The Dirac Impulses and their covariance matrix respectively are given by

$$\Delta g^* = G^{-1}\ell \tag{2-44}$$

$$\Sigma_{\Delta g^*} = G^{-1}\Sigma_\ell G^{-T} \tag{2-45}$$

(ii) Overdetermined case ($m < n$):

In this case the traditional least-squares method [Uotila, 1985] applies and the solution is

$$\Delta g^* = (G^T\Sigma_\ell^{-1}G)^{-1}G^T\Sigma_\ell^{-1}\ell \tag{2-46}$$

$$\Sigma_{\Delta g^*} = (G^T\Sigma_\ell^{-1}G)^{-1} \tag{2-47}$$

The a posteriori variance of unit weight $\hat{\sigma}_0^2$ is given by

$$\hat{\sigma}_0^2 = \sigma_0{}^2\,\frac{\ell^T\Sigma_\ell{}^{-1}\ell - \ell^T\Sigma_\ell{}^{-1}G\Delta g^*}{n - m} \tag{2-48}$$

where σ_0^2 is the a priori variance of unit weight.

It should be kept in mind that the property of the reproducibility of the observations is lost in this case.

(iii) Underdetermined case ($m > n$):

In this case equation (2-43) represents a system of equations with an infinite number of solutions since G has full row rank [Dermanis, 1985, p. 215]. From this infinite number of solutions, one particular solution may be chosen by the minimum-norm criterion $\Delta g^{*T}\cdot\Delta g^* = \min$. This solution is unique in the sense that the norm of any other solution is at least as large as the norm of Δg^* or larger. In order to find the solution that minimizes the norm of Δg^* and satisfies (2-43) one needs to find Δg^* that satisfies

$$\phi = \Delta g^{*T}\Delta g^* + 2k^T(G\Delta g^* - \ell) = \min \tag{2-49}$$

The minimum of ϕ with respect to Δg^* is attained at

$$\frac{\partial\phi}{\partial\Delta g^*} = 0 \iff 2\Delta g^{*T} + 2k^TG = 0 \iff \Delta g^* = G^Tk \tag{2-50}$$

On the other hand

$$0 = G\Delta g^* - \ell = GG^Tk - \ell \iff k = (GG^T)^{-1}\ell, \text{ thus}$$

$$\Delta g^* = G^T(GG^T)^{-1}\ell \tag{2-51}$$

Obviously G is (nxm) with rank n (full row rank). Now GG^T is (nxn) with the same rank as G, thus GG^T is of full rank and therefore invertible. The covariance matrix of Δg^* can be computed from the law of propagation of covariances [Uotila, 1985, p. 4]:

$$\Sigma_{\Delta g^*} = G^T(GG^T)^{-1}\ \Sigma_\ell\ (G^T(GG^T)^{-1})^T = G^T(GG^T)^{-1}\ \Sigma_\ell\ (GG^T)^{-1}G, \text{ thus}$$

$$\Sigma_{\Delta g^*} = G^T(GG^T)^{-1}\ \Sigma_\ell\ (GG^T)^{-1}G \tag{2-52}$$

It is trivial to notice that the solution (2-51) is the pseudo inverse solution. For a full row rank matrix G one has [Uotila, 1982b]

$$G^+ = G^T(GG^T)^{-1} \tag{2-53}$$

thus (2-51) and (2-52) can be written as

$$\Delta g^* = G^+\ell \tag{2-54}$$

$$\Sigma_{\Delta g^*} = G^+\ \Sigma_\ell\ (G^+)^T \tag{2-55}$$

The uniqueness of the pseudo inverse quarantees that Δg^* in (2-54) is unique.

2.5 Propagation of Data Noise into the Predictions

Let us assume that we will perform predictions at q stations. The vector f of predictions will be of dimension q and it will be given by

$$f = R\cdot\Delta g^* \tag{2-56}$$

where the elements of the (qxm) matrix R will be given by (2-28) for Δg predictions and by (2-34) for (ξ,η) predictions. The covariance matrix Σ_f of the prediction vector f will be given by [Uotila, 1985, p.4]

$$\Sigma_f = R\cdot\Sigma_{\Delta g^*}\cdot R^T \tag{2-57}$$

where $\Sigma_{\Delta g^*}$ is the covariance matrix of Δg^* as computed from (2-45) for the exact case, (2-47) for the overdetermined case and (2-55) for the underdetermined case.

2.6 On the Location of the Dirac Impulses

From the theoretical standpoint there is no reason to prefer any location over any other for the location of the Dirac Impulses. From the numerical standpoint however, one should prefer the location that yields optimal stability in the sense of maximal diagonal dominance of the matrix to be inverted as done in Bjerhammar [1986, p. 30]. The matrix G in (2-44) will be selected to investigate the location issue since this issue is only numerically and not theoretically relevant. The resulting location is going to be used regardless of the observation type and of the solution type (i.e., exact solution, adjustment solution or minimum norm solution). The development will follow Bjerhammar's ideas [ibid, p. 30].

Let the Dirac Impulse Δg^* corresponding to some observation Δg at r, ϕ, λ be located at r_0, ϕ_0, λ_0.

The corresponding element of G in the main diagonal will be (see eq. (2-28))

$$g = \frac{t^2(1-t^2)}{d^3} - 3t^3\cos\omega - t^2 \tag{2-58}$$

with $d = \{1 + t^2 - 2t\cos\omega\}^{1/2}$ (2-59)

and $\cos\omega = \sin\phi\sin\phi_0 + \cos\phi\cos\phi_0\cos(\lambda-\lambda_0)$ (2-60)

The maximum of $g = g(\omega)$ with respect to ω will be attained at $\frac{\partial g}{\partial\omega} = 0$, thus

$$0 = \frac{\partial g}{\partial\omega} = t^2(1-t^2)\frac{(-3)}{d^4}\frac{\partial d}{\partial\omega} - 3t^3(-\sin\omega) =$$

$$= -\frac{3t^2(1-t^2)}{d^4}\frac{t\sin\omega}{d} + 3t^3\sin\omega \Rightarrow$$

$$0 = \frac{\partial g}{\partial\omega} = 3t^3\left[\frac{t^2-1}{d^5} + 1\right]\sin\omega \tag{2-61}$$

which vanishes identically for $\omega = 0$, i.e., $\phi_0 = \phi$, $\lambda_0 = \lambda$. This is the argument originally given by Bjerhammar [1986, p. 30]. However, in order for $\omega=0$ to be a maximum $(\partial^2 g/\partial w^2)(\omega=0) < 0$ must be satisfied. It holds that

$$\frac{\partial^2 g}{\partial\omega^2} = \frac{\partial}{\partial\omega}\left[3t^3\sin\omega + \frac{3t^3(t^2-1)}{d^5}\sin\omega\right] = 3t^3\cos\omega + 3t^3(t^2-1)\frac{\partial}{\partial\omega}\left[\frac{\sin\omega}{d^5}\right] \Rightarrow$$

$$\frac{\partial^2 g}{\partial\omega^2} = 3t^3\cos\omega + \frac{3t^3(t^2-1)\cos\omega}{d^5} - \frac{15t^4(t^2-1)\sin^2\omega}{d^7} \tag{2-62}$$

Now for $\omega = 0 \Rightarrow \sin\omega = 0$, $\cos\omega = 1$, hence

$$d = [1 + t^2 - 2t\cos\omega]^{1/2} \Rightarrow d = 1 - t, \text{ thus}$$

$$\frac{\partial^2 g}{\partial\omega^2}(\omega = 0) = 3t^3 + \frac{3t^3(t^2-1)}{(1-t)^5}, \text{ or upon simplification}$$

$$\frac{\partial^2 g}{\partial\omega^2}(\omega = 0) = \frac{3t^3}{(1-t)^4}[(1-t)^4 - (1+t)] \tag{2-63}$$

Now for $0<t<1 \Rightarrow -1<-t<0 \Rightarrow 0<1-t<1 \Rightarrow (1-t)^4<1$ (2-64)

Also $0<t \Rightarrow 1<1+t$, thus

$$(1-t)^4<1<1+t \Rightarrow (1-t)^4 - (1+t)<0 \tag{2-65}$$

which yields $\frac{\partial^2 g}{\partial\omega^2}(\omega=0)<0$ and thus $\omega=0$ is indeed a maximum for g.

Therefore, the optimal positions for the Dirac Impulses corresponding to gravity anomaly observations are at the nadir points of the observation stations.

2.7 On the Optimal Radius of the Geosphere

A successful application of the Dirac Impulse method requires a suitable choice for the radius of the internal sphere. Some suggestions pertaining to gridded data can be found in Katsambalos [1981, p.76] and Bjerhammar [1985, p.7].

A suggestion for sparse data was made by Sjöberg [1978, p.64] according to which

$$r_o = R_E - R_E \frac{\bar{\psi}}{2} \tag{2-66}$$

where R_E is a mean earth radius (e.g. R_E=6371 km) and $\bar{\psi}$ is the average angular distance between neighboring points. Alternatively, one can attempt to compute r_o from the given data if this is possible. Two methods can be considered. The first one was somewhat differently regarded in Bjerhammar [1986, p.20]. He considered a least-squares solution whereas here a minimum norm solution will be investigated. The system in (2-43) can be written as

$$\ell_a = G \cdot \Delta g_a^* = F(X_a) \tag{2-67}$$

with $X_a = \begin{bmatrix} \Delta g_a^* \\ r_o^a \end{bmatrix}$, $X_o = \begin{bmatrix} \Delta g_o^* \\ r_o^o \end{bmatrix}$, $X = \begin{bmatrix} \delta\Delta g^* \\ \delta r_o \end{bmatrix}$ and $\ell_a = \ell_b + V$.

Equation (2-67) represents a non-linear system in the unknowns. Linearizing by Taylor's theorem and neglecting terms of order 2 and higher yields

$$\ell_a = F(X_o) + \frac{\partial F}{\partial X_a}(X_a - X_o), \text{ or upon letting}$$

$$\ell_o = F(X_o);\ \ell = \ell_a - \ell_o;\ \frac{\partial F}{\partial X_a} = \left[\frac{\partial F}{\partial \Delta g_a^*};\ \frac{\partial F}{\partial r_o}\right] = B, \text{ one then gets}$$

$$BX - \ell = 0. \tag{2-68}$$

In the case of n observations (2-68) represents a system of n equations in (n+1) unknowns with B having full row rank, therefore the condition X^TX=min will yield (see eq. (2-49) through (2-55))

$$X = B^T(BB^T)^{-1}\ell \tag{2-69}$$

with

$$\Sigma_X = B^T(BB^T)^{-1}\Sigma_\ell(BB^T)^{-1}B. \tag{2-70}$$

Now let us write B as

$$B = [G\ a], \tag{2-71}$$

where $a = \frac{\partial F}{\partial r_o}$ is an (nxl) vector. Denoting by ℓ_{a_i} the i-th element of ℓ_a, the i-th element a_i of the vector a will be $a_i = \frac{\partial \ell_{a_i}}{\partial r_o}$. In order to evaluate a_i for Δg, ξ and η observations one will need the following derivatives

(i) $\frac{\partial t^n}{\partial r_o} = nt^{n-1}\frac{\partial t}{\partial r_o} = n\frac{t^n}{r_o}$, (2-72)

(ii) $\frac{\partial d}{\partial r_o} = \frac{\partial d}{\partial t}\frac{\partial t}{\partial r_o}$; $\frac{\partial u}{\partial r_o} = \frac{\partial u}{\partial t}\frac{\partial t}{\partial r_o}$. Recalling (2-21) and (2-22) one gets

$$\frac{\partial d}{\partial r_o} = \frac{t(t-\cos\omega)}{r_o d};\ \frac{\partial u}{\partial r_o} = \frac{t}{2r_o}\left[\frac{t-\cos\omega}{d} - \cos\omega\right]. \tag{2-73}$$

Now, rewriting the i-th equation of (2-67) as

$$\ell_{a_i} = \sum_{j=1}^{n} g_{ij}\Delta g_{a_j}^* \tag{2-74}$$

one has

$$a_i = \frac{\partial \ell_{a_i}}{\partial r_o} = \sum_{j=1}^{n}\frac{\partial g_{ij}}{\partial r_o}\Delta g_{a_j}^* \tag{2-75}$$

where for gravity anomalies, from (2-28)

$$g_{ij}^{\Delta g} = \frac{t^2(1-t^2)}{d^3} - 3t^3\cos\omega - t^2 \tag{2-76}$$

and for vertical deflections, from (2-34)

$$\begin{Bmatrix} g^{\xi}_{ij} \\ g^{\eta}_{ij} \end{Bmatrix} = \frac{t^3}{\gamma}\left[8 - \frac{2}{d^3} - \frac{3(d+1)^2}{2ud} + 3\ell n u\right]\sin\omega \begin{Bmatrix} \cos\alpha \\ \sin\alpha \end{Bmatrix}. \tag{2-77}$$

The differentiation of the g_{ij} coefficients required in (2-75) yields (Appendix A.3):

$$\frac{\partial g_{ij}^{\Delta g}}{\partial r_0} = \frac{t^2}{r_0}\left[\frac{2}{d^3}(1-2t^2) - \frac{3t(1-t^2)(t-\cos\omega)}{d^5} - 9t\cos\omega - 2\right] \tag{2-78}$$

for gravity anomalies. For vertical deflections it yields (Appendix A.4)

$$\begin{Bmatrix} \dfrac{\partial g^{\xi}_{ij}}{\partial r_0} \\ \dfrac{\partial g^{\eta}_{ij}}{\partial r_0} \end{Bmatrix} = \frac{3t^3\sin\omega}{r_0\gamma}\left[8 - \frac{2}{d^3} - \frac{3(d+1)^2}{2ud} + 3\ell n u + \frac{t(t-\cos\omega)}{d^2}\left(\frac{2}{d^3} + \frac{(d+1)^2}{4u^2} + \frac{1}{2ud}\right)\right.$$

$$\left. - \frac{t\cos\omega}{2u}\left(\frac{(d+1)^2}{2ud} + 1\right)\right]\begin{Bmatrix} \cos\alpha \\ \sin\alpha \end{Bmatrix}. \tag{2-79}$$

Equations (2-78) and (2-79) can be used to form the elements of the vector a in (2-71). Equation (2-69) can be used to solve for the vector X of the unknowns, the last element of which is r_0.

For the actual implementation of (2-69) it is worth noting that since G in (2-67) is of full rank, then [Boullion and Odell, 1971, p. 18]

$$B^+ = \begin{bmatrix} G^{-1} - G^{-1}ab \\ b \end{bmatrix}$$

where $b = [1 + (G^{-1}a)^T G^{-1}a]^{-1}(G^{-1}a)^T G^{-1}$

Another method of solving for r_0 is to separate the data in two groups ℓ^1_s and ℓ^2_s of n_1 and n_2 observations respectively. Denoting by Δg^* the Dirac Impulses corresponding to ℓ^1_s, one has the following linear system:

$$\ell^1_s = R\Delta g^*. \tag{2-80}$$

Solving (2-80) for Δg^* one gets

$$\Delta g^* = R^{-1}\ell^1_s. \tag{2-81}$$

On the other hand, knowing Δg^* one can predict ℓ^2_s as

$$\ell_a^2 = SAg^* \tag{2-82}$$

Substituting (2-81) in (2-82) one gets

$$\ell_a^2 - SR^{-1}\ell_a^1 = 0 \tag{2-83}$$

Equation (2-83) can serve as the mathematical model of the form $F(X_a,L_a) = 0$ in an adjustment scheme with r_0 as the only unknown. Following Uotila [1985] one can write

$$\left(\begin{array}{l} X_a = {}_1[r_0^a]_1;\; X_0 = {}_1[r_0^0]_1;\; X = {}_1[\delta r_0]_1;\; \ell_a = {}_{n_1+n_2}\begin{bmatrix}\ell_a^1\\ \ell_a^2\end{bmatrix}_1 \\[2ex] \qquad \ell_b = \begin{bmatrix}\ell_b^1\\ \ell_b^2\end{bmatrix};\; V = \begin{bmatrix}V_1\\ V_2\end{bmatrix};\; n \doteq n_1+n_2 \end{array}\right) \tag{2-84}$$

Linearizing (2-83) by Taylor's theorem and neglecting powers of (X_a-X_0) of orders 2 and higher one gets

$$AX + BV + W = 0 \tag{2-85}$$

with

$$\underset{n_2 x n}{B} = \frac{\partial F}{\partial \ell a} = [\underset{n_2 x n_1}{-SR^{-1}};\; \underset{n_2 x n_2}{I}]. \tag{2-86}$$

Also

$$\underset{n_2 x 1}{A} = \frac{\partial F}{\partial X_a} = \frac{\partial F}{\partial r_0} = \frac{\partial}{\partial r_0}(\ell_a^2 - SR^{-1}\ell_a^1) = \frac{\partial}{\partial r_0}(\ell_a^2) - \frac{\partial}{\partial r_0}(SR^{-1}\ell_a^1) \tag{2-87}$$

From Dermanis [1985, p.187] one has that

$$\frac{d}{dt}(AB) = \frac{dA}{dt}B + A\frac{dB}{dt}\text{ , and} \tag{2-88}$$

$$\frac{d}{dt}(A^{-1}) = -A^{-1}\frac{dA}{dt}A^{-1}. \tag{2-89}$$

where A,B are matrix-functions of the variable t such that AB and A^{-1} are defined. Applying (2-88) and (2-89) in (2-87) one gets

$$A = \left(SR^{-1}\frac{\partial R}{\partial r_0} - \frac{\partial S}{\partial r_0}\right)R^{-1}\ell_a^1 \tag{2-90}$$

The elements of the matrices A and B are given by (2-90) and (2-86) respectively. The least-squares solution of (2-85) is given by Uotila [1985]

$$P = \sigma_0^2 \Sigma_{\ell_b}^{-1} \tag{2-91}$$

$$W = F(X_0, \ell_b) \tag{2-92}$$

$$M = BP^{-1}B^T \tag{2-93}$$

$$X = -(A^T M^{-1} A)^{-1} A^T M^{-1} W \tag{2-94}$$

$$X_a = X_0 + X \tag{2-95}$$

$$\Sigma_{x_a} = \sigma_0^2 (A^T M^{-1} A)^{-1}. \tag{2-96}$$

Since the problem is non-linear, iterations will be needed. Following the iteration scheme described in Uotila [1982a] one can write (for the i-th iteration) the following:

- Evaluate A,B at $X_0^i = X_a^{i-1}$, $\ell_0^i = \ell_a^{i-1}$ (2-97)

- $W^i = F(X_0^i, \ell_0^i) + B^i(\ell_b - \ell_0^i)$ (2-98)

- $M^i = (B^i)P^{-1}(B^i)^T; \ P = \sigma_0^2 \Sigma_{\ell_b}^{-1}$ (2-99)

$$\left\{\begin{aligned} X^i &= -[(A^i)^T(M^i)^{-1}A^i]^{-1}(A^i)^T(M^i)^{-1}W^i \\ V_i &= -P^{-1}(B^i)^T(M^i)^{-1}(A^iX^i + W^i) \end{aligned}\right\} \tag{2-100}$$

$$\left\{\begin{aligned} \ell_a^i &= \ell_b + V^i \\ X_a^i &= X_0^i + X^i \end{aligned}\right\} \tag{2-101}$$

In this particular case it is worth noting that

$$W^i = \ell_0^2 - S^i(R^i)^{-1}\ell_0^i. \tag{2-102}$$

Yet another method to be considered for optimal r_0 computations is the following. A measure s^2 of the quality of the results is assumed to be a second order polynomial in r_0. According to Bjerhammar, [1986, p.17] s^2 is the variance of unit weight or the RMS error of a residual field [ibid, p.18] (note that in the case where s^2 = RMS ($d\Delta g$) then the units of s^2 are mgals rather than mgal^2). Thus

$$s^2 = a + br_0 + cr_0^2 \tag{2-103}$$

The value of r_0 at which s^2 is an extremum will be the root of

$\frac{\partial s^2}{\partial r_o} = 0$, or equivalently of $2cr_o + b = 0$

The root of this equation is

$$r_o = -\frac{b}{2c} \tag{2-104}$$

Furthermore, for $c>0$, the extremum in (2-104) is a minimum. Assuming that three different radii r_{o_1}, r_{o_2}, r_{o_3}, *resulted in* s_1^2, s_2^2, s_3^2 respectively, one can write from (2-103)

$$\begin{bmatrix} s_1^2 = a + br_{o_1} + cr_{o_1}^2 \\ s_2^2 = a + br_{o_2} + cr_{o_2}^2 \\ s_3^2 = a + br_{o_3} + cr_{o_3}^2 \end{bmatrix}. \tag{2-105}$$

This linear system of three equations in three unknowns a,b,c can be solved to yield the following

$$\begin{bmatrix} a = s_3^2 - \dfrac{r_{o_1}r_{o_3}(s_2^2 - s_3^2)}{(r_{o_1}-r_{o_2})(r_{o_2}-r_{o_3})} + \dfrac{r_{o_2}r_{o_3}(s_1^2 - s_3^2)}{(r_{o_1}-r_{o_2})(r_{o_1}-r_{o_3})} \\ b = \dfrac{(r_{o_2}+r_{o_3})(s_1^2-s_3^2)}{(r_{o_1}-r_{o_2})(r_{o_3}-r_{o_1})} - \dfrac{(r_{o_1}+r_{o_3})(s_2^2-s_3^2)}{(r_{o_1}-r_{o_2})(r_{o_2}-r_{o_3})} \\ c = \dfrac{s_2^2 - s_3^2}{(r_{o_1}-r_{o_2})(r_{o_2}-r_{o_3})} - \dfrac{s_1^2 - s_3^2}{(r_{o_1}-r_{o_2})(r_{o_3}-r_{o_1})} \end{bmatrix}. \tag{2-106}$$

The substitution of b and c from (2-106) in (2-104) yields

$$\hat{r}_o = \frac{(r_{o_1}^2-r_{o_3}^2)(s_2^2-s_3^2) - (r_{o_2}^2-r_{o_3}^2)(s_1^2-s_3^2)}{2[(r_{o_1}-r_{o_3})(s_2^2-s_3^2)-(r_{o_2}-r_{o_3})(s_1^2-s_3^2)]} \tag{2-107}$$

If $r_{o_1} = r_o-h$, $r_{o_2} = r_o$, $r_{o_3} = r_o+h$ *is selected,* one obtains from (2-107)

$$\hat{r}_o = r_o - \frac{h(s_3^2-s_1^2)}{2s_1^2 + 2s_3^2 - 4s_2^2} \tag{2-108}$$

which is the original formula derived by Bjerhammar [1986, p.18] after correcting a minus sign error.

The actual implementation of (2-107) will be to apply the predictors three times with three different radii and record the resulting s^2 values. The selection of the three initial radii is quite arbitrary. However, in order to make (2-107) most effective one should keep in mind that (2-103) is a parabola and its minimum will be best computed if one has a point in the ascending part of the curve, one point in the descending part of the curve and one point between the two.

CHAPTER III

THE BIHARMONIC POTENTIAL - HARDY'S METHOD

3.1 Introduction

The gravitational potential of a mass distribution with density σ occupying a volume U is given by [Heiskanen and Moritz, 1967, p. 3]

$$V = G\iiint_{U} \frac{\sigma}{\ell}\, d\upsilon \tag{3-1}$$

where G = Newton's gravitational constant
$d\upsilon$ = differential volume element
ℓ = distance between $d\upsilon$ and the evaluation point.

Let the volume and the gravitational potential of the Earth with mass distribution σ_1 be denoted by U_1 and V_1 respectively. The gravity potential of the Earth is then given by

$$W_1 = V_1 + \Phi_1 \tag{3-2}$$

where $\Phi_1 = ½\omega_1^2(x^2+y^2)$ is the centrifugal potential [ibid, p.47] and ω_1 is the Earth's angular velocity.

Introducing the standard notion of the reference ellipsoid with density σ_2, volume U_2, gravitational potential V_2, gravity potential W_2 and angular velocity $\omega_2=\omega_1$, one has

$$V_1 = G\iiint_{U_1} \frac{\sigma_1}{\ell}\, d\upsilon \tag{3-3}$$

$$V_2 = G\iiint_{U_2} \frac{\sigma_2}{\ell}\, d\upsilon \tag{3-4}$$

$$W_2 = V_2 + \Phi_2 \tag{3-5}$$

The disturbing potential T is defined as

$$T = W_1 - W_2. \tag{3-6}$$

Therefore

$$T = W_1 - W_2 = V_1 + \Phi_1 - V_2 - \Phi_2 = G\iiint_{U_1} \frac{\sigma_1}{\ell}\, dv + \frac{1}{2}\,\omega_1^2(x^2+y^2) - G\iiint_{U_2} \frac{\sigma_2}{\ell}\, dv - \frac{1}{2}\,\omega_2^2(x^2+y^2)$$

and since $\omega_1 = \omega_2$ one gets

$$T = G\iiint_{U_2} \frac{\sigma_1}{\ell}\, dv - G\iiint_{U_2} \frac{\sigma_2}{\ell}\, dv + G\iiint_{U_1 - U_2} \frac{\sigma_1}{\ell}\, dv$$

It will be assumed that the integral of σ_1 over the difference of the two volumes U_1 and U_2 is negligible. Denoting by σ the density anomaly function, i.e., $\sigma = \sigma_1 - \sigma_2$ and also denoting U_2 by Ω one finally gets

$$T = G\iiint_{\Omega} \frac{\sigma}{\ell}\, dv \tag{3-7}$$

3.2 Hardy's proposal and its consequences

3.2.1 Existence of the biharmonic potential

The representation of the disturbing potential in (3-7) is singular at points that induce potential since at these points $\ell=0$. On the other hand, since there are infinitely many mass distributions σ_1 that have V_1 as their exterior potential [Heiskanen and Moritz, 1967, p.17], there are infinitely many density anomaly functions σ that have T as their exterior disturbing potential.

Hardy and Nelson [1986] proposed to select a particular family of σ functions, namely the ones that are zero together with their normal derivatives at the boundary. They also defined a function p such that

$$p = \tfrac{1}{2}\Delta\sigma \tag{3-8}$$

where the Laplacian operator Δ in (3-8) is defined as usual, i.e.,

$$\Delta = \frac{\partial^2}{\partial x^2} + \frac{\partial^2}{\partial y^2} + \frac{\partial^2}{\partial z^2}$$

and it refers to the point that induces potential. Then they showed that the disturbing potential T can be written as

$$T = G\iiint_{\Omega} p\,\ell\, dv \tag{3-9}$$

In order to prove (3-9) one needs to show the following: Let Ω be some volume of mass with density anomaly function σ, satisfying $\sigma = 0$ and $\partial\sigma/\partial n=0$ at the boundary S of Ω. The function p defined by $2p=\Delta\sigma$ is such that

$$\iiint_{\Omega}\left(\frac{\sigma}{\ell} - p\ell\right)dv = 0 \qquad (3\text{-}10)$$

The proof will in principle follow Hardy and Nelson [1986, p.19]. One can easily establish that $\Delta(\ell/2) = 1/\ell$ at points with $\ell \neq 0$.

We will distinguish two cases, one for exterior and one for interior points, due to the singularity at $\ell = 0$.

<u>(a) Exterior points:</u>

If the point at which the integral in (3-10) is evaluated is outside the volume Ω then by Green's identity for the functions $\ell/2$ and σ one can write [Heiskanen and Moritz, 1967, p.11]

$$\iiint_{\Omega}\left(\frac{\ell}{2}\,\Delta\sigma - \sigma\Delta\left(\frac{\ell}{2}\right)\right)dv = \iint_{S}\left(\frac{\ell}{2}\,\frac{\partial\sigma}{\partial n} - \sigma\,\frac{\partial}{\partial n}\left(\frac{\ell}{2}\right)\right)ds = \iint_{S}\left(\frac{\ell}{2}\,\frac{\partial\sigma}{\partial n} - \frac{\sigma}{2}\,\frac{\partial\ell}{\partial n}\right)ds.$$

But, on S, both σ and $\frac{\partial\sigma}{\partial n}$ are zero. Therefore $\iint_{S}\left(\frac{\ell}{2}\,\frac{\partial\sigma}{\partial n} - \frac{\sigma}{2}\,\frac{\partial\ell}{\partial n}\right)ds = 0.$

On the other hand $p = \frac{1}{2}\Delta\sigma$ and $\Delta\left(\frac{\ell}{2}\right) = \frac{1}{\ell}$, hence

$$\iiint_{\Omega}\left(\frac{\ell}{2}\,\Delta\sigma - \sigma\Delta\left(\frac{\ell}{2}\right)\right)dv = 0 \iff \iiint_{\Omega}\left(p\ell - \frac{\sigma}{\ell}\right)dv = 0, \text{ q.e.d.}$$

<u>(b) Interior points:</u>

Let us denote by Ω_r the volume that will remain if one excises from Ω the volume of a sphere with center at P and radius r. The boundary of Ω_r is denoted by S_r. A schematic representation is given in Figure 3.

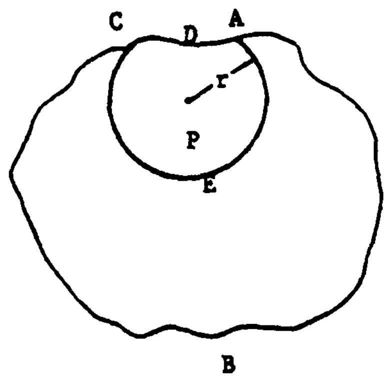

Figure 3. Derivation of the Alternate Integral for the Disturbing Potential at points Interior to the Mass.

The surface ABCDA is the boundary S of Ω. The surface ABCEA is the boundary S_r of Ω_r. The surface ABC is $S \cap S_r$ = {points $Q \varepsilon S$: $Q \varepsilon S_r$}. The surface AEC is $S_r - S$ = {points $Q \varepsilon S_r$, $Q \notin S$}.

By Green's identity for σ and $\ell/2$ one has

$$\iiint_{\Omega_r}\left(\frac{\ell}{2}\Delta\sigma - \sigma\Delta\left(\frac{\ell}{2}\right)\right)dv = \iint_{S_r}\left(\frac{\ell}{2}\frac{\partial\sigma}{\partial n} - \sigma\frac{\partial}{\partial n}\left(\frac{\ell}{2}\right)\right)ds = \iint_{S_r}\left(\frac{\ell}{2}\frac{\partial\sigma}{\partial n} - \frac{\sigma}{2}\frac{\partial\ell}{\partial n}\right)ds =$$

$$= \iint_{S \cap S_r}\left(\frac{\ell}{2}\frac{\partial\sigma}{\partial n} - \frac{\sigma}{2}\frac{\partial\ell}{\partial n}\right)ds + \iint_{S_r - S}\left(\frac{\ell}{2}\frac{\partial\sigma}{\partial n} - \frac{\sigma}{2}\frac{\partial\ell}{\partial n}\right)ds$$

The first integral in the above formula is zero since $\sigma = \partial\sigma/\partial n = 0$ on S and $S \cap S_r \subset S$. If one considers Ω_r small enough such that $(\ell/2)(\partial\sigma/\partial n) - (\sigma/2)(\partial\ell/\partial n) \approx$ constant = c [Scheik, 1986] the second integral can be written as follows:

$$\iint_{S_r - S}\left(\frac{\ell}{2}\frac{\partial\sigma}{\partial n} - \frac{\sigma}{2}\frac{\partial\ell}{\partial n}\right)ds = c\iint_{S_r - S} ds = c \cdot 4\pi r^2$$

which of course goes to zero like r^2. Therefore

$$\iiint_{\Omega}\left(\ell p - \frac{\sigma}{\ell}\right)dv = \iiint_{\Omega}\left(\frac{\ell}{2}\Delta\sigma - \sigma\Delta\left(\frac{\ell}{2}\right)\right)dv = \lim_{r\to o}\left[\iiint_{\Omega_r}\left(\frac{\ell}{2}\Delta\sigma - \sigma\Delta\left(\frac{\ell}{2}\right)\right)dv\right]$$

$$= \lim_{r\to o}\left[\iint_{S_r - S}\left(\frac{\sigma}{2} - \frac{r}{2}\frac{\partial\sigma}{\partial r}\right)ds\right] = 0, \text{ q.e.d.}$$

Therefore

$$\iiint_{\Omega}\left(p\ell - \frac{\sigma}{\ell}\right)dv = 0 \Longleftrightarrow \iiint_{\Omega} p\ell dv = \iiint_{\Omega}\frac{\sigma}{\ell}dv \Longleftrightarrow G\iiint_{\Omega} p\ell dv = G\iiint_{\Omega}\frac{\sigma}{\ell}dv \tag{3-11}$$

and the representations of T in (3-7) and (3-9) are identical.

<u>3.2.2 The biharmonic equation</u>

The Poisson equation

$$\Delta T = -4\pi G\sigma \tag{3-12}$$

corresponds to the representation (3-7) for the disturbing potential. The same way as above, a potential represented by (3-9) is called biharmonic because then it satisfies

$$\Delta^2 T = \frac{\partial^4 T}{\partial x^4} + \frac{\partial^4 T}{\partial y^4} + \frac{\partial^4 T}{\partial z^4} + 2\frac{\partial^4 T}{\partial x^2 \partial y^2} + 2\frac{\partial^4 T}{\partial y^2 \partial z^2} + 2\frac{\partial^4 T}{\partial x^2 \partial z^2} = -8\pi G p \tag{3-13}$$

which is the biharmonic equation. However, the derivatives

$$\frac{\partial^2\sigma}{\partial x^2},\ \frac{\partial^2\sigma}{\partial y^2},\ \frac{\partial^2\sigma}{\partial z^2} \tag{3-14}$$

must exist [Hardy and Nelson, 1986, p.19]. Outside the masses, where $p=0$, T satisfies

$$\Delta^2 T = 0. \tag{3-15}$$

3.2.3 The biharmonic potential

It is shown in Appendix A.5 that the solutions of the homogeneous biharmonic equation ($\Delta^2 T = 0$) are

$$T_i(r,\theta,\lambda) = \sum_{n=0}^{\infty} r^n \sum_{m=0}^{n} [(a_{nm}+r^2c_{nm})\cos m\lambda+(b_{nm}+r^2d_{nm})\sin m\lambda]P_{nm}(\cos\theta) \tag{3-16}$$

$$T_e(r,\theta,\lambda)= \sum_{n=0}^{\infty} \frac{1}{r^{n+1}} \sum_{m=0}^{n} [(a_{nm}+r^2c_{nm})\cos m\lambda+(b_{nm}+r^2d_{nm})\sin m\lambda]P_{nm}(\cos\theta) \tag{3-17}$$

where a_{nm}, b_{nm}, c_{nm} and d_{nm} are arbitrary constants. Therefore a biharmonic function T can be represented as

$$T = H_1 + r^2 H_2 \tag{3-18}$$

where H_1 and H_2 harmonic. If H_2 vanishes identically then T degenerates to a harmonic function.

Equations (3-16) and (3-17) are general. Every function which is biharmonic inside a certain sphere can be expanded into a series (3-16) whereas every function which is biharmonic outside a certain sphere can be expanded into a series (3-17).

3.2.4 Further consequences

The definition $p=\frac{1}{2}\Delta\sigma$ is a partial differential equation of the Poisson type. Therefore, the above definition together with the boundary conditions $\sigma = \partial\sigma/\partial n = 0$ uniquely determine σ [Kellogg, 1929, p.215]. Actually, since the earth is not homogeneous, one should write

$$\frac{\partial}{\partial x}\left[f_1\frac{\partial\sigma}{\partial x}\right] + \frac{\partial}{\partial y}\left[f_2\frac{\partial\sigma}{\partial y}\right] + \frac{\partial}{\partial z}\left[f_3\frac{\partial\sigma}{\partial z}\right] = 2p$$

where f_1, f_2, f_3 are functions characterizing the inhomogeneity of the medium [Volyskii and Bukhman, 1965, p.36].

In order to solve $p = \frac{1}{2}\Delta\sigma$ one can use Green's third identity [Heiskanen and Moritz, 1967, pp.11-12] to get

$$\iiint_{\Omega} \frac{1}{\ell} \Delta\sigma dv = -k\sigma + \iint_{S} \left(\frac{1}{\ell} \frac{\partial \sigma}{\partial n} - \sigma \frac{\partial}{\partial n} \left(\frac{1}{\ell} \right) \right) ds$$

where

$$k = \begin{cases} 4\pi & \text{if the evaluation point Q is inside S,} \\ 2\pi & \text{if the evaluation point Q is } on \text{ S,} \\ 0 & \text{if the evaluation point Q is outside S,} \end{cases}$$

and n is the normal to S directed outward. But since $\sigma = \frac{\partial \sigma}{\partial n} = 0$ on S and $p = \frac{1}{4}\Delta\sigma$ one gets

$$\iiint_{\Omega} \frac{p}{\ell} dv = -\frac{k\sigma}{2} \tag{3-19}$$

For points Q inside S one gets

$$\sigma = -\frac{1}{2\pi} \iiint_{\Omega} \frac{p}{\ell} dv \tag{3-20}$$

From equation (3-20) one can see that the singularity of T at $\ell=0$ is not avoided. It is simply transfered to a singularity in σ at the same point ($\ell=0$).

An obscure point in Hardy's derivation remains the existence of the fourth order partial derivatives of T in (3-13). The reason for this is that at least one of the second order partial derivatives of T must be discontinuous in the region from the geocenter to infinity [Heiskanen and Moritz, 1967, p. 5] following the discontinuities of σ.

On the other hand, the density anomaly function σ is assumed to possess properties that may not be physically reasonable. At first, the second partial derivatives of σ are assumed to exist. Since the earth's density function is very likely to exhibit discontinuities, the density function of the reference ellipsoid must be discontinuous in such a manner that both σ and its partials of first order be continuous. Furthermore, the density function of the reference ellipsoid must be such, that σ together with its normal derivative vanish at the boundary.

The aforementioned requirements of the method are not justified from the point of view of the physics of the problem. For example, since all the points of discontinuity of the Earth's density are not known, one cannot construct a reference ellipsoid such that the resulting density anomaly function σ and its partials of first order be continuous. The point of this discussion is that if the method yields not good predictions of gravity field related quantities, this should come as no surprise due to the aforementioned shortcomings of the method.

3.3 Approximation of the disturbing potential

Let data be given at n discrete points. Let us also subdivide Ω into regions V_i, i=1, 2, ..., n. The biharmonic sources (sources of biharmonic potential) are defined as follows [Hardy and Nelson, 1986, p. 19]

$$a_i = \iiint_{V_i} p\,dv \qquad (3\text{-}21)$$

Let P be the point at which the disturbing potential will be evaluated, q_i be one of the given data points and q be any point in V_i. Also, let ℓ_{pq_i} be the distance from p to q_i, ℓ_i be the distance of q to q_i and ℓ be the distance from p to q. The triangle inequality for p,q,q_i can be written as

$$\left|\ell-\ell_{pq_i}\right| \leq \ell_i \qquad (3\text{-}22)$$

Multiplying both sides by $|p|dv$ and forming the integral for V_i one gets

$$G\iiint_{V_i}\left|\ell-\ell_{pq_i}\right|\cdot|p|dv \leq G\iiint_{V_i} \ell_i|p|dv \qquad (3\text{-}23)$$

Summing over all of the V_i's one gets

$$G\sum_{i=1}^{n} \iiint_{V_i} \left|\ell-\ell_{pq_i}\right|\cdot|p|dv \leq G\sum_{i=1}^{n} \iiint_{V_i} \ell_i|p|dv \qquad (3\text{-}24)$$

Now

$$\left|\sum_{i=1}^{n} G\iiint_{V_i}\ell p dv - \sum_{i=1}^{n} G\iiint_{V_i}\ell_{pq_i} p dv\right| = G\left|\iiint_{V_1}\ell p dv + \ldots + \iiint_{V_n}\ell p dv - \iiint_{V_1}\ell_{pq_1} p dv\right.$$

$$\left. - \iiint_{V_n}\ell_{pq_n} p dv\right| =$$

$$= G\left|\iiint_{V_1}\ell p dv - \iiint_{V_1}\ell_{pq_1} p dv + \ldots + \iiint_{V_n}\ell p dv - \iiint_{V_n}\ell_{pq_n} p dv\right| \leq$$

$$\leq G\left|\iiint_{V_1}\ell p dv - \iiint_{V_1}\ell_{pq_1} dv\right| + \ldots + G\left|\iiint_{V_n}\ell p dv - \iiint_{V_n}\ell_{pq_n} p dv\right| \leq$$

$$\leq G\iiint_{V_1}\left|\ell_p-\ell_{pq_1}\right|\cdot|p|dv + \ldots + G\iiint_{V_n}\left|\ell_p-\ell_{pq_n}\right|\cdot|p|dv, \text{ hence,}$$

$$\left|\sum_{i=1}^{n} G\iiint_{V_i} \ell p dv - \sum_{i=1}^{n} G\iiint_{V_i} \ell_{pq_i} p dv\right| \leq \sum_{i=1}^{n} G\iiint_{V_i} \left|\ell_p - \ell_{pq_i}\right| \cdot |p| dv$$

which, upon substitution in (3-24) yields

$$\left|G \sum_{i=1}^{n} \iiint_{V_i} \ell p dv - G \sum_{i=1}^{n} \iiint_{V_i} \ell_{pq_i} p dv\right| \leq G \sum_{i=1}^{n} \iiint_{V_i} \ell_i |p| dv \tag{3-25}$$

Now $G \sum_{i=1}^{n} \iiint_{V_i} \ell p dv = T_p$ from the basic integral (3-9). Also, since ℓ_{pq_i} is constant for each V_i (3-25) can be rewritten as

$$\left|T_p - G \sum_{i=1}^{n} \ell_{pq_i} \iiint_{V_i} p dv\right| \leq G \sum_{i=1}^{n} \iiint_{V_i} \ell_i |p| dv \tag{3-26}$$

Let us denote by ε_i the distance of q_i to the furthermost q in V_i, i.e., $\varepsilon_i > \ell_{qq_i}$ for all $q \in V_i$. Also, let us denote by ε the maximum ε_i, i.e., $\varepsilon = \max(\varepsilon_i)$ for i=1,2,...,n. Then $\ell_i \leq \varepsilon$ for i=1,2,...,n and recalling (3-21), (3-26) can be written as

$$\left|T_p - G \sum_{i=1}^{n} \ell_{pq_i} a_i\right| \leq \varepsilon G \sum_{i=1}^{n} \iiint_{V_i} |p| dv \tag{3-27}$$

Equation (3-27) implies that the approximation

$$T = G \sum_{i=1}^{n} \ell_i a_i \tag{3-28}$$

can be made arbitrarily good by an appropriate choice of ε, i.e., of the size of the subregions V_i (note that ℓ_{pq_i} was substituted by ℓ_i in (3-28)).

3.4 Linear functionals of the disturbing potential

3.4.1 Gravity anomalies

From the fundamental equation of physical geodesy (2-7) one has

$$\Delta g = -\frac{\partial T}{\partial r} - \frac{2T}{r} \tag{3-29}$$

If one denotes by r the geocentric distance to the evaluation point, by r_i the geocentric distance to the biharmonic source a_i and by $\phi,\lambda,\phi_i,\lambda_i$ their geodetic coordinates respectively one has from (2-11) and (2-10)

$$\ell_i = (r^2 + r_i^2 - 2rr_i\cos\omega)^{\frac{1}{2}} \tag{3-30}$$

$$\cos\omega = \sin\phi\sin\phi_i + \cos\phi\cos\phi_i\cos(\lambda-\lambda_i). \tag{3-31}$$

Thus

$$\frac{\partial T}{\partial r} = G\sum_{i=1}^{n} a_i\frac{\partial \ell_i}{\partial r}, \text{ with } \frac{\partial \ell_i}{\partial r} = \frac{1}{2\ell_i}(2r-2r_i\cos\omega). \text{ Hence}$$

$$\frac{\partial T}{\partial r} = G\sum_{i=1}^{n} a_i\frac{r-r_i\cos\omega}{\ell_i}, \text{ and therefore}$$

$$\Delta g = -G\sum_{i=1}^{n} a_i\left[\frac{r-r_i\cos\omega}{\ell_i} + \frac{2\ell_i}{r}\right]. \tag{3-32}$$

3.4.2 Deflections of the vertical

Recall equation (2-30)

$$\begin{Bmatrix}\xi\\ \eta\end{Bmatrix} = \frac{1}{\gamma r}\frac{\partial T}{\partial \omega}\begin{Bmatrix}\cos\alpha\\ \sin\alpha\end{Bmatrix}. \tag{3-33}$$

The required derivative $\frac{\partial T}{\partial \omega}$ is

$$\frac{\partial T}{\partial \omega} = G\sum_{i=1}^{n} a_i\frac{\partial \ell_i}{\partial \omega} = G\sum_{i=1}^{n} a_i\frac{rr_i\sin\omega}{\ell_i}, \text{ thus, using (2-33) one gets}$$

$$\begin{Bmatrix}\xi\\ \eta\end{Bmatrix} = \frac{G}{\gamma}\sum_{i=1}^{n}\frac{a_i r_i}{\ell_i}\begin{Bmatrix}\cos\phi\sin\phi_i - \sin\phi\cos\phi_i\cos(\lambda_i-\lambda)\\ \cos\phi_i\sin(\lambda_i-\lambda)\end{Bmatrix}. \tag{3-34}$$

3.5 The biharmonic sources on the geosphere

If one places the biharmonic sources on the surface of the geosphere with radius r_0, equations (3-32), (3-34) will become

$$\Delta g = -G\sum_{i=1}^{n} a_i\left[\frac{r-r_0\cos\omega}{\ell} + \frac{2\ell}{r}\right] \tag{3-35}$$

$$\begin{Bmatrix}\xi\\ \eta\end{Bmatrix} = \frac{G}{\gamma}\sum_{i=1}^{n}\frac{a_i r_0}{\ell}\begin{Bmatrix}\cos\phi\sin\phi_i - \sin\phi\cos\phi_i\cos(\lambda_i-\lambda)\\ \cos\phi_i\sin(\lambda_i-\lambda)\end{Bmatrix} \tag{3-36}$$

with

$$\ell = \{r^2+r_0^2 - 2rr_0\cos\omega\}^{1/2} \tag{3-37}$$

Introducing t and d by

$$t = \frac{r_0}{r} \tag{3-38}$$

and $d = \{1+t^2-2t\cos\omega\}^{1/2}$ (3-39)

one gets

$$\ell = \{r^2+r_0^2-2rr_0\cos\omega\}^{1/2} = r\{1+t^2-2t\cos\omega\}^{1/2} = rd; \text{ hence}$$

$$\Delta g = -G\sum_{i=1}^{n}\left[\frac{1-t\cos\omega}{d} + 2d\right]a_i, \tag{3-40}$$

$$\begin{Bmatrix}\xi \\ \eta\end{Bmatrix} = \frac{Gt}{\gamma}\sum_{i=1}^{n}\frac{a_i}{d}\begin{Bmatrix}\cos\phi\sin\phi_i - \sin\phi\cos\phi_i\cos(\lambda_i-\lambda) \\ \cos\phi_i\sin(\lambda_i-\lambda)\end{Bmatrix}. \tag{3-41}$$

Finally, letting

$$c_i = Ga_i \tag{3-42}$$

one can write (3-40), (3-41) as

$$\Delta g = -\sum_{i=1}^{n}\left[\frac{1-t\cos\omega}{d} + 2d\right]c_i, \tag{3-43}$$

$$\begin{Bmatrix}\xi \\ \eta\end{Bmatrix} = \frac{t}{\gamma}\sum_{i=1}^{n}\frac{c_i}{d}\begin{Bmatrix}\cos\phi\sin\phi_i - \sin\phi\cos\phi_i\cos(\lambda_i-\lambda) \\ \cos\phi_i\sin(\lambda_i-\lambda)\end{Bmatrix}. \tag{3-44}$$

Equations (3-43), (3-44) can be used to compute c_i from observed Δg, ξ and η and/or to predict Δg, ξ, η from previously computed c_i values. The associated linear system and its solution will be identical to the one described in Section 2.4. Also, the propagation of the data noise into the predictions will be performed in a manner identical to the one described in Section 2.5.

CHAPTER IV

THE DATA

4.1 Introduction

The White Sands Test Area is located at the western outskirts of the Rio Grande Rift System in New Mexico. The tests of the two methods were performed with data in the portion of White Sands bound by the parallels 32°N and 34°N and the meridians 253°E and 254°E. This area is mainly a plateau at a level of 1200 m to 1400 m (Figure 4). The Oscura and San Andres mountain chains cross the area in a North-South direction. The geological constitution of the area is mainly young mesozoic sediments complimented by some late tertiary volcanics [Schwarz, 1983, p. 2].

The bulk of the White Sands Test data were made available to the Special Study Group 4.70 of the International Association of Geodesy by the National Geodetic Survey, NOS, NOAA, Rockville, Maryland. C.C. Tscherning did some initial data screening and then arranged the different files for the tests [Schwarz, 1983]. The test data used were made available to us by C.C. Tscherning and were identical to the data used in the collocation solution of the report "White Sands Revisited" [Kearsley et al., 1985].

4.2 The Two Solutions

For each method two independent solutions were employed. One for the (1°x1°) area bound by parallels 33°N and 34°N and called the North Block (NB) and one for the (1°x1°) area bound by parallels 32°N and 33°N and called the South Block (SB).

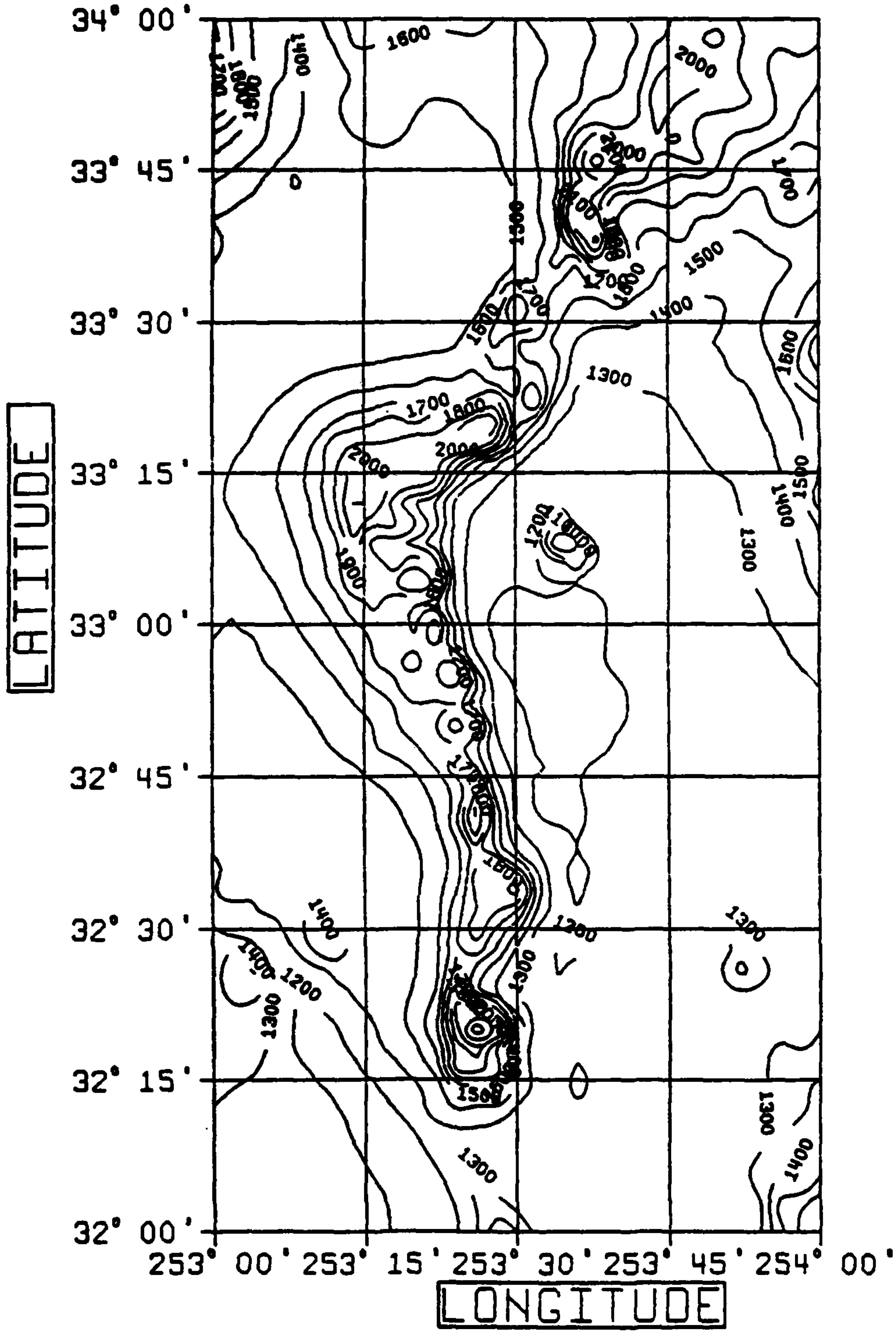

Figure 4. Topographic Map of the New Mexico Test Area From a 2′x2′ DTM (CI = 100m).

4.3 Gravity Anomalies

The gravity anomaly data are free-air values referenced to the Geodetic Reference System 1967. Their geodetic latitude and longitude are given in the NAD27, their height is orthometric and their standard deviation is $\pm$ 2 mgals. There are 384 observations in the NB (Figure 5), 548 observations in the SB (Figure 6), 82 control values in the NB (Figure 7) and 123 control values in the SB (Figure 8).

4.4 Deflections of the Vertical

The vertical deflection data are astrogeodetic values referenced to the NAD27. Their geodetic coordinates are given in the NAD27, their height is orthometric and their standard deviation is $\pm 0''.3$. There are 67 (ξ,η) observed pairs in the NB (Figure 9), 63 observed pairs in the SB (Figure 10), 176 control pairs in the NB (Figure 11) and 208 control pairs in the SB (Figure 12).

4.5 Conversion of the data to an approximately geocentric system

The system in which all the calculations were carried out was an approximately geocentric system with the ellipsoidal parameters of GRS80. The datum transformation parameters from NAD27 to the new system are [Schwarz, 1983, p. 13], [Tscherning, 1987]

$$\Delta x = -22\text{m},\ \Delta y = 157\text{m},\ \Delta z = 176\text{m},\ \varepsilon = 0,\ \psi = 0,\ \omega = -0''.7,\ \Delta L = 0 \qquad (4\text{-}1)$$

The geodetic latitude and longitude can be transformed to the new system by

$$\begin{Bmatrix} \phi_{NEW} = \phi_{NAD27} + d\phi \\ \lambda_{NEW} = \lambda_{NAD27} + d\lambda \end{Bmatrix} \qquad (4\text{-}2)$$

with [Rapp, 1981, pp.70,77]

$$\begin{pmatrix} d\phi = -\dfrac{\sin\phi\cos\lambda}{M+h}\Delta x - \dfrac{\sin\phi\sin\lambda}{M+h}\Delta y + \dfrac{\cos\phi}{M+h}\Delta z + \dfrac{e^2\sin\phi\cos\phi}{W(M+h)}\Delta a \\ \qquad + \dfrac{\sin\phi\cos\phi(2N+e'^2M\sin^2\phi)}{M+h}(1-f)\Delta f \\ d\lambda = -\dfrac{\sin\lambda}{(N+h)\cos\phi}\Delta x + \dfrac{\cos\lambda}{(N+h)\cos\phi}\Delta y - \omega \end{pmatrix} \qquad (4\text{-}3)$$

and [Rapp, 1984, pp.21,30,35]

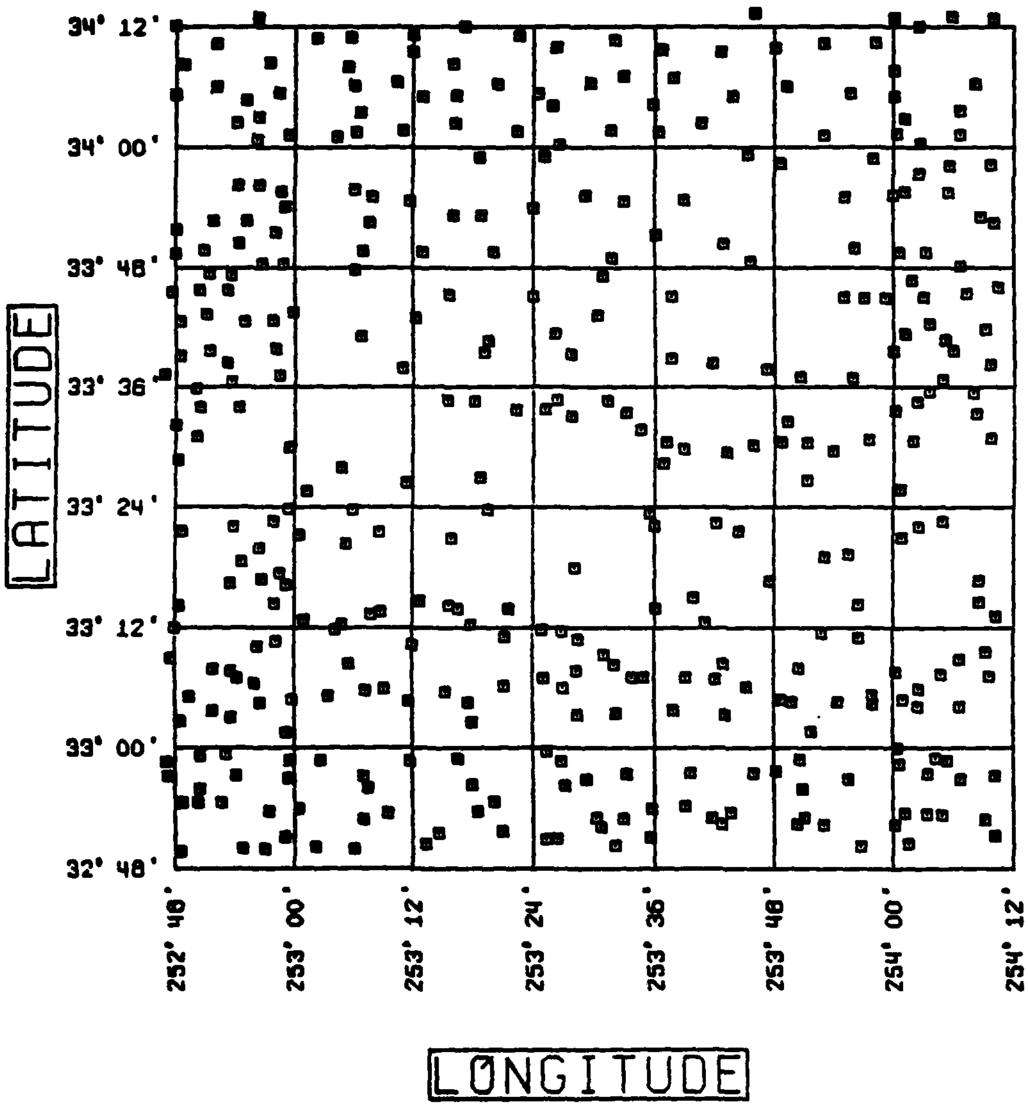

Figure 5. Distribution of the 384 Gravity Observations at the North Block of the White Sands Test Area.

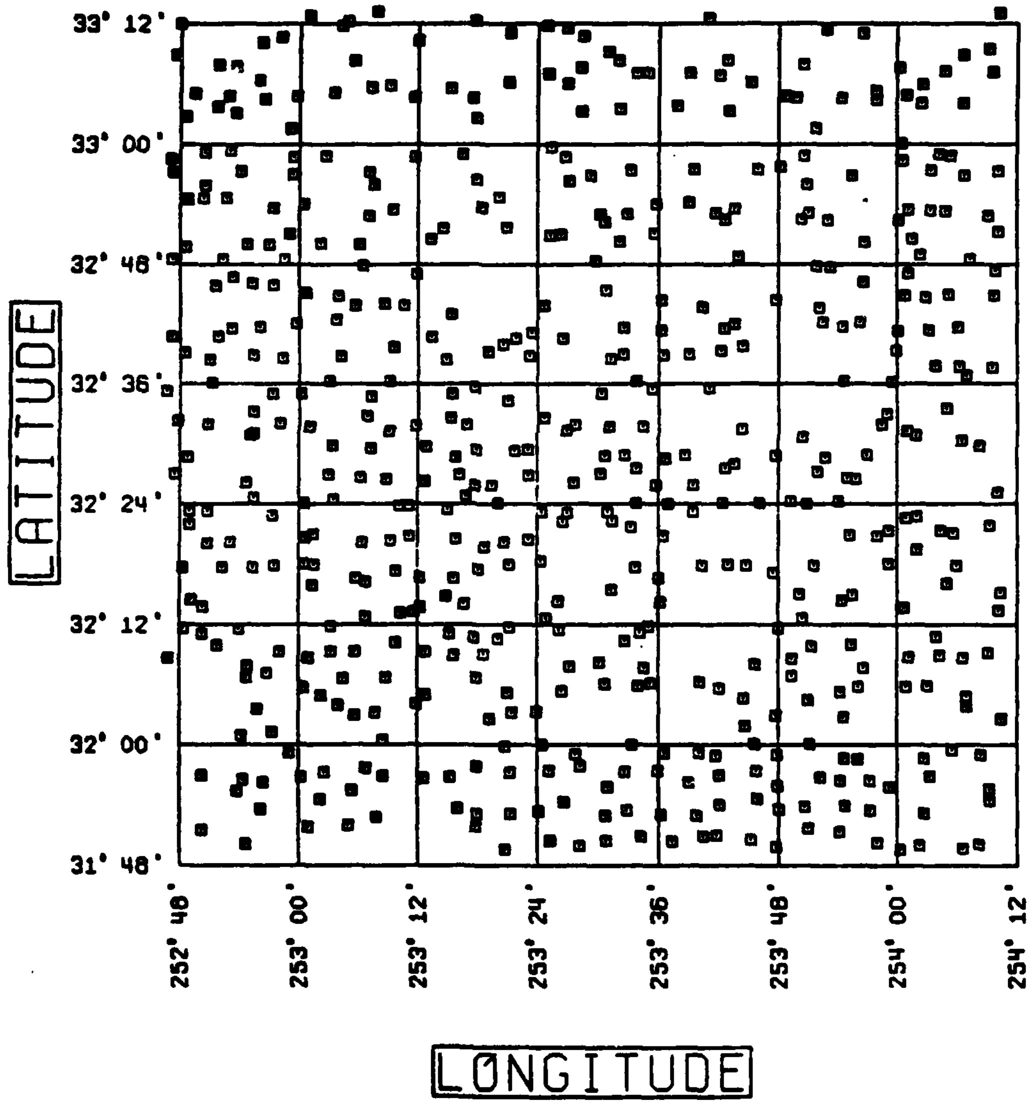

Figure 6. Distribution of the 548 Gravity Observations at the South Block of the White Sands Test Area.

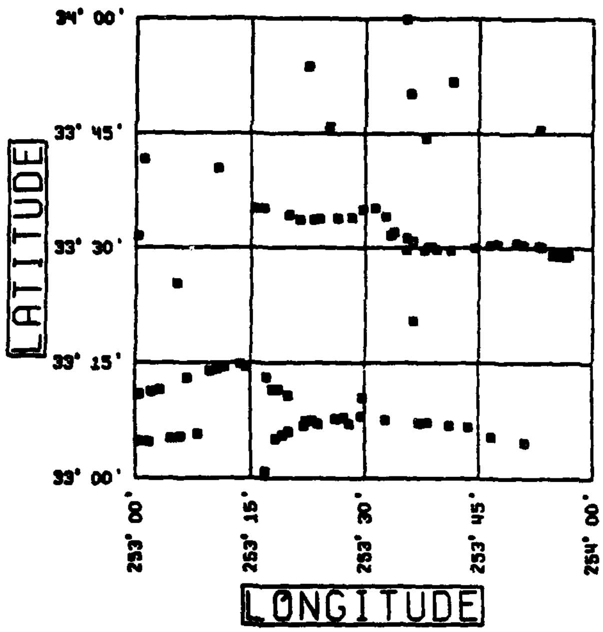

Figure 7. Distribution of the 82 Gravity Control Stations at the North Block of the White Sands Test Area.

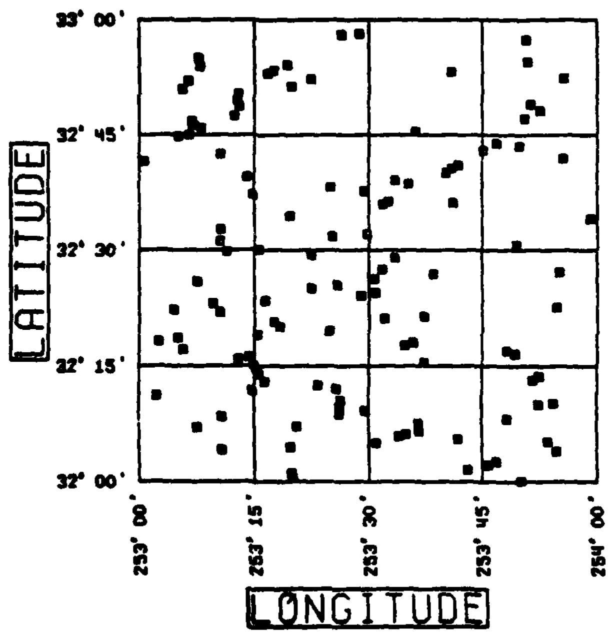

Figure 8. Distribution of the 123 Gravity Control Stations at the South Block of the White Sands Test Area.

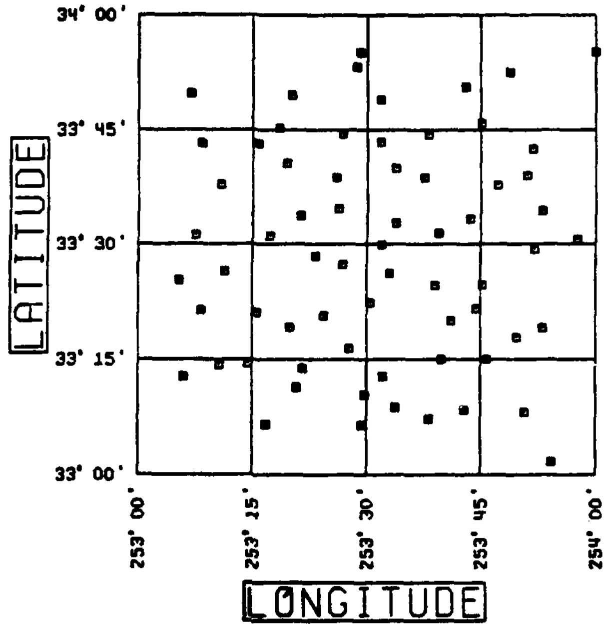

Figure 9. Distribution of the 67 Observed Vertical Deflection Pairs at the North Block of the White Sands Test Area.

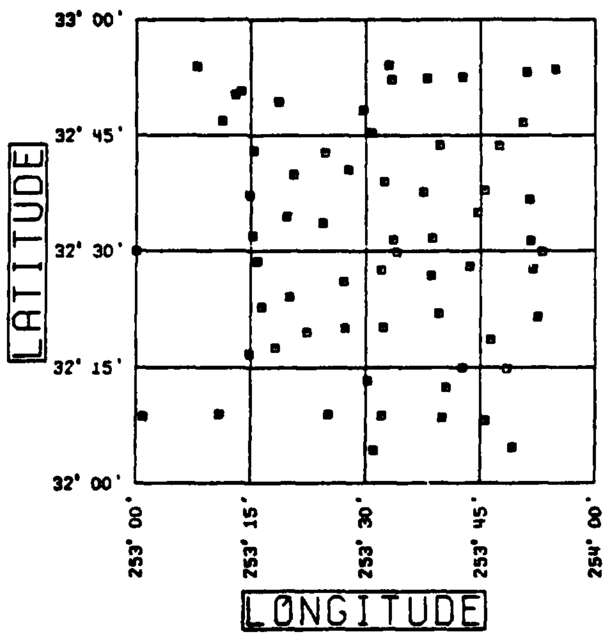

Figure 10. Distribution of the 63 Observed Vertical Deflection Pairs at the South Block of the White Sands Test Area.

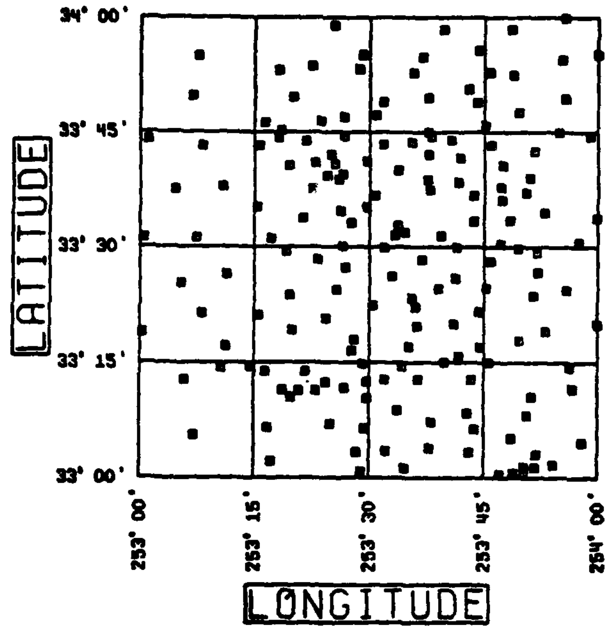

Figure 11. Distribution of the 176 Vertical Deflection Control Stations at the North Block of the White Sands Test Area.

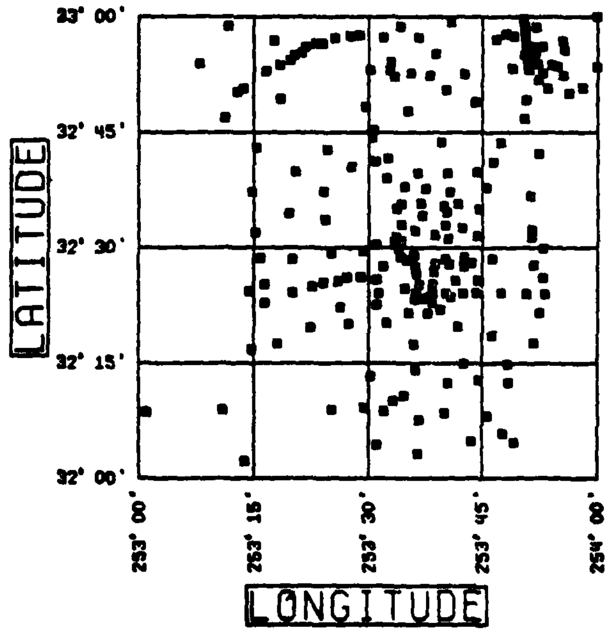

Figure 12. Distribution of the 208 Vertical Deflection Control Stations at the South Block of the White Sands Test Area.

$$W^2 = 1-e^2\sin^2\phi;\ M = \frac{a(1-e^2)}{W^3};\ N = \frac{a}{W} \tag{4-4}$$

Also [Rapp, 1984, p.169]

$$\begin{aligned} a_{NAD27} &= 6378206.4 \text{ m} \\ f_{NAD27} &= 1/294.978698 \\ a_{NEW} &= 6378137 \text{ m} \\ f_{NEW} &= 1/298.257222101 \end{aligned}$$

and $\Delta a = a_{NEW} - a_{NAD27}$

$$\delta f = f_{NEW} - f_{NAD27}$$

The error in using orthometric height instead of geometric height in (4-3) is less than 0".001.

Similarly for the vertical deflections one has

$$\begin{bmatrix} \xi_{NEW} = \xi_{NAD27} + d\xi \\ \eta_{NEW} = \xi_{NAD27} + d\eta \end{bmatrix} \tag{4-5}$$

where [Rapp, 1981, p. 74]

$$\begin{pmatrix} d\xi = -d\phi \\ d\eta = -d\lambda\cos\phi \end{pmatrix} \tag{4-6}$$

The relation between normal gravity computed with the GRS80 and the GRS67 reference ellipsoid is [Schwarz, 1983, p. 13]

$$\gamma_{1980} = \gamma_{1967} + (0.8316 + 0.0782\sin^2\phi - 0.0007\sin^4\phi) \tag{4-7}$$

Furthermore, in Section 2.2.1 it was assumed that the space outside the boundary is empty which implies that the atmospheric and the tidal effects have been removed from the observed gravity. As far as the tidal corrections are concerned it is assumed that they have been modeled during the observation reduction process. The atmospheric corrections will be computed by [Wichiencharoen, 1982, p. 5]

$$\delta g_A = (0.8658 - 9.727\text{x}10^{-5}H + 3.482\text{x}10^{-9}H^2)\text{mgals} \tag{4-8}$$

where H is the orthometric height in meters.

Therefore the gravity anomalies referenced to GRS80 and corrected for atmospheric effects are given by

$$\Delta g_{GRS80} = \Delta g_{GRS67} - 0.8316 - 0.0782\sin^2\phi_{NEW} + 0.0007\sin^4\phi_{NEW} + \delta g_A \tag{4-9}$$

Contour maps of the observations at both the North and the South Block of the White Sands Test Area are shown in Figures 13 through 18.

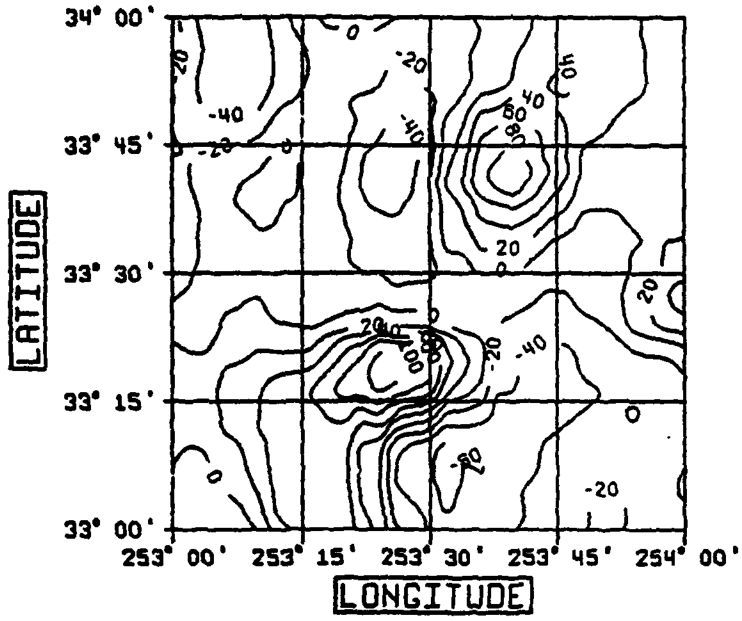

Figure 13. Contour Map From the Observed Gravity Anomalies at the North Block of the White Sands Test Area. (CI=20 mgals).

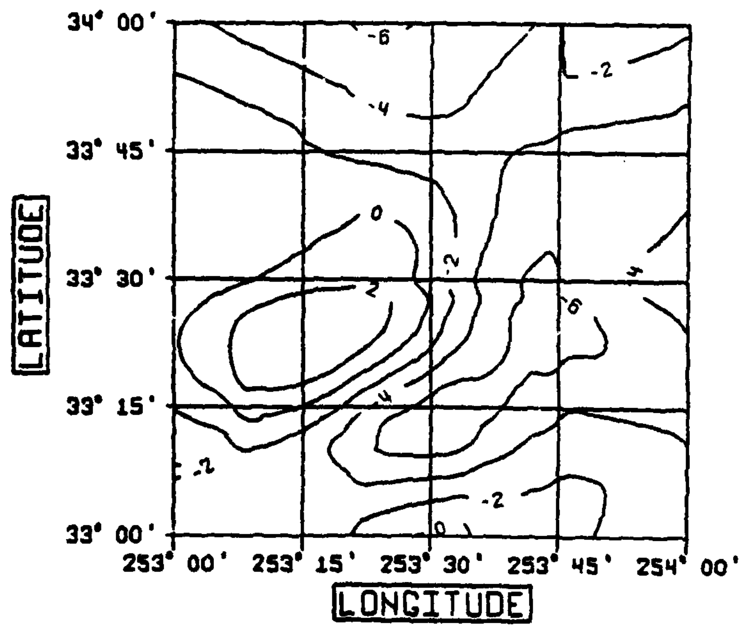

Figure 14. Contour Map From the Observed Meridional Deflections at the North Block of the White Sands Test Area. (CI=2").

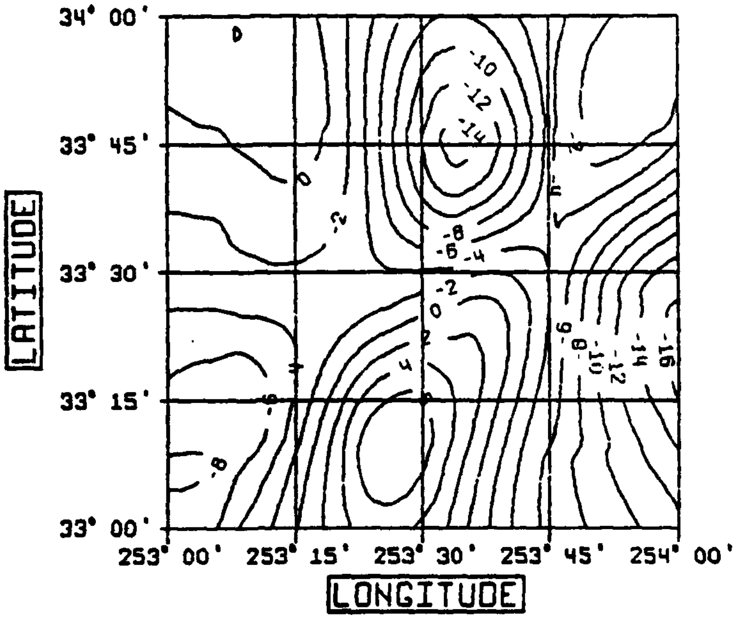

Figure 15. Contour Map From the Observed Prime Vertical Deflections at the North Block of the White Sands Test Area. (CI=2").

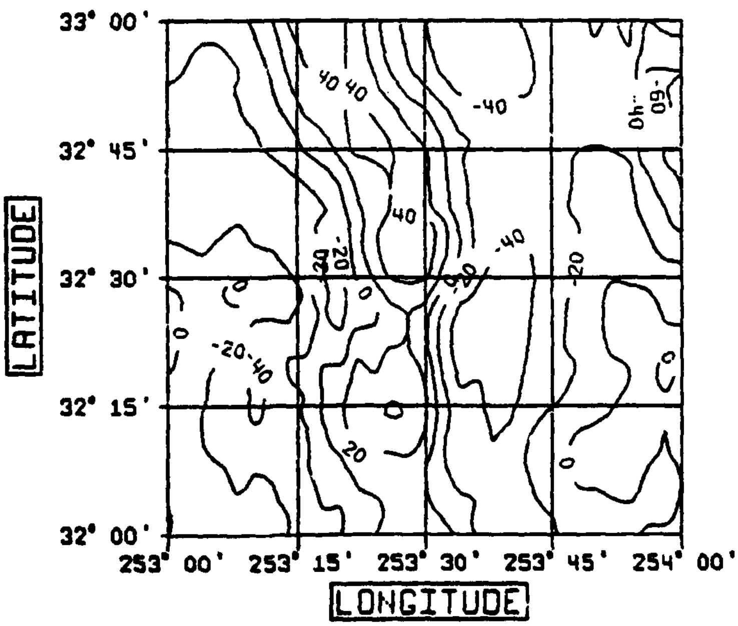

Figure 16. Contour Map From the Observed Gravity Anomalies at the South Block of the White Sands Test Area. (CI=20 mgals).

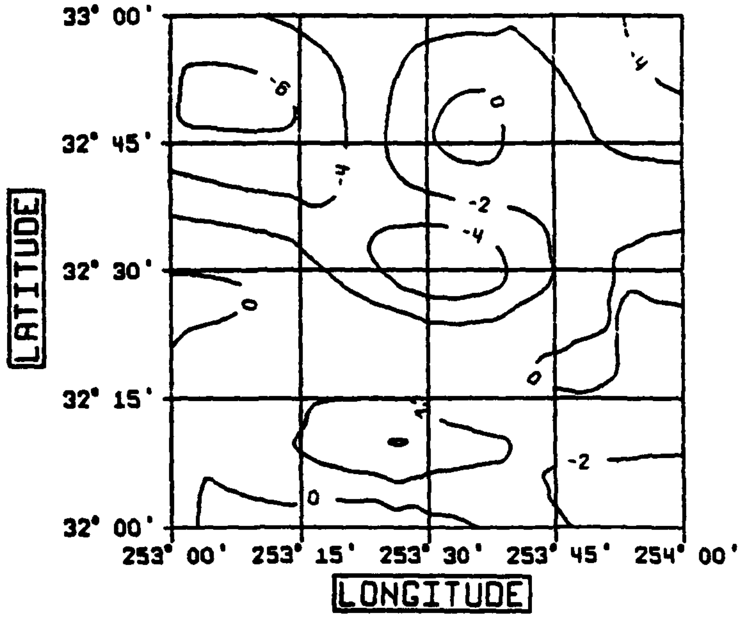

Figure 17. **Contour Map From the Observed Meridional Deflections at the South Block of the White Sands Test Area. (CI=2").**

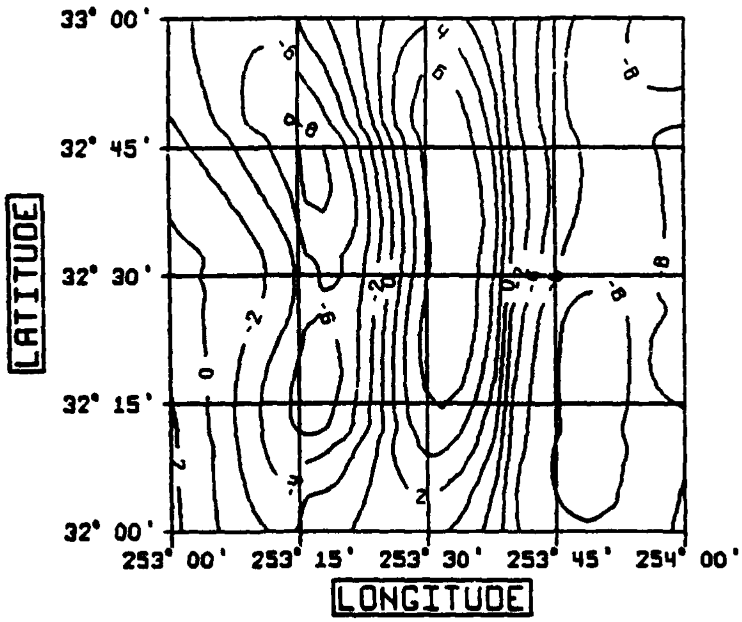

Figure 18. **Contour Map From the Observed Prime Vertical Deflections at the South Block of the White Sands Test Area. (CI=2").**

4.6 Removal of Reference Field and Residual Terrain Model (RTM) Effects

The predictors will be applied to the mid-frequencies of the anomalous potential spectrum. The low frequency effects, corresponding to wavelengths of about 1° (~111 km) or larger will be accounted for by the OSU86F reference field to degree and order 180 [Rapp and Cruz, 1986]. The reference field computations will be performed as described in [Rapp, 1982b].

The Residual Terrain Model (RTM) effect is the effect of the masses between the actual topography and a mean elevation surface, on the gravity anomalies and the deflections of the vertical. The actual topography is represented by a detailed DTM whereas the aforementioned mean elevation surface, termed the reference surface, is a coarse DTM which is usually derived from the detailed DTM by averaging. The residual topography is modeled as an assembly of rectangular prisms with a constant positive or negative density depending on whether the terrain surface is above or below the reference surface [Kearsley et al., 1985, p. 53]. The effect of the residual topography on the gravity anomalies and the vertical deflections is removed computationally, so that the residual quantities refer to the reference surface rather than the actual topography [Forsberg, 1988]. Therefore, the RTM effects account for the short wavelength features of the anomalous potential spectrum [Kearsley et al., 1985, p. 55].

The question of the optimal RTM computations has not been completely answered yet. For example, Forsberg and Tscherning [1981] used two different grid sizes as reference surfaces for testing purposes. On the other hand, Cruz [1985, p. 74] used a spherical harmonic expansion of the topography as the reference surface. Moreover, Kearsley et al. [1985, p. 55] performed tests using different DTMs as reference surfaces. These tests indicated that the coarser the reference surface the smoother the residual field. However, different reference surfaces have an insignificant impact on the predictions due to the remove-restore operation [ibid, p. 55].

The RTM effects used in this investigation were computed by R. Forsberg and C.C. Tscherning [Forsberg, 1988]. The same RTM effect values were also used in other tests with the White Sands data [Schwarz, 1983] and [Kearsley et al., 1985]. A (30"x30") elevation grid which extends over the area $31°30' < \phi < 35°$ and $252° < \lambda < 255°$ was used as the detailed DTM, whereas a (30'x30') grid was used as the reference surface. Consequently, the majority of the signal of the anomalous field at wavelengths of 30' (~55 km) or smaller was removed by the RTM computations. The remaining part of the signal (between wavelengths 55 km and 110 km) was left to be handled by the predictors [Forsberg, 1988].

Tables 1 and 2 show the results of the removal of both the reference field and the RTM effects from the observed and the control values respectively. The residual quantities V in these tables are defined as

$$\left\{\begin{array}{l} V_{\Delta g} = \Delta g_{GRS80} - \Delta g_{OSU86F} - \Delta g_{RTM} \\ V_{\xi} = \xi_{NEW} - \xi_{OSU86F} - \xi_{RTM} \\ V_{\eta} = \eta_{NEW} - \eta_{OSU86F} - \eta_{RTM} \end{array}\right\} \tag{4-10}$$

Table 1. RMS Values of OSU86F and RTM Effects on Observations.

	OBSERVATION	OSU86F	RTM	RESIDUAL(V)
Δg(mgal)	26.59	14.86	19.64	17.68
ξ (")	3.73	2.60	1.95	1.80
η (")	6.42	4.53	3.34	4.09

Table 2. RMS Values of OSU86F and RTM Effects on Control Data.

	CONTROL	OSU86F	RTM	RESIDUAL(V)
Δg(mgal)	25.54	10.94	15.95	19.35
ξ (")	3.82	2.66	1.76	1.63
η (")	6.78	4.65	3.42	4.33

Tables 1 and 2 indicate that the residual field is smoother than the original field. Figures 19 through 24 show contours from the residual observations in both the NB and the SB. Comparison of Figures 13 to 19, 14 to 20, 15 to 21 for the North Block and 16 to 22, 17 to 23, 18 to 24 for the South Block reveals that the basic signature of the anomalous potential is not lost by the removal of the OSU86F and RTM effects. However, some irregularities of the original field have been smoothed out by these computations.

The CPU time required to compute reference field effects is about 0.5 sec/station and to compute RTM effects is about 0.5 sec/station on the IBM 3081 main frame.

In conclusion, the computation scheme will be to remove the OSU86F and RTM effects from the observations, perform the predictions with the residual field and then restore the OSU86F and RTM effects at the prediction stations.

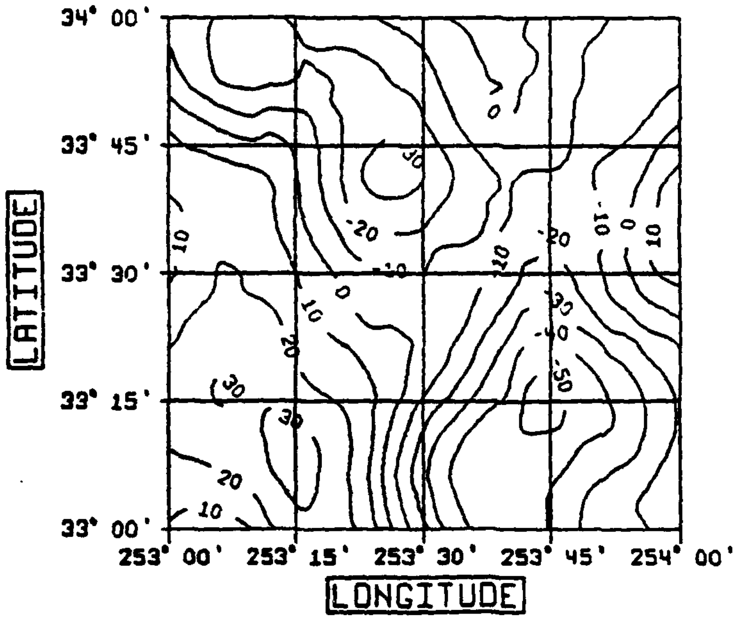

Figure 19. Contour Map of the Residual Observations at the North Block of the White Sands Test Area. Gravity Anomalies (CI=10 mgals).

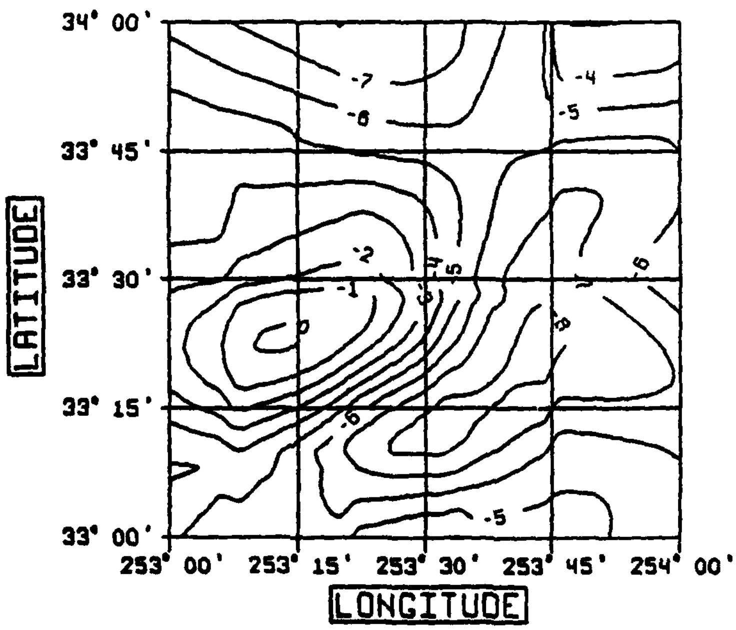

Figure 20. Contour Maps of the Residual Observations at the North Block of the White Sands Test Area. Meridional Deflections (CI=1").

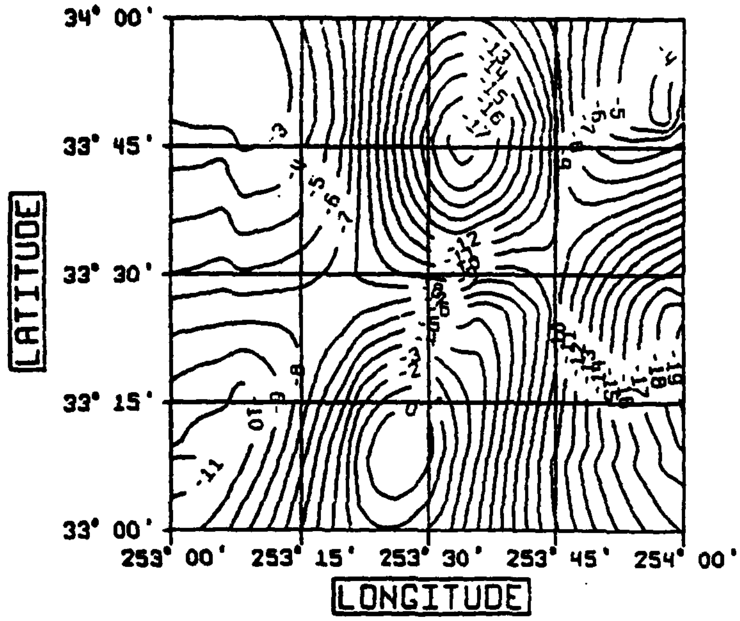

Figure 21. Contour Map of the Residual Observations at the North Block of the White Sands Test Area. Prime Vertical Deflections (CI=1").

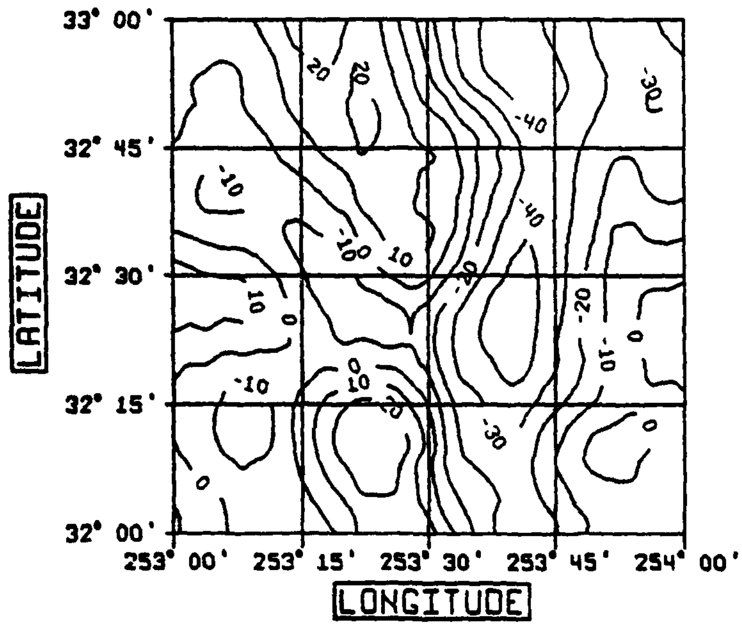

Figure 22. Contour Map of the Residual Observations at the South Block of the White Sands Test Area. Gravity Anomalies (CI=10 mgals).

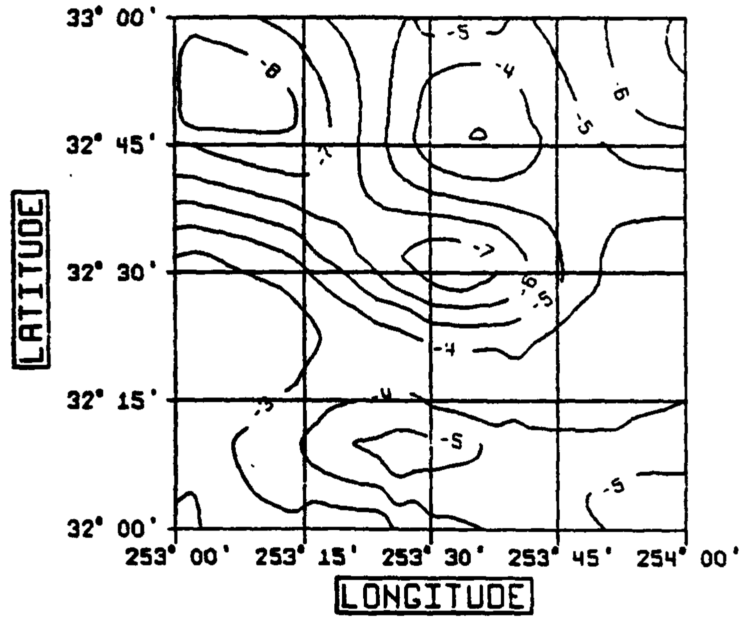

Figure 23. Contour Map of the Residual Observations at the South Block of the White Sands Test Area. Meridional Deflections (CI=1").

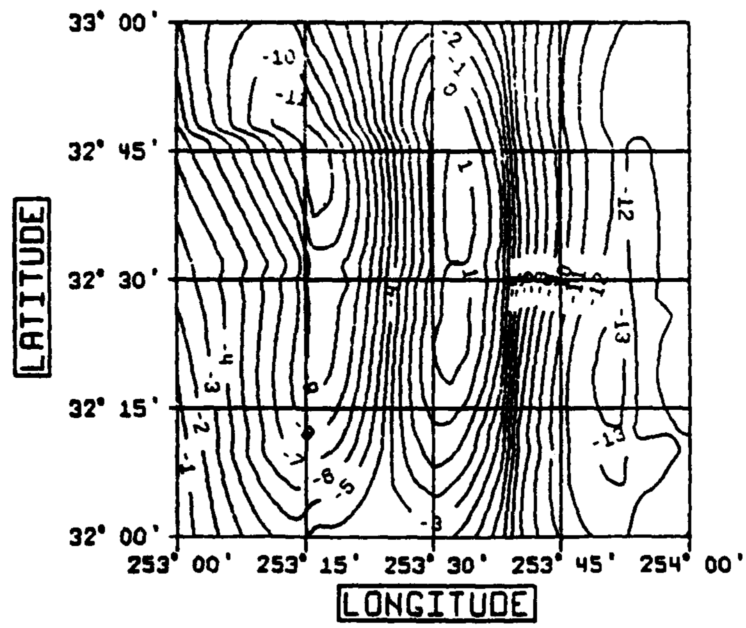

Figure 24. Contour Map of the Residual Observations at the South Block of the White Sands Test Area. Prime Vertical Deflections (CI=1").

CHAPTER V

ANALYSIS OF THE RESULTS

5.1 Introduction

The Bjerhammar and Hardy predictors were tested with data in the portion of the White Sands Test Area bound by parallels 32°N and 34°N and meridians 253°E and 254°E. For each method tested two independent solutions were employed. One for the 1°x1° area bound by parallels 33°N and 34°N and called the North Block (NB) solution and one for the 1°x1° area bound by parallels 32°N and 33°N and called the South Block (SB) solution.

Two factors that contribute greatly to the quality of predictions of quantities related to the Earth's gravity field are the topography and the data coverage of the area of interest. The 2°x1° area at which the two predictors were tested presents significant variations in both of these factors. As far as the terrain is concerned, Figure 4 reveals relatively large valleys and rather high mountain peaks, the NB being more irregular than the SB. In relation to data coverage, the SB is superior to the NB in terms of gravity anomalies. It possesses more observations the distribution of which is more even than the ones of the NB (Figures 5 and 7). However, in terms of vertical deflections, Figures 6 and 8 show that the NB is superior to the SB as related to both amount and distribution of data.

Furthermore, both the terrain and the data coverage vary significantly within blocks. Therefore, in order to understand the performance of each method better, the area was divided into eight 0°.5x0°.5 sub-blocks (hereafter to be referred to as "the 0°.5 blocks" or simply "blocks") following Kearsley et al. [1985, p.61]. The eight 0°.5 blocks are shown in Figure 25.

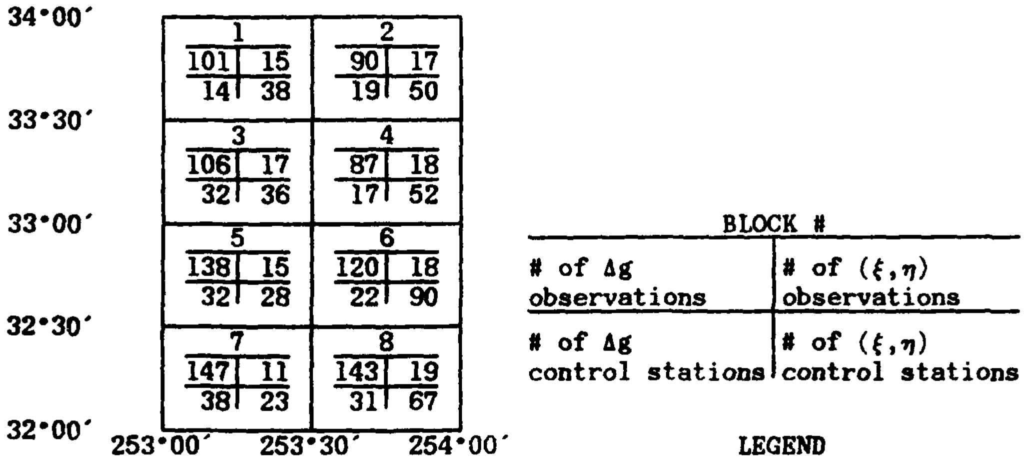

Figure 25. The eight 0°.5 blocks used to test the performance of the two predictors at the White Sands Test Area.

The "goodness of representation" factor R can be defined as follows [Kearsley et al., 1985, p.63]

$$R = 10^{-3} C \sigma_H \qquad (5\text{-}1)$$

where σ_H is the RMS height variation with respect to the mean elevation of the area and C in km²/station is the average coverage of the area defined as

$$C = \frac{A}{n} \qquad (5\text{-}2)$$

where A is the area and n is the number of stations in A.

A large R value indicates either few observations or highly varying terrain or both. It is essential to realize that R is a relative quantity for intercomparison of the eight 0°.5 blocks. This is to say that an R value of 10 for the observed deflections represents a good sub-block whereas it may represent a very poor sub-block in terms of gravity control stations. As a specific example, block #8 with $R_{\Delta g} = 6.1$ for the control stations is considered as representing the area well whereas blocks #2 and 3 with $R_{\Delta g}$ equal to 5.7 and 5.3 respectively for the observation stations is considered as representing the area poorly. The following table shows these details by sub-block. In this table P stands for Poor, M for Medium and G for Good sub-blocks.

Table 3. Terrain Characteristics and Data Coverage in the Test Area.

BLOCK #	TERRAIN TYPE	σ_H (m)	OBSERVATIONS						CONTROL STATIONS					
			C		R		TYPE		C		R		TYPE	
			Δg	ξ,η	Δg	ξ,η	Δg	ξ,η	Δg	ξ,η	Δg	ξ,η	Δg	ξ,η
1	Hilly → Flat	81	25	171	2.1	13.9	M	M	184	68	14.9	5.5	M	M
2	Mountainous	200	29	151	5.7	30.2	P	M	135	51	27.0	10.3	P	M
3	Mountainous	217	24	152	5.3	33.0	P	M	81	72	17.5	15.6	M	M
4	Hilly → Flat	128	30	144	3.8	18.4	M	M	152	50	19.5	6.4	M	M
5	Mountainous	176	19	173	3.3	30.5	M	M	81	93	14.3	16.3	M	M
6	Hilly → Flat	90	22	144	1.9	13.0	G	M	118	29	10.6	2.6	M	G
7	Hilly → Flat	187	18	238	3.3	44.4	M	P	69	114	12.9	21.2	M	M
8	Hilly → Flat	72	18	138	1.3	9.9	G	G	84	39	6.1	2.8	G	G

Table 3 quantifies the differences by sub-block in terms of both terrain characteristics and data coverage. For example, the difference between the SE 30′x30′ portion of the SB (sub-block #7) and the SW 30′x30′ portion of the SB (sub-block #8) in terms of vertical deflection observations is clearly demonstrated by the $R_{\xi,\eta}$ factors which are 44.4 and 9.9 respectively. From Table 3 one can see that the SB solution should be considered more representative of the capabilities of the method under consideration than the NB one. Furthermore, in terms of gravity anomaly observations, sub-blocks #2 and 3 are not anticipated to contribute greatly to a possible good NB solution, whereas sub-blocks #6 and 8 are capable of being the major contributors to a possible high quality of the SB solution. On the other hand, the gravity anomaly control data coverage in sub-block #2 is poor rendering the comparison of results not very reliable in this block, whereas block #8 is good for this purpose. Also, reliable sub-blocks for vertical deflection comparison in terms of control values are blocks 6 and 8.

In order to evaluate the two predictors the differences

$$\left\{\begin{aligned} d\Delta g &= \Delta g_c - \Delta g_p \\ d\xi &= \xi_c - \xi_p \\ d\eta &= \eta_c - \eta_p \end{aligned}\right\} \qquad (5\text{-}3)$$

will be examined where the subscript c refers to the control values and the subscript p refers to the results of either the Bjerhammar or the Hardy method. The differences in (5-3) are due to errors in the prediction as well as errors in the control data.

5.2 Results of the Bjerhammar Method

5.2.1 Attempts to Compute an Optimal Geosphere Radius from the Data

One of the most important factors influencing the quality of the predictions with the Bjerhammar method is the radius r_0 of the internal sphere. Up to a certain extent r_0 is a coupling factor in the sense that the improvement of the predictions expected by a smooth terrain, by good data coverage and by the removal of reference field and residual terrain model effects can be easily nullified by an unsuccessful choice of r_0. More importantly, an inappropriate choice of r_0 can render the downward continuation impossible. Due to the aforementioned effects of r_0 on the predictions, efforts were made to compute it from the data.

Two methods never before tested with the Bjerhammar predictor were attempted. The first method is the minimum norm (pseudo) solution given by equations (2-67) to (2-70). It was tested in the NB with 384 gravity anomalies as observations. The unknowns were both 384 Dirac Impulses and the optimal radius of the geosphere, a total of 385 unknowns. An approximate value of 6350 km for the optimal radius r_0 resulted after 2 iterations in an adjusted value of 6350 $\pm$ 0.17×10^{-5} km. The residuals were in the order of 10^{-9} mgals, V^TPV was 7×10^{-15} and the standard deviations of the Dirac Impulses exceeded the values of the Impulses. Similar results were attained after two iterations when the approximate value for r_0 was 6360 km. The order of magnitude of the residuals and V^TPV can be explained by the fact that no redundant observations are present in the solution. The large standard deviations of the Impulses stress that the values for the Impulses are evaluated with very large uncertainty. The only peculiar result is the small standard deviation of r_0 even though the adjusted value of r_0 is the same one as the approximate. At any rate this method did not seem to have computed an optimal radius of the geosphere.

The second method to compute r_0 from the data is to separate the observations into two groups and to consider the first group as observed values and the second one as control values. This type of solution is given by equations (2-80) through (2-102). In this case we only have one unknown, namely the optimal geosphere radius r_0 and therefore we have only one normal equation. This method was tested in the NB. The results of the solution (iteration #0) as well as some selected iterations are shown in Table 4. In Table 4, N is the normal matrix (of dimensions (1x1)) and U is the right hand side vector (of dimensions (1x1)) of the normal equations.

Table 4. Data Separation Method of Computing r_0. Bjerhammar Predictor.

ITERATION #	r_0^* (km)	N	U	δr_0(km)	r_0^a (km)
0	6360.000	0.000 015 520	0.045 439 743	-2.928	6357.072
1	6357.072	0.000 007 390	0.031 566 632	-4.272	6352.801
5	6346.544	0.000 001 266	0.002 313 902	-1.827	6344.717
10	6339.725	0.000 000 799	0.000 635 825	-0.816	6338.909
20	6335.527	0.000 000 578	0.000 082 876	-0.143	6335.384
30	6334.783	0.000 000 546	0.000 019 254	-0.035	6334.748
40	6334.576	0.000 000 537	0.000 003 724	-0.007	6334.569
45	6334.549	0.000 000 535	0.000 001 777	-0.003	6334.546
50	6334.536	0.000 000 535	0.000 000 948	-0.002	6334.534
52	6334.533	0.000 000 535	0.000 000 767	-0.001	6334.531
53	6334.531	0.000 000 535	0.000 000 485	-0.001	6334.530

From Table 4 one observes that the iteration criterion, the correction to r_0 be less than 1 m, was met after 53 iterations. Furthermore, the normal matrix stabilizes only at the 45th iteration and the rate at which the correction to r_0 tends to zero is very low. Most importantly, the resulting adjusted value of r_0^a = 6334.530 km yields RMS differences of control minus predicted values in the order of 7.73 mgals for Δg, 20.″53 for ξ and 30.″07 for η. These differences are much larger than the ones yielded with the same data type when an optimal radius was computed prior to the solution as it will be demonstrated in Subsection 5.2.2.1.

The overall conclusion from both of the aforementioned methods is that they did not yield an optimal geosphere radius. Therefore the s^2 method given by (2-103) to (2-108) will be used for optimal geosphere radius computations.

5.2.2 The Asymmetric Kernel Approach

The predictor defined by equations (2-8) through (2-34) is called the Asymmetric Kernel (AK) approach to be distinguished from the Symmetric Kernel (SK) Approach given by (2-35) through (2-42). The Symmetric Kernel Approach is given its name by Bjerhammar [1986, p. 48]. In the SK approach, t in (2-38) is a symmetric quantity, i.e., invariant with respect to i and j. Recall that t of the AK is not symmetric (see equation (2-15)). Furthermore, if the observations are only gravity anomalies, then the design matrix G in (2-43) is symmetric. The Asymmetric Kernel Approach was given this name in this investigation in order to distinguish it from the SK Approach. In what follows the Dirac Impulses will be located at the nadir points of the observations. In the tables that follow the differences in Δg, ξ and η are control minus predicted. The notation $\hat{r}_0^{\Delta g}$, $\hat{r}_0^{\xi}$ and $\hat{r}_0^{\eta}$ will be differences in Δg, ξ and η respectively as s^2 values. On the other hand, $\hat{r}_0$ will be defined as:

$$\hat{r}_0 = \frac{1}{3}\left(\hat{r}_0^{\Delta g} + \hat{r}_0^{\xi} + \hat{r}_0^{\eta}\right) \tag{5-4}$$

Every variation of each predictor will be tested and compared with similar results after the following cycle is completed:

(1) Perform three solutions with three different radii,
(2) Compute $\hat{r}_0^{\Delta g}$, $\hat{r}_0^{\xi}$ and $\hat{r}_0^{\eta}$ by (2-107),
(3) Compute $\hat{r}_0$ by (5-4).
(4) Perform the final solution with $r_0 = \hat{r}_0$.

5.2.2.1 Prediction Using Only Gravity Anomaly Data

In the case where only gravity anomalies are observed the exact solution as given by (2-44) and (2-45) applies. The elements of the design matrix G in (2-44) and (2-45) are given by (2-28). The results of both the NB and the SB solutions with three different radii are shown in Table 5.

Table 5. RMS Differences Between Predicted and Control Values with the Asymmetric Kernel Approach and Only Δg Observed. Bjerhammar Method.

SOLUTION	r_0(km)	Δg(mgal)	ξ(")	η(")
North Block	6355	4.03	0.99	0.99
	6360	3.32	0.91	0.97
	6365	2.96	0.92	1.11
South Block	6355	3.87	1.00	1.17
	6360	3.80	0.92	1.13
	6365	3.89	0.89	1.19

Using the results of Table 5 with the s^2 method (eq. (2-107)) and the RMS differences one gets $\hat{r}_0$ = 6362.571 km for the NB and $\hat{r}_0$ = 6361.562 km for the SB solution. The results of the NB and the SB solutions with $r_0 = \hat{r}_0$ are shown in Table 6.

Table 6. RMS Differences Between Predicted and Control Values with the Asymmetric Kernel, Only Δg Observed and the Optimal Radius of the Geosphere r_o, by 0°.5 Block. Bjerhammar Method.

BLOCK	RMS DIFFERENCES		
SUB-BLOCK	Δg(mgal)	ξ(")	η(")
North	3.08	0.90	1.00
1	4.27	0.91	0.81
2	2.54	0.64	0.99
3	2.84	1.26	0.70
4	2.86	0.81	1.28
South	3.79	0.90	1.13
5	3.43	1.27	1.36
6	6.22	0.94	1.28
7	3.20	0.58	0.75
8	2.23	0.74	0.89

From Table 6 one observes that the best Δg predictions were performed at sub-block #8 and the best ξ and η predictions were performed at sub-block #7.

5.2.2.2 Prediction Using Both Gravity and Vertical Deflection Data

In the case where both Δg and (ξ,η) are observed the least squares solution applies with as many degrees of freedom as deflection pairs. This type of solution is given by (2-46) through (2-48) and the elements of the design matrix G are given by (2-28) for gravity anomaly observations and by (2-32) for vertical deflection observations. The results for three different radii are given in Table 7.

Table 7. RMS Differences Between Predicted and Control Values with the Asymmetric Kernel Approach and Both Δg and (ξ,η) Observed. Bjerhammar Method.

SOLUTION	r_o(km)	Δg(mgal)	ξ(")	η(")
North Block	6355	3.78	0.87	0.73
	6360	3.56	0.78	0.73
	6365	3.76	0.77	0.77
South Block	6360	4.52	0.84	0.92
	6364	4.34	0.82	0.91
	6368	5.59	1.10	1.14

Using the RMS differences of Table 7 in equation (2-107) we obtain $\hat{r}_o$ = 6360.248 km for the NB and $\hat{r}_o$ = 6362.312 km for the SB solution. The results of the NB and the SB solution with $r_o = \hat{r}_o$ are shown in Table 8.

Table 8. RMS Differences Between Predicted and Control Values with the Asymmetric Kernel Approach, Both Δg and (ξ,η) Observed and With the Optimal Radius of the Geosphere, by 0°.5 Block. Bjerhammar Method.

BLOCK	RMS DIFFERENCES		
SUB-BLOCK	Δg(mgal)	ξ(")	η(")
North	3.58	0.77	0.73
1	4.04	0.84	0.58
2	2.54	0.79	0.87
3	3.47	0.91	0.57
4	4.32	0.72	0.77
South	4.54	0.84	0.93
5	3.83	1.26	1.27
6	7.35	0.92	1.04
7	4.01	0.46	0.34
8	2.94	0.54	0.73

From Table 8 one can see that using both Δg and (ξ,η) observations one can predict Δg on the average to about 4 mgals and ξ and η to about 0".8. These results can vary from 2.54 mgals (sub-block #2) to 7.35 mgals (sub-block #6) for Δg, 0".46 (sub-block #7) to 1".26 (sub-block #5) for ξ and 0".34 (sub-block #7) to 1".27 (sub-block #5) for η.

5.2.2.3 Prediction Using Only Vertical Deflection Data

In the case where only vertical deflections are observed the least squares solution applies with as many degrees of freedom as observed deflection pairs. This type of solution is given by (2-46) through (2-48). The elements of the design matrix G are given by (2-32). Results with three radii for both the NB and the SB solutions are given in Table 9.

Table 9. RMS Differences Between Predicted and Control Values with the Asymmetric Kernel Approach and Only (ξ,η) Observed. Bjerhammar Method.

SOLUTION	r_0(km)	Δg(mgal)	ξ(")	η(")
North Block	6350	18.74	1.16	1.00
	6360	9.01	1.47	1.31
	6365	10.06	1.84	1.84
South Block	6340	58.57	1.18	1.14
	6350	9.46	1.06	0.99
	6360	9.19	1.64	1.19

The RMS differences of Table 9 in (2-107) yield $\hat{r}_0$ = 6354.221 km for the NB and $\hat{r}_0$ = 6350.352 km for the SB solution. Using these $\hat{r}_0$ values one gets the results in Table 10.

Table 10. RMS Differences Between Predicted and Control Values with the Asymmetric Kernel Approach, Only (ξ,η) Observed and With the Optimal Radius of the Geosphere. Bjerhammar Method.

BLOCK	RMS DIFFERENCES		
SUB-BLOCK	Δg(mgal)	$\xi('')$	$\eta('')$
North	13.19	1.25	1.06
1	11.98	1.06	0.91
2	8.15	0.76	0.74
3	16.00	1.00	0.80
4	12.85	1.79	1.50
South	9.19	1.08	0.99
5	10.62	1.58	1.25
6	7.34	1.11	0.89
7	10.20	1.00	1.35
8	7.25	0.75	0.85

From Table 10 one can see poor Δg predictions. On the other hand ξ was predicted to about 1".17 and η to about 1".03 on the average, with variations from 0".75 to 1".79 for ξ and 0".74 to 1".50 for η.

5.2.3 The Symmetric Kernel Approach

In this series of tests with the SK approach the Dirac Impulses will be located at the nadir points of the observations. Also, the optimal geosphere radius will be computed via (5-4) in order to use it for the final solution as described in Section 5.2.2.

5.2.3.1 Prediction Using Only Gravity Anomaly Data

In this case the exact solution as described by (2-44) and (2-45) applies. The elements of the design matrix G are given by (2-41). The results of both the NB and the SB solutions with three different radii are shown in Table 11.

Using the RMS differences of Table 11 in equation (2-107) one obtains $\hat{r}_0$ = 6366.339 km for the NB and $\hat{r}_0$ = 6365.267 km for the SB solution. The results of the NB and the SB solutions with $r_0 = \hat{r}_0$ are shown in Table 12.

Table 11. RMS Differences Between Predicted and Control Values with the Symmetric Kernel Approach and Only Δg Observed. Bjerhammar Method.

SOLUTION	r_0(km)	Δg(mgal)	ξ(")	η(")
North Block	6360	5.31	2.03	1.42
	6365	3.62	0.95	0.96
	6370	3.59	1.11	1.61
South Block	6360	4.00	1.84	1.67
	6365	3.82	0.95	1.13
	6370	4.78	0.99	1.58

Table 12. RMS Differences Between Predicted and Control Values with the Symmetric Kernel Approach, Only Δg Observed and the Optimal Radius of the Geosphere $\hat{r}_0$. Bjerhammar Method.

BLOCK	RMS DIFFERENCES		
SUB-BLOCK	Δg(mgal)	ξ(")	η(")
North	3.29	0.92	0.97
1	4.47	0.88	0.82
2	2.56	0.66	1.00
3	3.03	1.32	0.75
4	3.33	0.80	1.15
South	3.81	0.94	1.13
5	3.57	1.36	1.44
6	5.97	0.96	1.23
7	3.30	0.58	0.79
8	2.44	0.78	0.92

In this case one can see in Table 12 that the good sub-block #8 in the sense of Table 3 gave the best Δg predictions whereas the best ξ and η predictions were performed at sub-block #7. Overall, with only Δg observations the SK approach on the average predicted Δg to about 3.6 mgals, ξ to about 0".9 and η to about 1".05.

5.2.3.2 Prediction Using Both Gravity and Vertical Deflection Data

In the event that both Δg and (ξ,η) are observed the least-squares solution given by (2-46) to (2-48) applies, and one has as many degrees of freedom as observed deflection pairs. The elements of the design matrix G are given by (2-41) for Δg observations and by (2-42) for (ξ,η) observations. Table 13 shows the results for this case with three different radii.

Table 13. RMS Differences Between Predicted and Control Values with the Symmetric Kernel Approach and Both Δg and (ξ,η) Observed. Bjerhammar Method.

SOLUTION	r_0(km)	Δg(mgal)	ξ(")	η(")
North Block	6363	3.29	0.86	0.72
	6365	3.38	0.81	0.72
	6367	3.67	0.72	0.70
South Block	6365	4.31	0.88	0.89
	6367	4.55	0.84	0.93
	6369	4.20	0.82	0.91

The application of (2-107) and (5-4) with the results of Table 13 yielded $\hat{r}_0$ = 6362.867 km for the NB and $\hat{r}_0$ = 6368.049 km for the SB solution. The results of the NB and SB solutions with $r_0 = \hat{r}_0$ are shown in Table 14.

Table 14. RMS Differences Between Predicted and Control Values with the Symmetric Kernel, Both Δg and (ξ,η) Observed and the Optimal Radius of the Geosphere $\hat{r}_0$. Bjerhammar Method.

BLOCK	RMS DIFFERENCES		
SUB-BLOCK	Δg(mgal)	ξ(")	η(")
North	3.26	0.87	0.72
1	3.90	0.67	0.54
2	2.49	0.77	0.71
3	3.25	1.15	0.83
4	3.45	0.85	0.75
South	4.33	0.82	0.91
5	3.58	1.23	1.23
6	7.01	0.90	1.01
7	3.83	0.48	0.37
8	2.85	0.52	0.72

From Table 14 one observes Δg to be predicted to about 3.5 mgals, ξ to about 0."85 and η to about 0."8 on the average.

5.2.3.3 Prediction Using Only Vertical Deflection Data

When only vertical deflections are observed the least-squares solution applies with as many degrees of freedom as observed (ξ,η) pairs. This type of solution is given by (2-46) to (2-48) and the elements of the design matrix G are given by (2-42). Both the NB and the SB solutions with three different radii are shown in Table 15.

Table 15. RMS Differences Between Predicted and Control Values with the Symmetric Kernel Approach and Only (ξ,η) Observed. Bjerhammar Method.

SOLUTION	r_0(km)	Δg(mgal)	$\xi('')$	$\eta('')$
North Block	6355	50.88	1.04	1.03
	6360	22.98	1.12	1.00
	6365	10.19	1.36	1.18
South Block	6355	93.96	1.31	1.23
	6360	13.05	0.97	0.99
	6365	8.38	1.48	1.12

Using the RMS differences of Table 15 in (2-107) yields $\hat{r}_0$ = 6359.982 km for the NB and $\hat{r}_0$ = 6361.017 km for the SB solution. The NB and SB solutions with these optimal radii are shown in Table 16.

Table 16. RMS Differences Between Predicted and Control Values with the Symmetric Kernel, Only (ξ,η) Observed and $r_0 = \hat{r}_0$. Bjerhammar Method.

BLOCK	RMS DIFFERENCES		
SUB-BLOCK	Δg(mgal)	$\xi('')$	$\eta('')$
North	23.05	1.12	1.00
1	20.82	0.97	1.08
2	17.16	0.79	0.74
3	27.34	0.99	0.77
4	21.65	1.51	1.25
South	9.84	1.05	0.99
5	11.35	1.53	1.22
6	8.25	1.08	0.90
7	10.69	1.01	1.33
8	7.93	0.73	0.86

From Table 16 one can see that Δg were poorly predicted with only (ξ,η) observations. Also, the best ξ predictions were performed at sub-block #8 whereas sub-block #2 yielded the best η predictions.

5.2.4 Comments on the Results of the Asymmetric and Symmetric Kernel Approaches

Comparison of Tables 6 and 8 shows that in the AK approach when (ξ,η) observations are introduced vertical deflection predictions are improved by about $0.''3$, whereas the gravity anomaly predictions were downgraded by about 0.6 mgals. Furthermore, inspection of Tables 12 and 14 yields very similar comparison for the SK approach for the introduction of (ξ,η) observations.

Comparison of Tables 8 and 10 for the AK and 14 and 16 for the SK approach demonstrates deterioration of both the Δg and the (ξ,η) predictions when no Δg observations are used.

Comparison of Tables 6 to 12, 8 to 14 and 10 to 16 shows that the results of the predictions with the AK and the SK approaches are practically identical. Actually, the only difference in the two approaches is the radius that yielded the optimal results. Table 17 shows the optimal radii for the two approaches.

Table 17. Optimal Radii in km for the AK and the SK Approaches in Both the NB and the SB Solutions with Different Observation Types. Bjerhammar Method.

Type of Observations	Optimal radius r_0 (km) Asymmetric Kernel		Optimal radius r_0 (km) Symmetric Kernel	
	North Block	South Block	North Block	South Block
Δg	6362.571	6361.562	6366.339	6365.267
Δg and (ξ,η)	6360.248	6362.312	6362.867	6368.049
(ξ,η)	6354.221	6350.352	6359.982	6361.017

From Table 17 one can see that larger radii yield the optimal results in the SK than in the AK approach.

5.2.5 Dirac Impulses on a Grid

Up to this point the Dirac Impulses were located at the nadir points of the observations. However, one potential location for the Impulses is on a grid at the surface of the geosphere. In this case it holds that r_i in (2-38) is equal to r_0 and therefore t is the same for both the AK and the SK approach. Consequently their respective formulae namely (2-28) and (2-41) for Δg and (2-32) and (2-42) for (ξ,η) become identical. This scheme of computing Δg^* on a grid was tested for four different grid sizes for both the NB and the SB. The grids were selected with two considerations in mind. The first one was to have integer minutes in the mesh size. The second one was to have less number of grid vertices (unknowns) than observations so that the least squares solution as given by (2-46) to (2-48) be applicable. Also, it should be kept in mind that very coarse grids are not desirable since information that exists on the data cannot be transferred to Δg^* values and the resulting predictions become inaccurate. The selected grids are shown in Table 18.

Table 18. Details of the Four Grids Used at the White Sands Test Area.

GRID	GRID CELL SIZE	# OF VERTICES IN ϕ DIRECTION	# OF VERTICES IN λ DIRECTION	TOTAL # OF VERTICES
1	6′x4′	15	22	330
2	6′x6′	15	15	225
3	7′x7′	13	13	169
4	12′x12′	8	8	64

The grids of Table 18 were used in two cases. One with only Δg observations and one with both Δg and (ξ,η) observations. In the case of only (ξ,η) observations two grids were used. The criteria were the same as the ones in the selection of the grids of Table 18. The first grid had a grid cell size of 7′x12′ with 13 and 8 vertices in the latitude and longitude directions respectively and a total of 104 vertices. The second grid was identical to grid #4 of Table 18. The computational scheme will be to use three arbitrary values for r_0 and record the resulting RMS differences of control minus predicted values for Δg, ξ and η. Subsequently, these values will be used in conjunction with (2-107) and (5-2) to yield the optimal geosphere radius. The optimal radius of the geosphere is used in the final solution.

5.2.5.1 Prediction Using Only Gravity Anomaly Data

In this case, the elements of the design matrix G are given by either (2-28) or (2-41). The results of both the NB and the SB solutions are shown in Table 19.

Table 19. RMS Differences Between Predicted and Control Values with the Four Grids and Only Δg Observed. Bjerhammar Method.

Optimal	NORTH BLOCK			GRID	Optimal	SOUTH BLOCK		
radius(km)	Δg(mgal)	ξ(")	η(")	#	radius(km)	Δg(mgal)	ξ(")	η(")
6347.269	8.86	6.07	10.69	1	6353.852	4.38	0.93	1.20
6348.500	3.21	1.55	1.69	2	6351.250	4.39	0.87	1.10
6342.500	3.41	0.94	1.24	3	6351.250	4.82	0.80	1.08
6330.576	4.85	0.77	1.01	4	6347.500	6.49	0.83	1.49

From Table 19 one can see that gravity anomaly predictions are best performed with grid #2. Furthermore, the best (ξ,η) predictions were performed with grid #4 for the NB and with grid #3 for the SB. Most importantly, with gravity data alone, the downward continuation on a grid can yield similar results to the ones obtained with the downward continuation to the nadir points of the observations (compare with results of Tables 6 and 12).

5.2.5.2 Prediction Using Both Gravity and Vertical Deflection Data

In this case the elements of the design matrix G are given by either (2-28) and (2-32) or (2-41) and (2-42). The results of both the NB and the SB solutions with the four grids of Table 18 are shown in Table 20.

Table 20. RMS Differences Between Predicted and Control Values with the Four Grids and Both Δg and (ξ,η) Observed. Bjerhammar Method.

Optimal radius(km)	NORTH BLOCK Δg(mgal)	$\xi('')$	$\eta('')$	GRID #	Optimal radius(km)	SOUTH BLOCK Δg(mgal)	$\xi('')$	$\eta('')$
6356.389	3.49	0.71	0.75	1	6350.143	3.57	0.64	0.73
6349.166	3.18	0.68	0.61	2	6341.548	3.94	0.63	0.86
6346.167	3.56	0.65	0.65	3	6345.833	4.69	0.62	0.92
6326.624	4.39	0.72	0.89	4	6325.686	6.28	0.80	1.29

From Table 20 one observes that grid #2 yielded the best Δg predictions in the NB whereas grid #1 was the favorite for the SB. As far as the meridional deflection predictions are concerned grid #3 gave the best results. However, in terms of η predictions grid #2 performed best in the NB whereas grid #1 performed best in the SB. Comparing Tables 19 and 20 one sees that the introduction of vertical deflection observations resulted in improved predictions in all cases. Finally, comparison of Table 20 to Tables 8 and 14 reveals slightly better results from the downward continuation onto a grid. However, the downward continuation onto a grid has the drawback of having to try different mesh-sizes in order to get the best predictions, which is impossible in the absence of control data.

5.2.5.3 Prediction Using Only Vertical Deflection Data

For this application the elements of the design matrix G are given by either (2-32) or (2-42). The results of the NB and the SB solutions are shown in Table 21.

Table 21. RMS Differences Between Predicted and Control Values with Two Grids and Only (ξ,η) Observed. Bjerhammar Method.

Optimal radius(km)	NORTH BLOCK Δg(mgal)	$\xi('')$	$\eta('')$	GRID #	Optimal radius(km)	SOUTH BLOCK Δg(mgal)	$\xi('')$	$\eta('')$
6330.232	5424.63	123.57	41.82	1	6347.498	10708.15	293.05	66.84
6347.420	314.77	4.98	3.66	2	6348.443	332.27	7.21	4.33

From Table 21 one observes very poor predictions for both grids with only (ξ,η) observations.

5.2.6 The Best Δg and (ξ,η) Predictions

The best gravity anomaly predictions were obtained with the Asymmetric Kernel (Table 6) approach and with only gravity anomalies as observations. The Dirac Impulses were located on the geosphere at the nadir points of the observations.

Inspecting Table 6 in light of the representation factors of Table 3 we see that even though the SB solution was expected to be better than the NB one this was not the case. Actually they turned out about the same. Furthermore, from Table 3 one sees that sub-block #6 should yield very good predictions, which was not the case as Table 6 shows. Also, even though sub-block #2 is characterized poor in Table 3, it yielded good predictions. These somewhat conflicting results force one to look at the individual results at each station.

Figures 26, 27, 28 and 29 show the differences control minus predicted value for each gravity control station at the four $0^{\circ}.5 \times 0^{\circ}.5$ sub-blocks of the NB and the SB solution respectively in the background of the gravity data. These differences are from the AK approach with only gravity observations and the Dirac Impulses located at the nadir points of the observations. In these Figures the gravity control stations are indicated by x and the convention is that a bar above the x indicates a positive difference whereas a bar below the x indicates a negative difference.

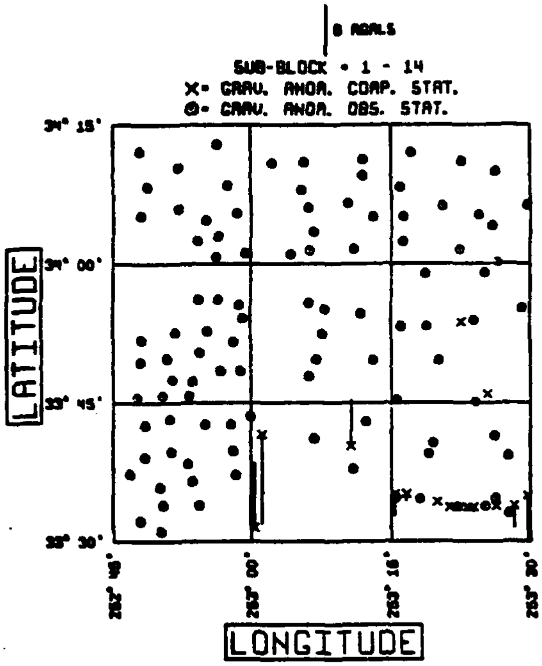

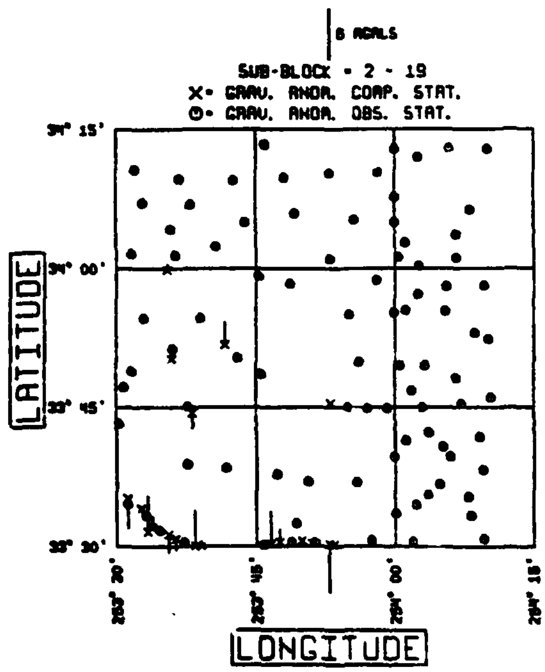

Figure 26. Comparison by Station of Control and Bjerhammar-Predicted Gravity Anomalies at the North Block of the Test Area. Sub-blocks #1 and 2.

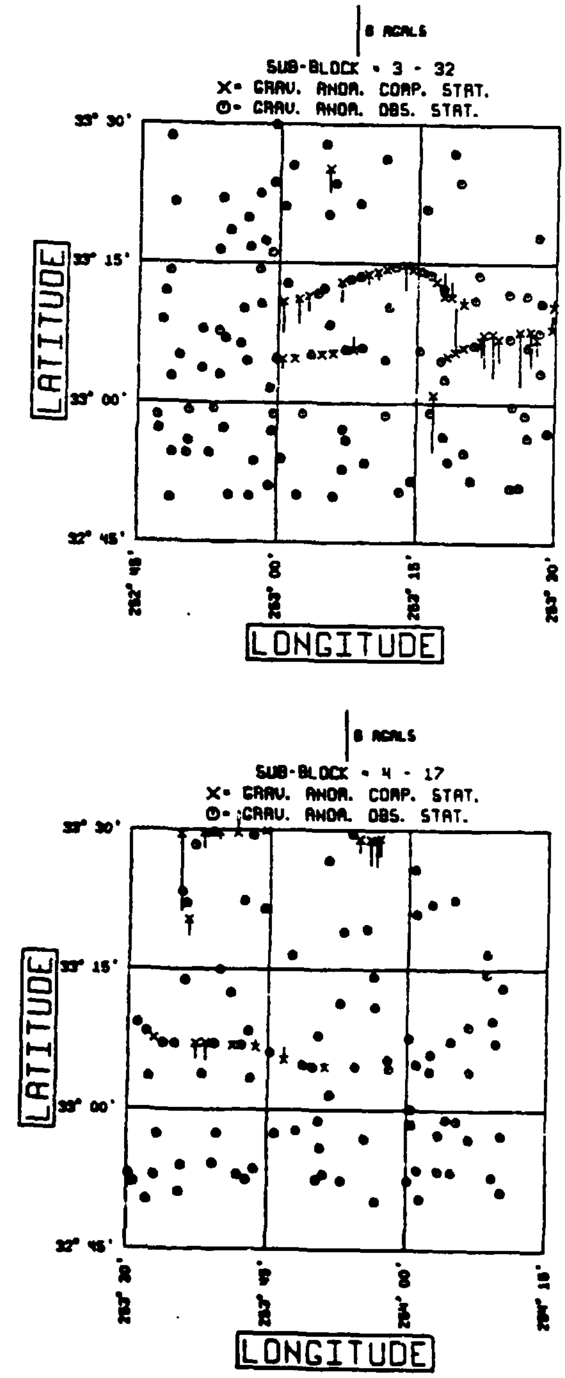

Figure 27. Comparison by Station of Control and Bjerhammar-Predicted Gravity Anomalies at the North Block of the Test Area. Sub-blocks #3 and 4.

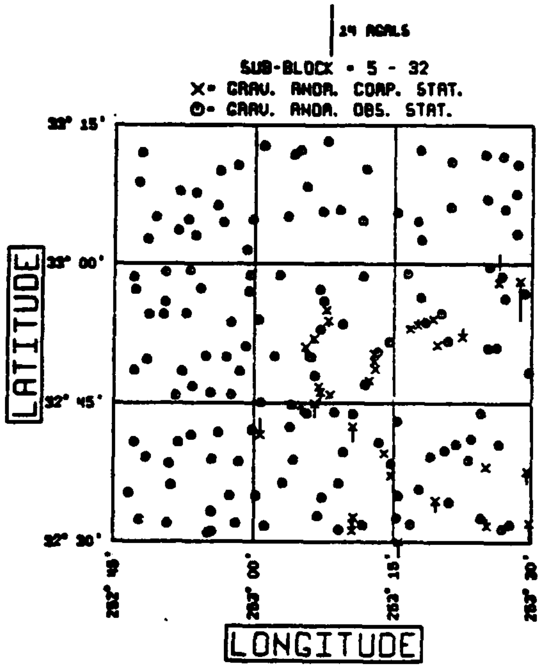

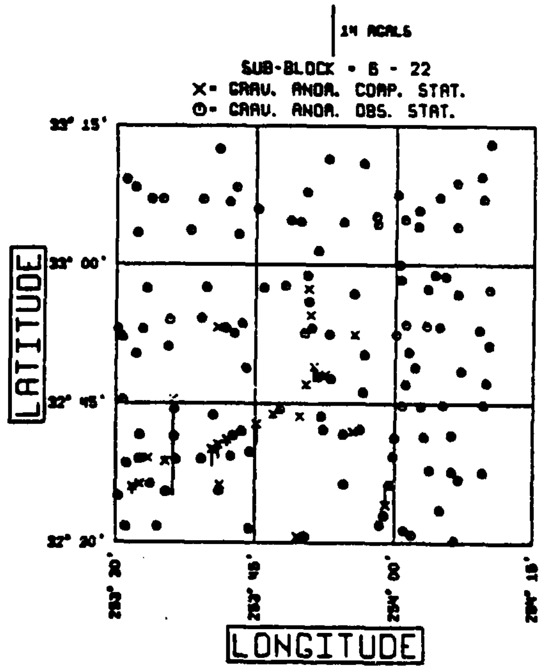

Figure 28. Comparison by Station of Control and Bjerhammar-Predicted Gravity Anomalies at the South Block of the Test Area. Sub-blocks #5 and 6.

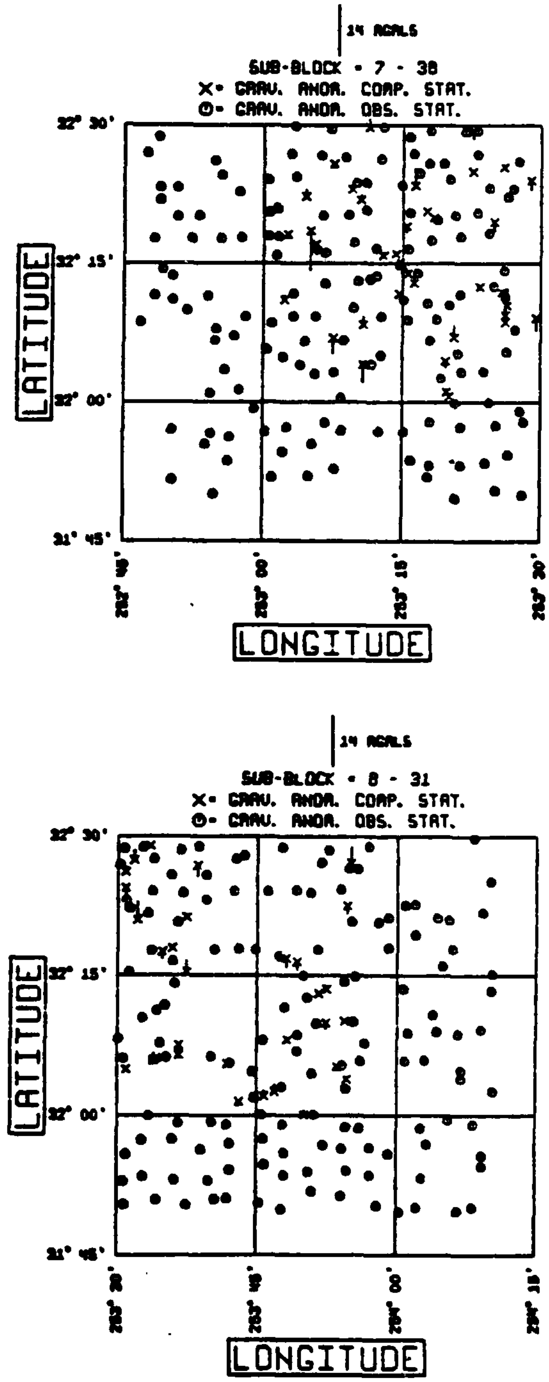

Figure 29. Comparison by Station of Control and Bjerhammar-Predicted Gravity Anomalies at the South Block of the Test Area. Sub-blocks #7 and 8.

Figures 26, 27, 28 and 29 indicate that the majority of the large differences occur at areas with insufficient data coverage. However, there are exceptions. For example, in block #2, station #7778 has a difference of -5.85 mgals whereas for station #7777 this difference is -0.08 mgals and these stations are only about 700 m apart. Similarly, in block #3, station #6717 which is between stations 6716 and 6718 and only a few km away from either one has a differences of 5.35 mgals whereas the other two stations have differences of 0.22 mgals and -0.32 mgals respectively. Also, Figures 26, 27, 28 and 29 demonstrate that the method can operate fairly well in clusters provided sufficient data coverage is present.

As far as the vertical deflection predictions are concerned, the best results were obtained when both gravity and deflection observations were included. The Dirac Impulses were located on grid #3 on the geosphere (Table 20). The results of this solution, by (0.°5x0.°5) sub-block are given in Table 22.

Table 22. RMS Differences Between Predicted with Δg and (ξ,η) Observed and the Optimal Radius of the Geosphere r_0. Dirac Impulses on Grid #3. Bjerhammar Method.

BLOCK	RMS DIFFERENCES		
SUB-BLOCK	Δg(mgal)	ξ(")	η(")
North	3.56	0.65	0.65
1	4.07	0.66	0.54
2	3.16	0.63	0.75
3	3.03	0.83	0.44
4	4.34	0.49	0.75
South	4.69	0.62	0.92
5	4.30	0.57	0.89
6	4.06	0.70	0.80
7	6.25	0.59	1.03
8	2.90	0.51	1.04

The results of Table 22 in light of Table 3 are conflicting in this case also. For example the "Medium" sub-block #4 yielded the best meridional deflection predictions and the prime vertical deflection predictions of the "Good" sub-block #8 were the worst η predictions. However, the "Good" sub-block #8 yielded the best gravity anomaly predictions and the second best meridional deflection predictions. Figures 30, 31, 32 and 33 show the differences control minus predicted value for each vertical deflection control station at the four 0.°5x0.°5 sub-blocks of the NB and the SB solution in the background of the gravity observations. These differences are from the solution where both Δg and (ξ,η) were observed and the Dirac Impulses were located on grid #3 at the surface of the geosphere. In these Figures the vertical deflection control stations are indicated by x and the convention is that a bar above the x indicates a positive difference in ξ, a bar to the

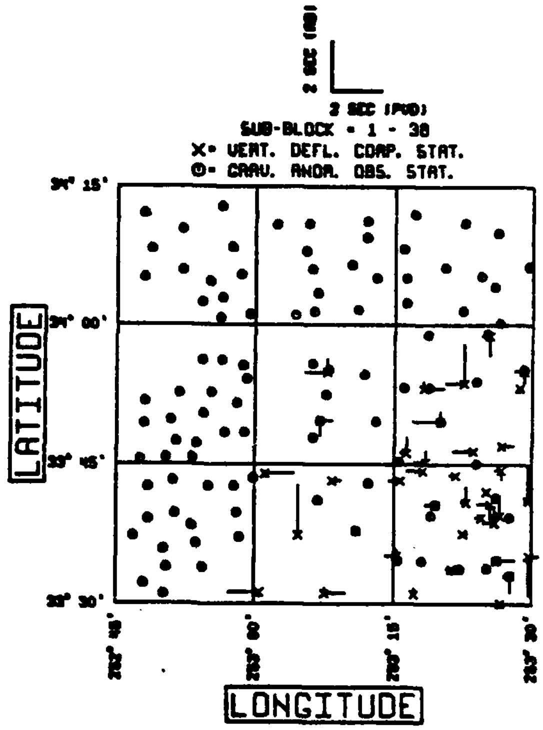

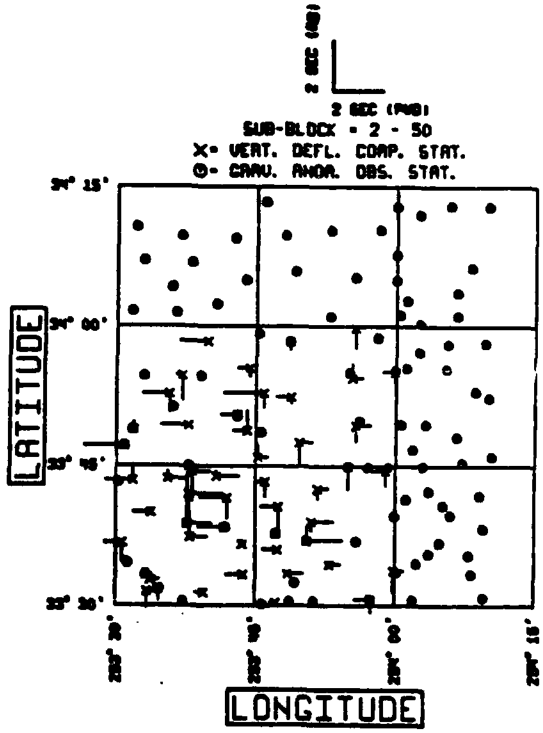

Figure 30. Comparison by Station of Control and Bjerhammar-Predicted Deflections of the Vertical at the North Block of the Test Area. Sub-blocks #1 and 2.

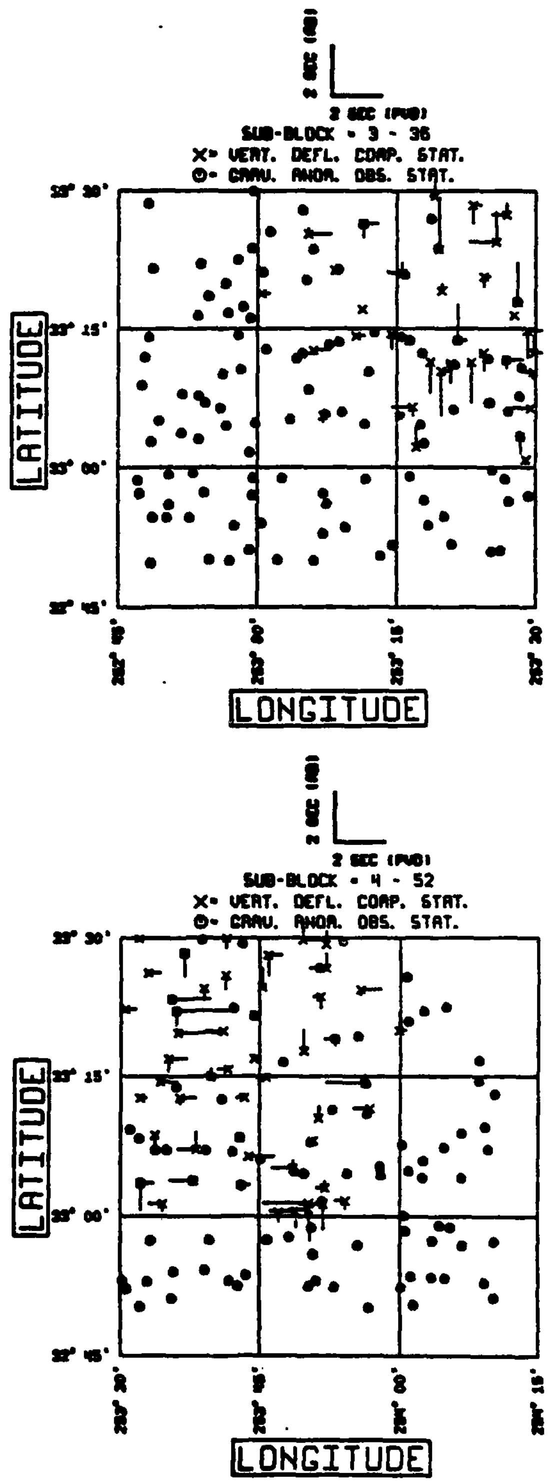

Figure 31. Comparison by Station of Control and Bjerhammar-Predicted Deflections of the Vertical of the North Block of the Test Area. Sub-blocks #3 and 4.

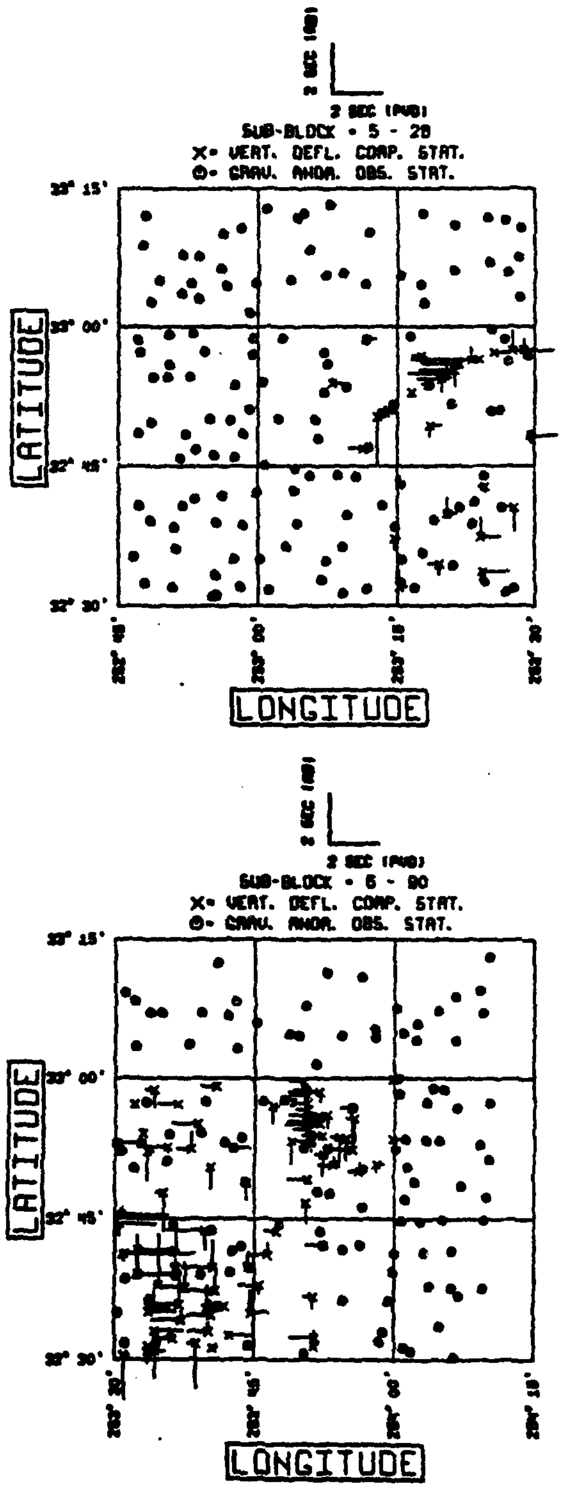

Figure 32. Comparison by Station of Control and Bjerhammar-Predicted Deflections of the Vertical at the South Block of the Test Area. Sub-blocks #5 and 6.

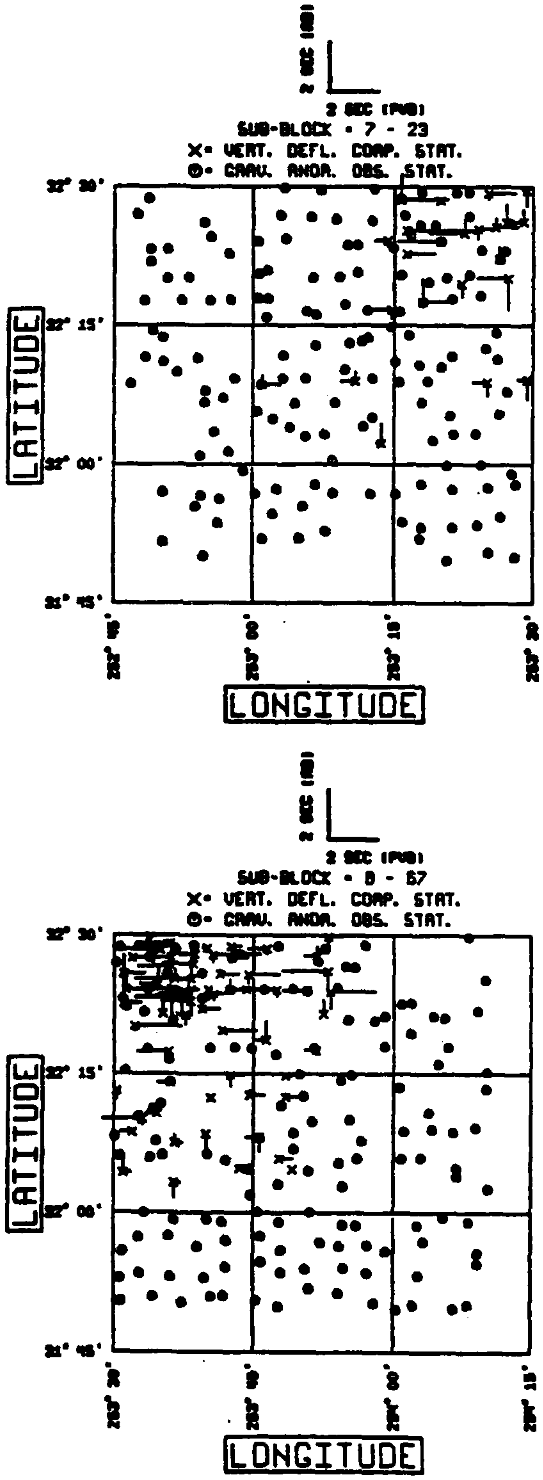

Figure 33. Comparison by Station of Control and Bjerhammar-Predicted Deflections of the Vertical at the South Block of the Test Area. Sub-blocks #7 and 8.

right indicates a positive η difference whereas a bar below x indicates a negative difference in ξ and a bar to the left indicates a negative difference in η.

Figures 30 through 33 illustrate that the majority of the large discrepancies between control and predicted values occur at areas poor in data coverage and rich in terrain variations. For example the hilly to flat sub-block #8 with good Δg and (ξ,η) observation coverage yielded the best Δg and second best ξ predictions. Moreover, in the "poor" sub-block #2, station 358 had ξ predicted within $0\overset{''}{.}1$ and η within $0\overset{''}{.}2$ due to the presence of gravity observation stations 7800, 7801 and 7802.

5.2.7 Errors of Predictions

In the solution with optimal radius of the geosphere for each variation of the predictor the standard deviations of the predicted values were computed according to (2-57). A close inspection of these standard deviations indicates that they cannot be considered a safe indicator of the quality of the predictions. This is to say that many poorly predicted quantities are associated with small standard deviations and many very well predicted quantities are associated with large standard deviations.

5.2.8 Conclusions from the Bjerhammar Predictor

At first the optimal radius r_0 of the geosphere could not be computed from the data. The results of two methods to perform this computations were discouraging. Therefore the s^2 method was used at which the RMS discrepancies (control minus predicted) in Δg, ξ and η were considered a second order polynomial in r_0.

If gravity predictions are required, then use only gravity data and position the Dirac Impulses at the nadir points of the observations. It is not significant whether the Asymmetric or the Symmetric Kernel is used in terms of the quality of the predictions. The only requirement to get the same prediction quality from both the AK and the SK is to associate the AK with radii about 6362 km and the SK with radii about 6366 km. The exact value for the optimal r_0 should be dictated by the specific data set with the s^2 method. In the event that no control data exist in an area, the observations can be separated in two groups, one of which will play the role of observations and the other one the role of control data so that an optimal r_0 can be computed by the s^2-method.

If vertical deflection predictions are sought, then include (ξ,η) observations with the gravity data and place the Dirac Impulses on a grid. When performing computations on scalar computers select the grid cell size keeping in mind that finer grids are more CPU time consuming withoug being necessarily more accurate. In the event that a super-computer is available, the grid cell size may not introduce a problem in terms of CPU time. This is the case with the Cray X-MP/24 which was used for our solutions. As for the grid size, the White Sands Test Area seems to indicate that it can be about twice the angular distance between gravity observations. A radius of about 6346 km yielded optimal results.

As far as the R factor (eq.(5-1)) is concerned, one may conclude that it is of limited importance. For example, from Table 22 one can see that the "Medium" sub-block #4 (see Table 3) yielded the best ξ predictions, the "Good" sub-block #8 yielded the worst η predictions, even though the "Good" sub-block #8 yielded the best Δg predictions and the "Poor" sub-block #7 yielded very poor η predictions.

For terrain height variations from the mean height of 70 m to 220 m, gravity data density of 20 to 30 km^2 per station and standard deviations of the data in the order of 2 mgals, the method can predict Δg within 4 mgals and (ξ,η) within 1". If vertical deflection observations as dense as 140 to 240 km^2 per station and as accurate as $0\overset{''}{.}3$ are added, then vertical deflections can be predicted to $0\overset{''}{.}7$ or better.

5.3 Results of the Hardy Method

5.3.1 Tests of Optimal Geosphere Radius Computation

The radius of the internal sphere is as important with Hardy's predictor as it is with Bjerhammar's predictor. The coupling effect of r_0 mentioned in subsection 5.2.1 is present here also. Therefore an optimal value for the radius was attempted to be computed from the data with this predictor as well.

The same two methods tested with the Bjerhammar predictor were tested with the Hardy predictor also. The first one was to use 384 Δg observations in the NB and solve for 384 biharmonic sources c_i plus the radius r_0 of the geosphere. An approximate value of 6350 for r_0 resulted after 4 iterations in an adjusted value of 6381585.4 $\pm$ 11.4 m. The residuals were in the order of 10^{-6} mgals; V^TPV was 10^{-9} and the standard deviations of the biharmonic sources c_i were larger than the c_i values. An approximate value of 6360 km for r_0 resulted after 10 iterations in an adjusted value of 6359324.1 $\pm$ 1018.1 m. The residuals were of the order of 10^{-3} mgals, V^TPV was 10^{-4} and the standard deviations of c_i were larger than the c_i values. The order of magnitude of the residuals and of V^TPV can be explained by the absence of redundant observations. The large standard deviations of the c_i values as well as the standard deviation of the adjusted r_0 simply stress that the resulted adjusted values have not been accurately determined. From the above results one cannot conclude in favor of a meaningful r_0 computation.

The second attempt was the data separation method (equation (2-80) through (2-102)). The method was tested in the NB and the results of the solution (iteration #0) as well as the six iterations required for convergence are shown in Table 23. In Table 23, N is the normal matrix (of dimensions (1x1)) and U is the right hand side vector (of dimensions (1x1)) of the normal equations.

Table 23. Data Separation Method of Computing r_0. Hardy Method.

ITERA-TION #	r_0^0 (km)	N	U	δr_0(km)	$\hat{r}_0$ (km)
0	6360.000	0.000 006 657	0.009 826 926	-1.476	6358.524
1	6358.524	0.000 005 277	-0.011 218 644	2.126	6360.650
2	6360.650	0.000 004 396	-0.024 550 281	5.585	6366.235
3	6366.235	0.000 027 438	-0.148 932 793	5.428	6371.663
4	6371.663	0.085 465 724	-38.874 943 956	0.455	6372.118
5	6372.118	1.708 862 581	-160.625 401 236	0.094	6372.212
6	6372.212	415.993 395 432	-106.240 406 225	0.000	6372.212

The adjustment yielded $\hat{r}_0$ = 6372.212 ± 5x10^{-5} km. Also, it yielded V^TPV = 5x10^4 and $\hat{\sigma}_0$ = 11.7. From Table 23 one observes that, after the second iteration, both N and U are increasing in absolute value. However, the correction δr_0 tends to zero after the third iteration. The adjusted value of the internal sphere was greater than the mean Earth radius of 6371 km. Using $r_0 = \hat{r}_0$ = 6372.212 km resulted in RMS discrepancies control minus predicted of 17.37 mgals for Δg, 93.''11 for ξ and 323.''81 for η. Conclusively, neither one of the two methods appears to be able to compute an optimal r_0 value. As a result, the s^2 method should be used for r_0 computations with the Hardy predictor.

5.3.2 Biharmonic Sources at the Nadir Points of the Observations

In this series of tests the biharmonic sources c_i will be located at the nadir points of the observations. The differences in the following tables will be control minus predicted and the s^2 method will be used for optimal r_0 computations. The final solutions for each variation of the method will be performed with the $\hat{r}_0$ value computed from (5-4) based on the RMS differences resulting from solutions with three different radii.

5.3.2.1 Prediction Using Only Gravity Anomaly Data

In the case where only Δg are considered as observations the exact solution applies as given by (2-44) and (2-45). The elements of the design matrix G are given by (3-43). The results from both the NB and the SB solutions with three different radii are shown in Table 24.

Table 24. RMS Differences Between Predicted and Control Values with Only Δg Observed. Hardy Method.

SOLUTION	r_0(km)	Δg(mgal)	ξ(")	η(")
North Block	6355	4.39	8.49	6.59
	6360	3.58	4.72	7.24
	6365	3.03	5.41	13.37
South Block	6355	3.90	2.57	4.43
	6360	3.82	2.57	7.51
	6365	3.75	4.53	15.55

Application of (5-4) with $\hat{r}_0^{g}$, $\hat{r}_0^{\xi}$, $\hat{r}_0^{\eta}$ as computed through (2-107) and the RMS differences of Table 24 yielded $\hat{r}_0$ = 6363.903 km for the NB and $\hat{r}_0$ = 6355.948 km for the SB solution. The NB and SB solutions with $r_0 = \hat{r}_0$ are shown in Table 25.

Table 25. RMS Differences Between Predicted and Control Values with Only Δg Observed and the Optimal Radius of the Geosphere $\hat{r}_0$. Hardy Method.

BLOCK	RMS DIFFERENCES		
SUB-BLOCK	Δg(mgal)	ξ(")	η(")
North	3.13	4.93	11.36
1	4.32	2.86	11.42
2	2.56	6.17	3.95
3	2.88	2.32	18.44
4	2.98	6.00	9.52
South	3.88	2.43	4.77
5	3.73	3.93	7.24
6	5.69	1.49	4.97
7	3.57	1.04	4.18
8	2.63	2.91	3.12

From Table 25 we can see that the NB solution is slightly better than the SB one in terms of gravity predictions. The best Δg predictions were performed in sub-block #2. However, the SB solution is better than the NB one in terms of vertical deflection predictions. The best ξ predictions were performed in sub-block #7 and the best η ones were performed in sub-block #8.

5.3.2.2 Prediction Using Both Gravity and Vertical Deflection Data

In the event that both Δg and (ξ,η) are utilized as observed quantities the least-squares solution applies as given by (2-46) through (2-48) and we have as many degrees of freedom as observed deflection pairs. The elements of the design matrix G are given by (3-43) for Δg observations and by (3-44) for (ξ,η) observations. The solutions for both the NB and the SB with three different radii are shown in Table 26.

Table 26. RMS Differences Between Predicted and Control Values with Both Δg and (ξ,η) Observed. Hardy Method.

SOLUTION	r_0(km)	Δg(mgal)	ξ(")	η(")
North Block	6360	6.88	2.23	2.31
	6365	12.73	2.43	3.09
	6370	20.09	3.15	3.74
South Block	6361	7.57	2.29	2.43
	6365	13.09	4.12	4.17
	6368	18.09	4.83	4.92

Using the results of Table 26 with the s^2 method (equation (2-107)) and the RMS differences we get $\hat{r}_0$ = 6365.402 km for the NB and the $\hat{r}_0$ = 6362.044 km for the SB solution. The $\hat{r}_0$ value for SB resulted in a normal matrix with numerically linearly dependent columns and therefore non-invertible. Alternatively the value of 6361 km was considered optimal for the SB. The results from the NB solution with $r_0 = \hat{r}_0$ and the SB solution for r_0 = 6361 km are shown in Table 27.

Table 27. RMS Differences Between Predicted and Control Values with Both Δg and (ξ,η) Observed, $\hat{r}_0$ = 6362.186 km for the NB and $\hat{r}_0$ 6361 km for the SB solution. Hardy Method.

BLOCK	RMS DIFFERENCES		
SUB-BLOCK	Δg(mgal)	ξ(")	η(")
North	13.37	2.45	3.19
1	9.12	1.65	1.79
2	5.08	2.32	3.10
3	18.55	1.84	2.43
4	10.85	3.29	4.32
South	10.13	3.70	3.11
5	8.00	2.76	1.91
6	13.84	4.85	4.30
7	10.25	1.04	0.75
8	8.73	2.69	1.86

From Table 27 we can see that Δg can be predicted from 5.08 mgals (sub-block #1) to 18.55 mgals (sub-block #3). Also, the RMS discrepancies vary from 1".04 (sub-block #7) to 4".85 (sub-block #6) for ξ and from 0".75 (sub-block #7) to 4".32 (sub-block #4) for η. Not surprisingly, comparison of Tables 25 and 27 reveals that the introduction of vertical deflection observations degrades the gravity predictions whereas it improves vertical deflection predictions.

5.3.2.3 Prediction Using Only Vertical Deflection Data

In the case where only vertical deflections are observed the least-squares solution applies with as many degrees of freedom as deflection pairs. This type of solution is given by (2-46) through (2-48). The elements of the design matrix G are given by (3-44). Results from both the NB and the SB solutions with three different radii are shown in Table 28.

Table 28. RMS Differences Between Predicted and Control Values with Only (ξ,η) Observed. Hardy Method.

SOLUTION	r_0(km)	Δg(mgal)	ξ(")	η(")
North Block	6355	16.33	0.97	0.99
	6360	15.15	1.01	1.01
	6365	15.78	1.07	1.09
South Block	6350	29.57	0.93	1.06
	6355	22.90	0.91	1.01
	6360	22.03	0.99	1.05

The s^2 method of equation (2-107) with the RMS differences of Table 28 yielded $\hat{r}_0$ = 6354.698 km for the NB and $\hat{r}_0$ = 6355.676 km for the SB solution. The NB and SB solutions with $r_0 = \hat{r}_0$ are shown in Table 29.

Table 29. RMS Differences Between Predicted and Control Values with Only (ξ,η) Observed and the Optimal Radius of the Geosphere r_0. Hardy Method.

BLOCK	RMS DIFFERENCES		
SUB-BLOCK	Δg(mgal)	ξ(")	η(")
North	16.48	0.97	0.98
1	11.68	0.87	1.16
2	5.93	0.74	0.77
3	23.62	0.97	0.88
4	10.43	1.20	1.09
South	12.61	0.91	1.01
5	6.49	1.46	1.23
6	20.09	0.80	0.93
7	10.90	0.97	1.37
8	12.46	0.72	0.86

From Table 29 one can see that the best Δg predictions are performed at sub-block #2. Sub-blocks #2, 6 and 8 did well for ξ

predictions as did sub-block #2, 3, 6 and 8 for η. Comparison of Table 29 to Tables 25 and 27 indicates further improvement of the (ξ,η) predictions and deterioration of the Δg predictions from the removal of Δg observations.

5.3.3 Biharmonic Sources on a Grid

Up to this point the biharmonic sources were located at the nadir points of the observations on the internal sphere (see Subsection 5.3.2). In the following sequence of tests the biharmonic sources will be placed on a grid at the surface of the geosphere. The scheme for selecting the grids was the same as previously employed (Subsection 5.2.4); the four grids of Table 18 were used. The computational scheme will be to use three arbitrary values for r_0 and record the resulting RMS differences of control minus predicted values for Δg, ξ and η. Subsequently, these values will be used in conjunction with (2-107) and (5-2) to yield the optimal geosphere radius. The optimal radius of the geosphere is used in the final solution.

5.3.3.1 Prediction Using Only Gravity Anomaly Data

In this case the least-squares solution applies as given by (2-46) to (2-48). The elements of the design matrix G are given by (3-43). The results of the NB and the SB solutions are shown in Table 30.

Table 30. RMS Differences Between Predicted and Control Values with the Four Grids and Only Δg Observed. Hardy Method.

Optimal	NORTH BLOCK			GRID	Optimal	SOUTH BLOCK		
radius(km)	Δg(mgal)	ξ(")	η(")	#	radius(km)	Δg(mgal)	ξ(")	η(")
6356.965	19.80	14.19	23.91	1	6356.973	4.39	2.81	4.06
6354.388	3.21	4.21	8.61	2	6351.499	4.39	2.72	2.81
6351.746	3.37	7.17	5.93	3	6362.912	4.77	3.08	8.07
6342.176	4.91	2.70	2.88	4	6354.502	6.51	3.37	5.15

From Table 30 one sees that grids #2, 3 in the NB and grids #1, 2, 3 in the SB yield satisfactory Δg predictions. However, the vertical deflections were predicted poorly from only gravity anomaly data.

5.3.3.2 Prediction Using Both Gravity and Vertical Deflection Data

Here the least-squares solution applies also. The elements of the design matrix G are given by (3-43) for gravity anomaly and by (3-44) for vertical deflection observations. The results of NB and SB adjustments are shown in Table 31.

Table 31. RMS Differences Between Predicted and Control Values with the Four Grids and Both Δg and (ξ,η) Observed. Hardy Method.

Optimal radius(km)	NORTH BLOCK			GRID #	Optimal radius(km)	SOUTH BLOCK		
	Δg(mgal)	ξ(")	η(")			Δg(mgal)	ξ(")	η(")
6352.264	4.85	1.16	1.39	1	6350.196	4.85	0.87	1.19
6343.865	4.36	0.98	0.86	2	6342.498	4.53	0.79	0.98
6335.444	4.50	0.81	0.77	3	6334.255	5.34	0.69	1.08
6312.865	5.18	0.76	1.09	4	6326.940	6.76	0.93	1.59

From Table 31 one observes that grid #2 is the preferred choice for Δg predictions at both the NB and the SB. However, grid #3 yielded best (ξ,η) for the NB and best ξ for the SB. The best η predictions at the SB were performed using grid #2.

Comparison of Tables 30 and 31 indicates that the introduction of (ξ,η) observations deteriorated the Δg predictions whereas it improved the (ξ,η) predictions.

5.3.3.3 Predictions Using Only Vertical Deflection Data

The two grids of subsection 5.2.4.3 were used in this case. The solution is of the least-squares type, and the elements of the design matrix G are given by (3-44). The results for both the NB and the SB adjustments are shown in Table 32.

Table 32. RMS Differences Between Predicted and Control Values with the Two Grids and Only (ξ,η) Observed. Hardy Method.

Optimal radius(km)	NORTH BLOCK			GRID #	Optimal radius(km)	SOUTH BLOCK		
	Δg(mgal)	ξ(")	η(")			Δg(mgal)	ξ(")	η(")
6177.393	194.41	4.48	5.39	1	6108.834	208.57	3.95	8.25
6328.837	777.24	3.28	3.78	2	6329.203	406.48	4.66	2.05

From Table 32 one sees that gravity anomalies are predicted unacceptably with both grids. Furthermore, the vertical deflection predictions are poor. Also, from Table 32 one sees that the value of the optimal radius of the geosphere for grid #1 is peculiar.

Comparison of Tables 31 and 32 indicates that removal of Δg observations deteriorated both the Δg and the (ξ,η) predictions.

5.3.4 The Best Δg and (ξ,η) Predictions

As far as the gravity anomaly predictions are concerned the best results were obtained using only gravity observations and locating the biharmonic sources at the nadir points of the observations. This solution yielded RMS differences in the order of 4 mgals for gravity anomalies and is shown in Table 25.

Inspecting Table 25, with the representation factor R of Table 3 in mind, we see that block #8 performed well as expected. Also, blocks #2, 3 and 4 performed well even though they were classified as not very good. The "promising" sub-block #6 according to Table 3 yielded the worst results. Figures 34, 35, 36 and 37 show the differences control minus predicted value for each gravity control station at eight $0°.5 \times 0°.5$ sub-blocks. The convention for positive and negative values is the one used in Figures 26, 27, 28 and 29.

The fact that the terrain type and the data coverage influences the predictions greatly is also illustrated in Figures 34 through 37. The problems of stations 7778 and 6717 mentioned at the Bjerhammar method exist with the Hardy predictor. The difference for station #7777 is also 0.10 mgals whereas for 7778 it is -5.69 mgals and the discrepancy for 6717 is 5.27 mgals whereas for 6716 it is 0.14 and for 6718 is -0.26 mgals.

In terms of vertical deflection predictions, the best results were attained when both Δg and (ξ,η) were observed and the biharmonic sources were located on grid #3 at the surface of the geosphere (Table 31). These solutions yielded good Δg predictions also and are shown in Table 33 by $(0°.5 \times 0°.5)$ sub-block.

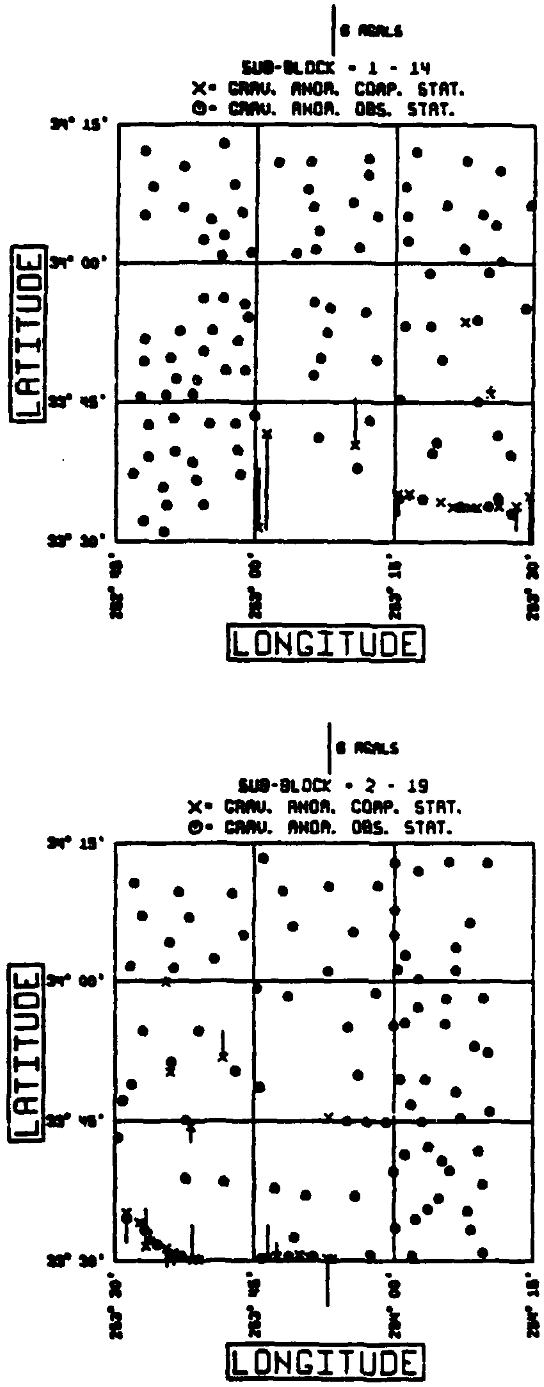

Figure 34. Comparison by Station of Control and Hardy-Predicted Gravity Anomalies at the North Block of the Test Area. Sub-blocks #1 and 2.

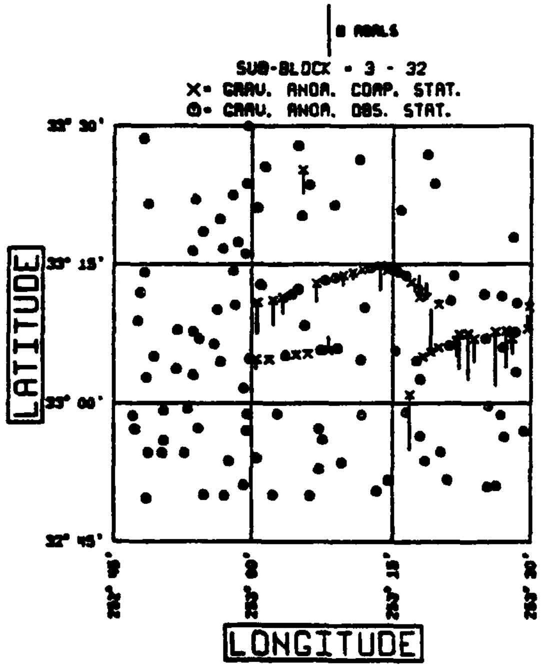

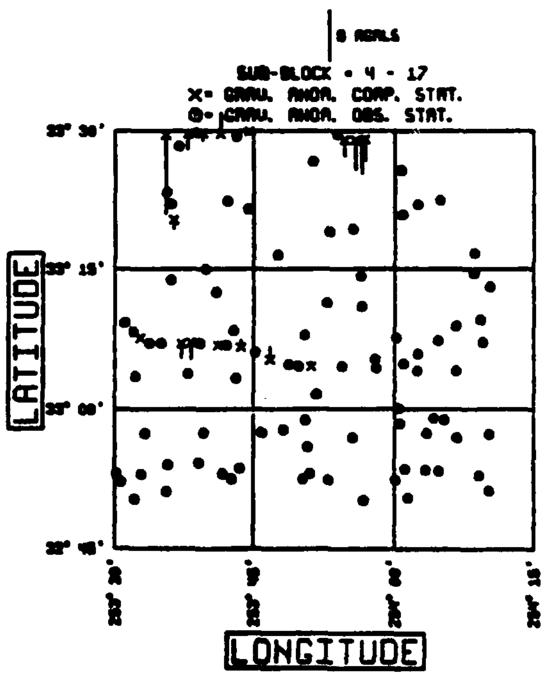

Figure 35. **Comparison by Station of Control and Hardy-Predicted Gravity Anomalies at the North Block of the Test Area. Sub-blocks #3 and 4.**

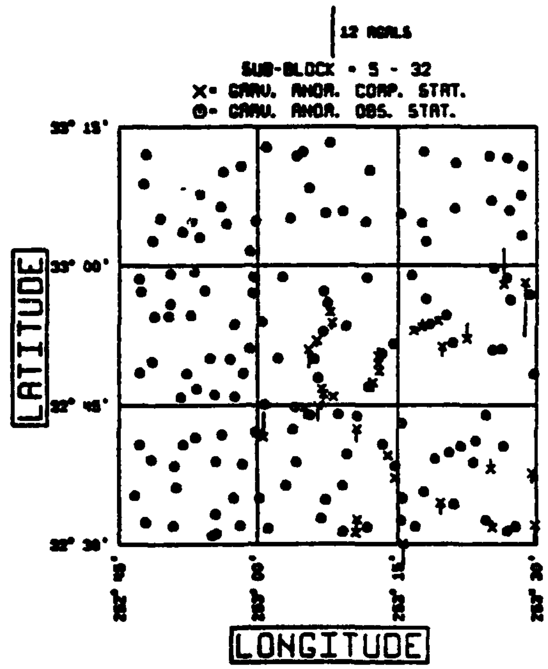

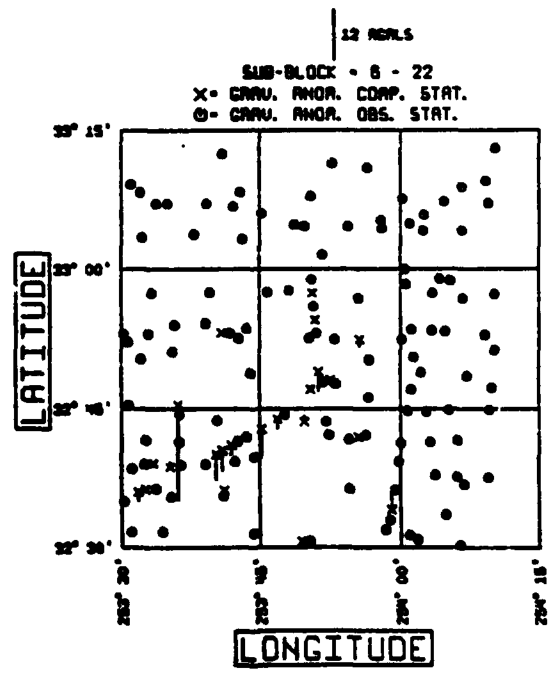

Figure 36. Comparison by Station of Control and Hardy-Predicted Gravity Anomalies at the South Block of the Test Area. Sub-blocks #5 and 6.

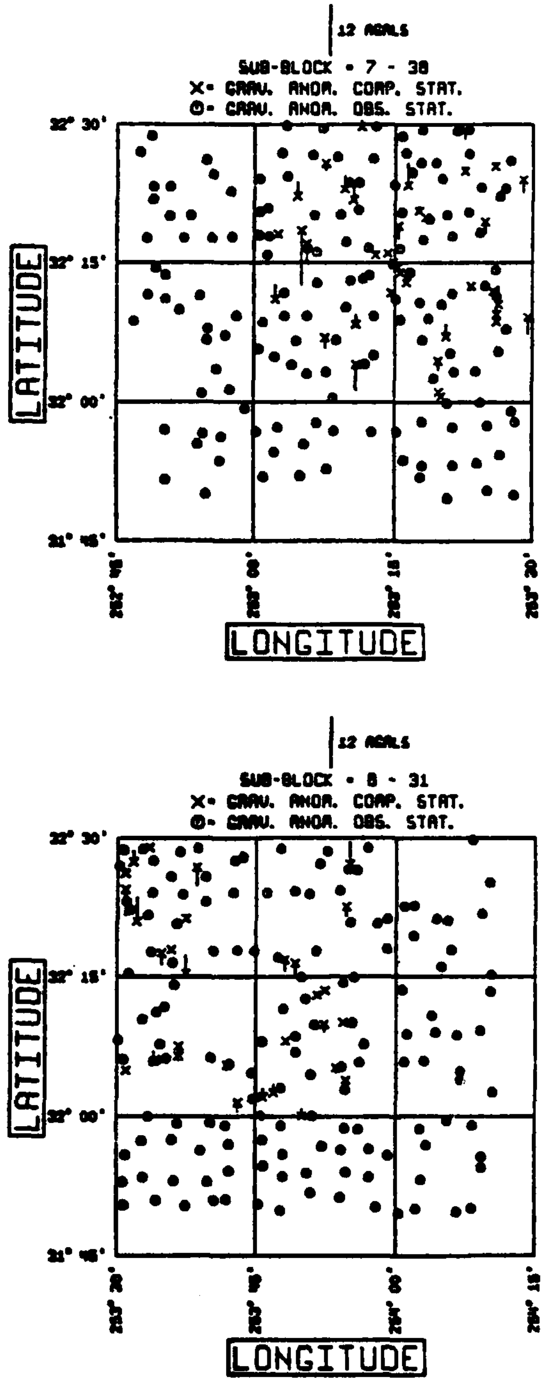

Figure 37. Comparison by Station of Control and Hardy-Predicted Gravity Anomalies at the South Block of the Test Area. Sub-blocks #7 and 8.

Table 33. RMS Differences Between Predicted and Control Values with Δg and (ξ,η) Observed and $r_0 = \hat{r}_0$. Biharmonic Sources on Grid #3. Hardy Method.

BLOCK	RMS DIFFERENCES		
SUB-BLOCK	Δg(mgal)	ξ(")	η(")
North	4.50	0.81	0.77
1	4.56	0.69	0.54
2	3.68	0.62	0.77
3	3.85	1.00	0.93
4	6.14	0.90	0.79
South	5.34	0.69	1.08
5	4.77	0.76	1.18
6	5.03	0.75	0.91
7	7.00	0.69	1.12
8	3.37	0.55	1.23

From Table 33 one can see that the "Good" sub-block #8 yielded the best ξ predictions and the "Medium" sub-block #1 yielded the best η predictions. Most importantly from Table 33 one sees that predictions below the 1" mark can be performed with the Hardy Method. Figures 38, 39, 40 and 41 show the differences control minus predicted value for the eight $0\overset{\circ}{.}5 \times 0\overset{\circ}{.}5$ sub-blocks. The convention for positive and negative differences is the one used in Figures 30, 31, 32 and 33.

Figures 38 through 41 demonstrate that large differences mostly occur at areas rich in terrain variations and poor in data coverage. With the Hardy predictor one observes that sub-blocks #8 and 7 yield the best and worst ξ predictions respectively and that sub-blocks #1 and 8 yield the best and worst η predictions respectively.

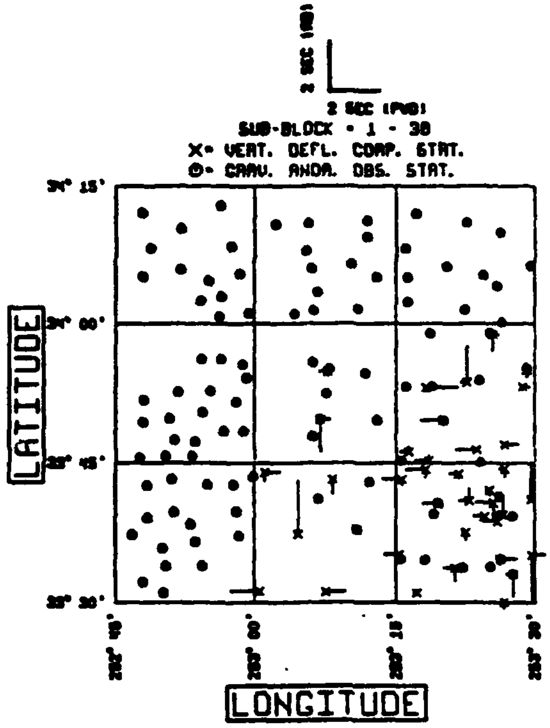

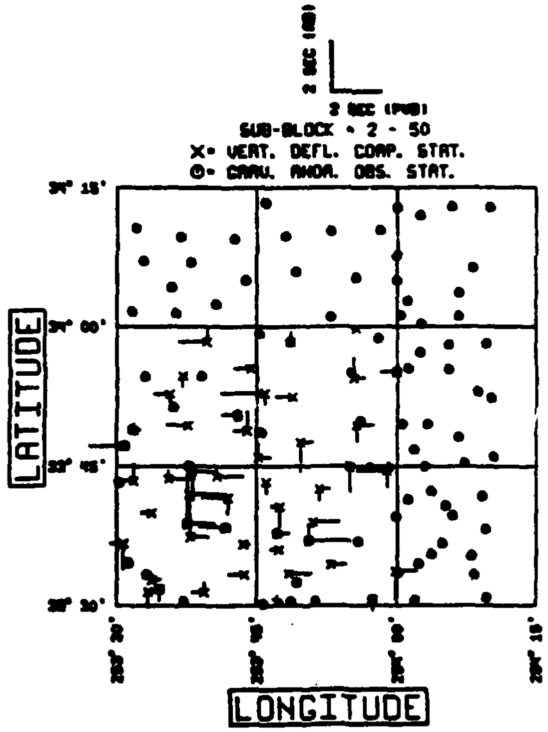

Figure 38. Comparison by Station of Control and Hardy-Predicted Vertical Deflections at the North Block of the Test Area. Sub-blocks #1 and 2.

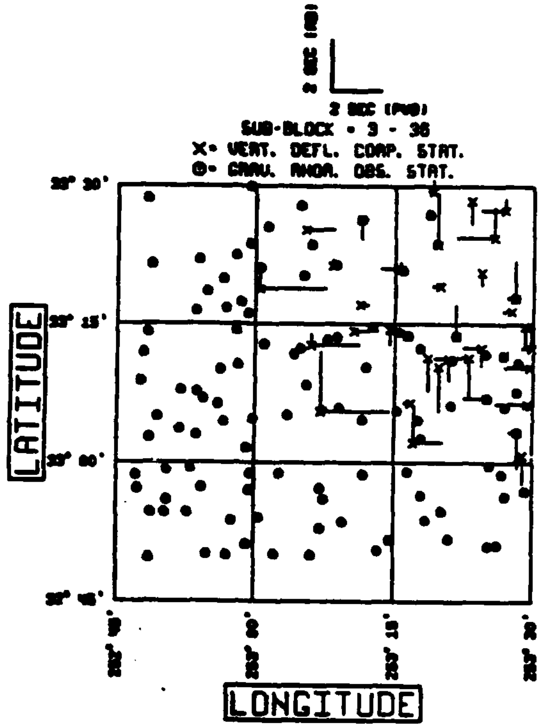

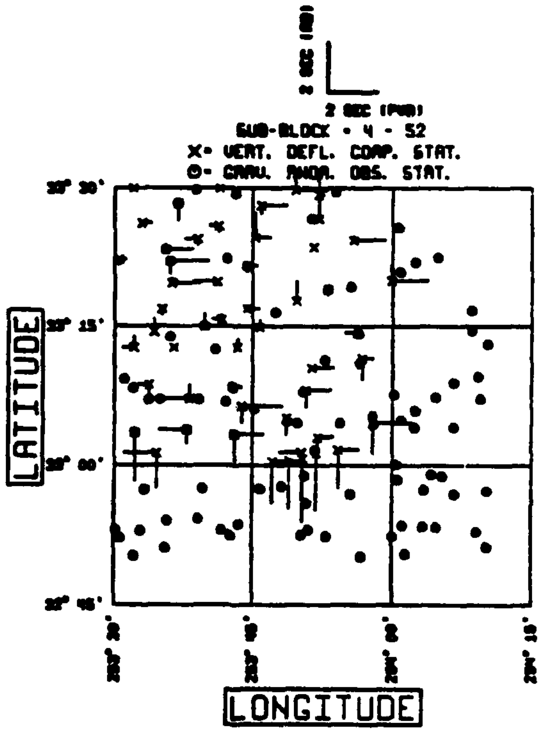

Figure 39. Comparison by Station of control and Hardy-Predicted Vertical Deflections at the North Block of the Test Area. Sub-blocks #3 and 4.

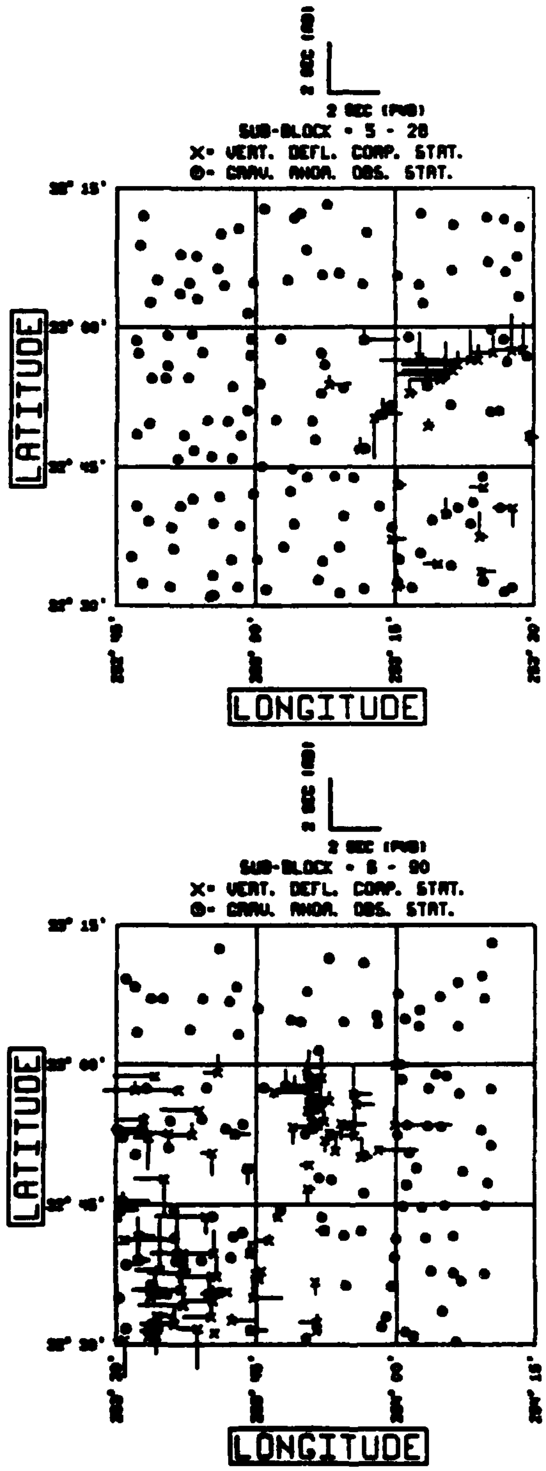

Figure 40. Comparison by Station of Control and Hardy-Predicted Vertical Deflections at the South Block of the Test Area. Sub-blocks #5 and 6.

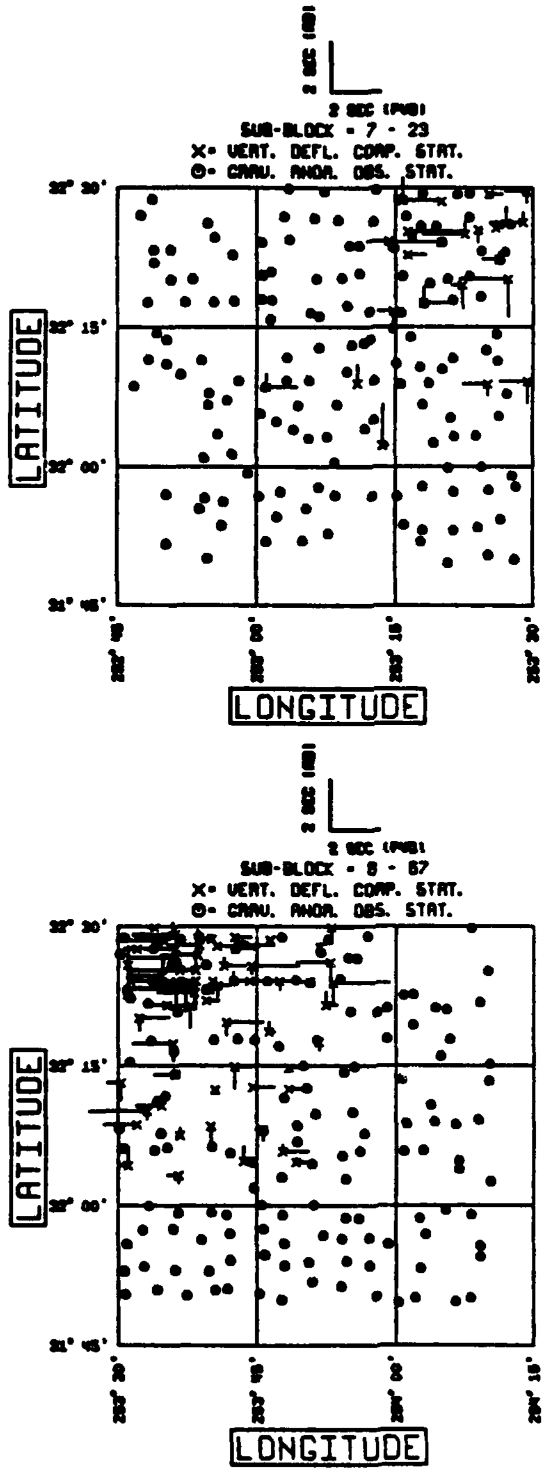

Figure 41. Comparison by Station of Control and Hardy-Predicted Vertical Deflections at the South Block of the Test Area. Sub-blocks #7 and 8.

5.3.5 Errors of Predictions

For every variation of the predictor the standard deviations σ of the predictions were computed at the solutions with the optimal radii $\hat{r}_0$ according to (2-57). These σ values are rather smooth and cannot indicate locations at which predictions are good or not.

5.3.6 Conclusions from the Hardy Predictor

At first, the results of the two methods to compute $\hat{r}_0$ from the data were not promising with the Hardy Predictor. As a result the s^2 method was used to compute $\hat{r}_0$.

If gravity predictions are required, use only gravity data and place the biharmonic sources at the nadir points of the observations on the geosphere. For White Sands, a radius of about 6356 km to 6363 km appears to be optimal.

If vertical deflection predictions are required use both Δg and (ξ,η) observations and locate the biharmonic sources on a grid at the surface of the geosphere. A radius of about 6335 km yielded optimal results for New Mexico.

The overall result of the tests of the Hardy Predictor seems to be that Δg can be predicted to about 3 to 4 mgals, ξ and η to about $0\overset{''}{.}8$ $0\overset{''}{.}9$.

5.3.7 Comparison of Bjerhammar and Hardy Predictors

Theoretically the predictors are very different. They even assume different behavior of the disturbing potential T. However, in practice they yielded very similar results. The best Δg and (ξ,η) predictions were performed with identical data requirements and downward continuation scheme and yielded similar results. A minor difference is the value of the optimal geosphere radius. The aforementioned results seem to stress that an improvement in the predictions of both Δg and (ξ,η) even in mountainous areas may not result from a theoretical breakthrough but from improved data coverage.

5.4 Prediction Using Least-Squares Collocation

For comparison purposes a Least-Squares Collocation solution was tested at the New Mexico Area. The model used for the disturbing potential covariance function was of the form [Kearsley et al., 1985; p. 50]

$$K(P,Q) = \sum_{n=181}^{\infty} \frac{AR_E^{\,2}}{(n-1)(n-2)(n+24)} \left(\frac{R_B^{\,2}}{r_P r_Q}\right)^{n+1} P_n(\cos\omega_{PQ}) \qquad (5\text{-}5)$$

where ω_{PQ} is the spherical distance between points P and Q, r_P and r_Q are geocentric radial distances to P and Q respectively, R_B is the radius to the Bjerhammar sphere and R_E is the mean Earth radius. The following values were used [Kearsley et al., 1985, p. 50].

$$R_E = 6371 \text{ km}, \quad R_B = 6369.75 \text{ km} \tag{5-6}$$

The variance $C_0^{V\Delta g}$ of the residual gravity anomalies as computed fr om 1137 point values was [Heiskanen and Moritz, 1967; p. 253]

$$C_0^{V\Delta g} = \mathrm{Var}(V_{\Delta g}) = 323.82 \text{ mgal}^2 \tag{5-7}$$

where $V_{\Delta g}$ is given by (4-10).

For each test two solutions were performed. One for the NB and one for the SB. The first test was to predict Δg and (ξ,η) from gravity data alone. The results of this test for both the NB and the SB are shown in Table 34.

Table 34. RMS Differences Between Predicted and Control Values with Only Δg Observed. Collocation Solution.

BLOCK	RMS DIFFERENCES		
SUB-BLOCK	Δg(mgal)	ξ(")	η(")
North	2.84	0.76	0.92
1	4.23	0.83	0.79
2	2.59	0.63	0.91
3	2.28	1.02	0.75
4	2.65	0.61	1.10
South	3.68	0.80	1.03
5	3.01	1.00	1.25
6	6.25	0.86	1.16
7	3.36	0.57	0.79
8	1.68	0.67	0.79

From Table 34 one sees RMS differences from 1.68 to 6.25 mgals for Δg, 0."57 to 1."02 for ξ and 0."75 to 1."25 for η resulting from different data coverage and terrain type within the eight sub-blocks. On the average Δg was predicted to about 3 mgals, ξ to about 0."8 and η to about 1."0.

The second test was to predict Δg and (ξ,η) from both Δg and (ξ,η) observations. The results of this attempt for both the NB and the SB solution are shown in Table 35.

Table 35. RMS Differences Between Predicted and Control Values with both Δg and (ξ,η) Observed. Collocation Solution.

BLOCK	RMS DIFFERENCES		
SUB-BLOCK	Δg(mgal)	ξ(")	η(")
North	2.93	0.58	0.56
1	4.08	0.59	0.48
2	2.40	0.49	0.60
3	2.56	0.82	0.31
4	3.00	0.44	0.68
South	3.44	0.64	0.66
5	3.37	0.89	1.06
6	4.61	0.70	0.59
7	3.70	0.31	0.37
8	1.82	0.49	0.59

From Table 35 one sees RMS differences from 1.82 to 4.61 mgals for Δg, 0".31 to 0".89 for ξ and 0".31 to 1".06 for η due to the terrain type and data coverage of the sub-blocks. On the average Δg was predicted to about 3.3 mgals and ξ and η to about 0".6.

The third test was to predict Δg and (ξ,η) from vertical deflection observations alone. The results of this test for both the NB and the SB solution are shown in Table 36.

Table 36. RMS Differences Between Predicted and Control Values with only (ξ,η) Observed. Collocation Solution.

BLOCK	RMS DIFFERENCES		
SUB-BLOCK	Δg(mgal)	ξ(")	η(")
North	5.41	0.67	0.86
1	6.02	0.65	0.87
2	3.75	0.52	0.66
3	5.91	0.73	0.83
4	5.46	0.76	1.02
South	7.36	0.72	0.86
5	5.92	1.31	1.27
6	3.49	0.58	0.79
7	10.70	0.53	0.64
8	5.47	0.60	0.80

From Table 36 one sees RMS differences from 3.49 to 10.70 mgals for Δg, 0".52 to 1".31 for ξ and 0".64 to 1".27 for η. The reason for this variation is the terrain type and the data coverage in the sub-blocks. On the average Δg was predicted to about 6.5 mgals, ξ to about 0".7 and η to about 0".9.

Comparison of Tables 34, 35 and 36 shows that the introduction of vertical deflection data slightly improved the (ξ,η) predictions and slightly deteriorated the Δg predictions. It is noteworthy that the RMS difference of 6.25 mgals at sub-block #6 was improved to 4.61 mgals by the introduction of (ξ,η) observations. The removal of gravity data resulted in degradation of the Δg predictions by about 3 mgals and a slight degradation of the (ξ,η) predictions. In conclusion, the best Δg predictions were obtained from Δg data alone (Table 34). This solution is shown by station in Figures 42, 43, 44 and 45. On the other hand, the best (ξ,η) predictions are obtained from both Δg and (ξ,η) data (Table 35) and this solution is shown in Figures 46, 47, 48 and 49 by station.

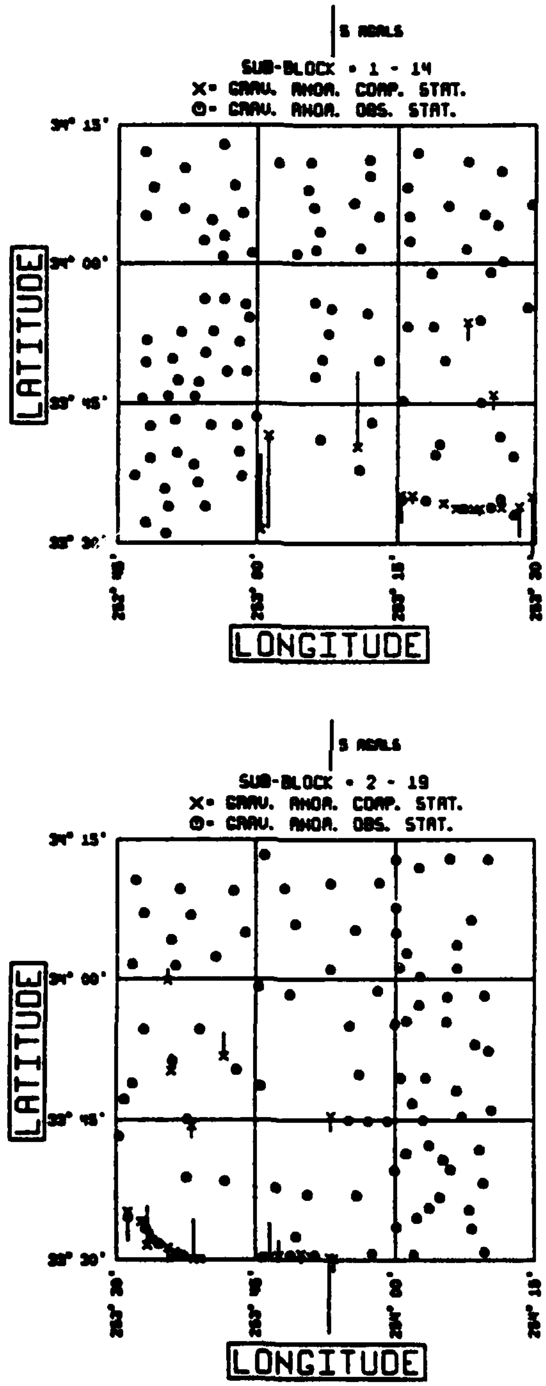

Figure 42. Comparison by Station of Control and Least Squares Collocation - Predicted Gravity Anomalies at the North Block of the Test Area. Sub-blocks #1 and 2.

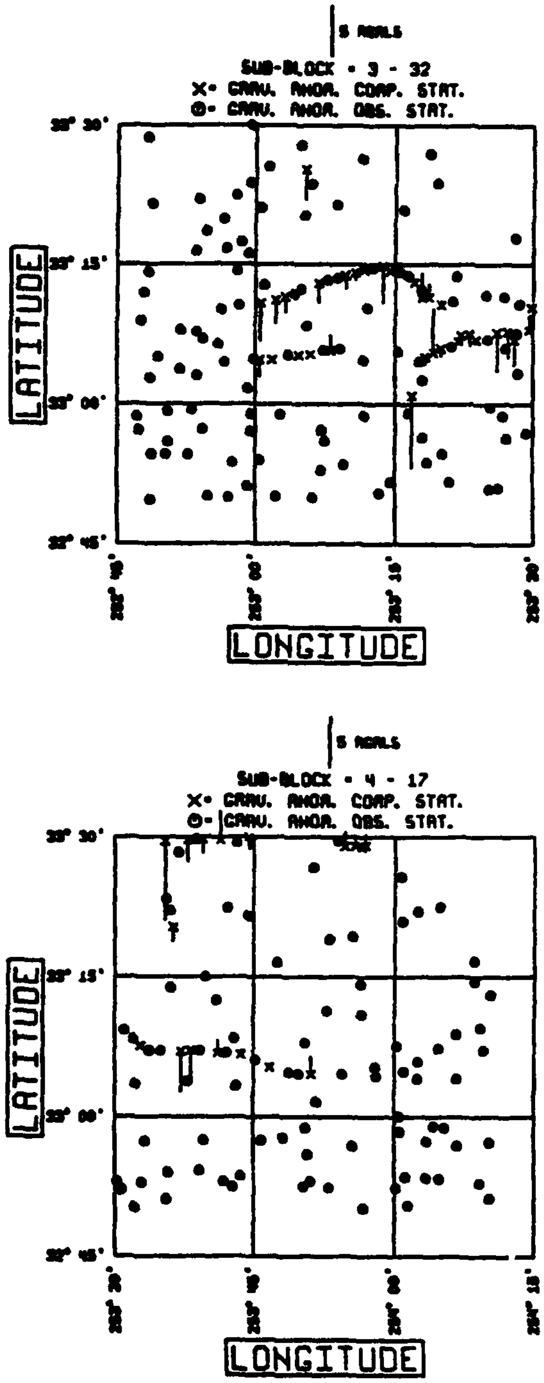

Figure 43. Comparison by Station of Control and Least Squares Collocation - Predicted Gravity Anomalies at the North Block of the Test Area. Sub-blocks #3 and 4.

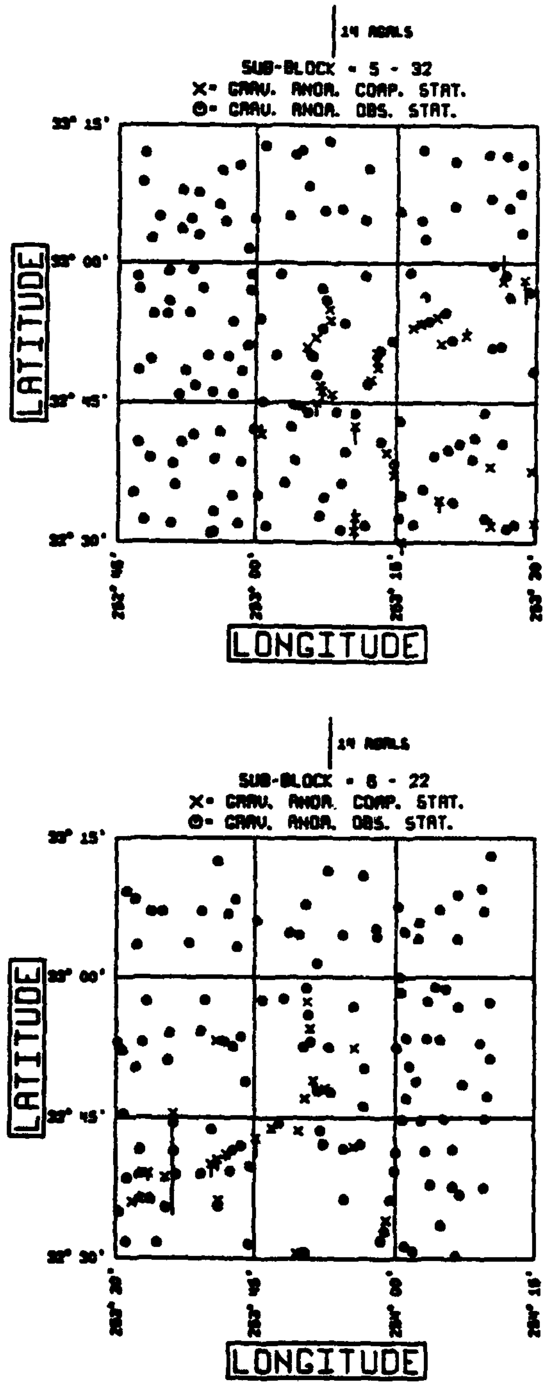

Figure 44. Comparison by Station of Control and Least Squares Collocation - Predicted Gravity Anomalies at the South Block of the Test Area. Sub-blocks #5 and 6.

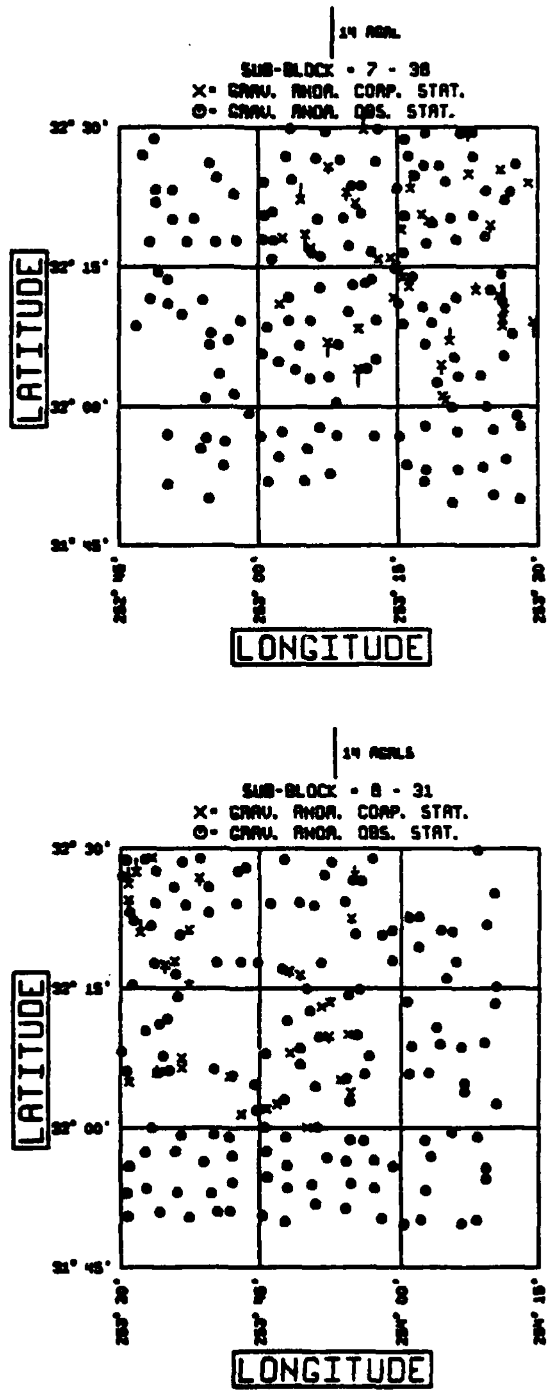

Figure 45. Comparison by Station of Control and Least Squares Collocation - Predicted Gravity Anomalies at the South Block of the Test Area. Sub-blocks #7 and 8.

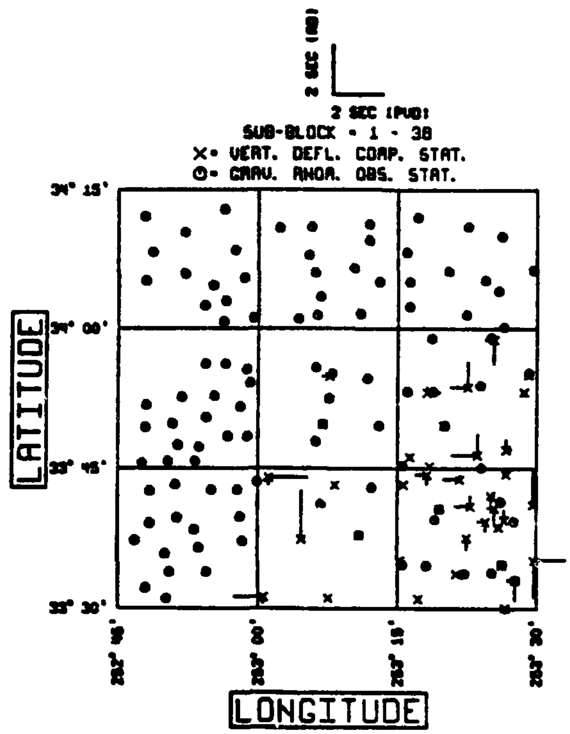

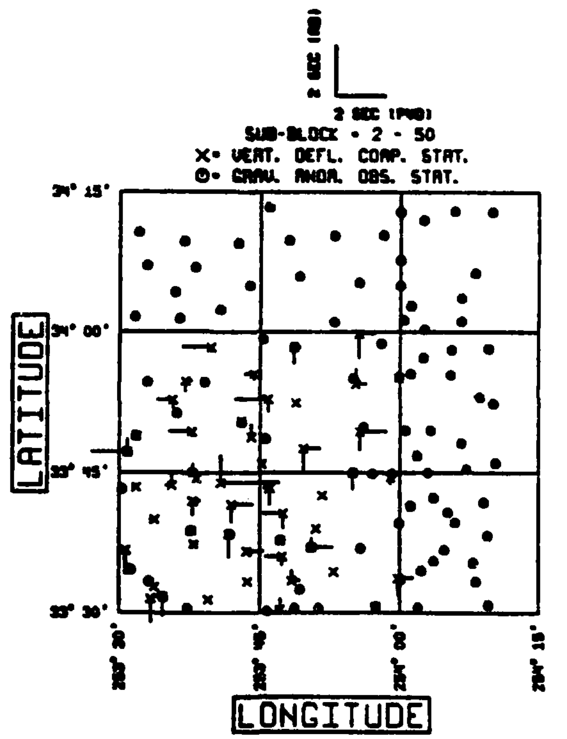

Figure 46. Comparison by Station of Control and Least Squares Collocation - Predicted Vertical Deflections at the North Block of the Test Area. Sub-blocks #1 and 2.

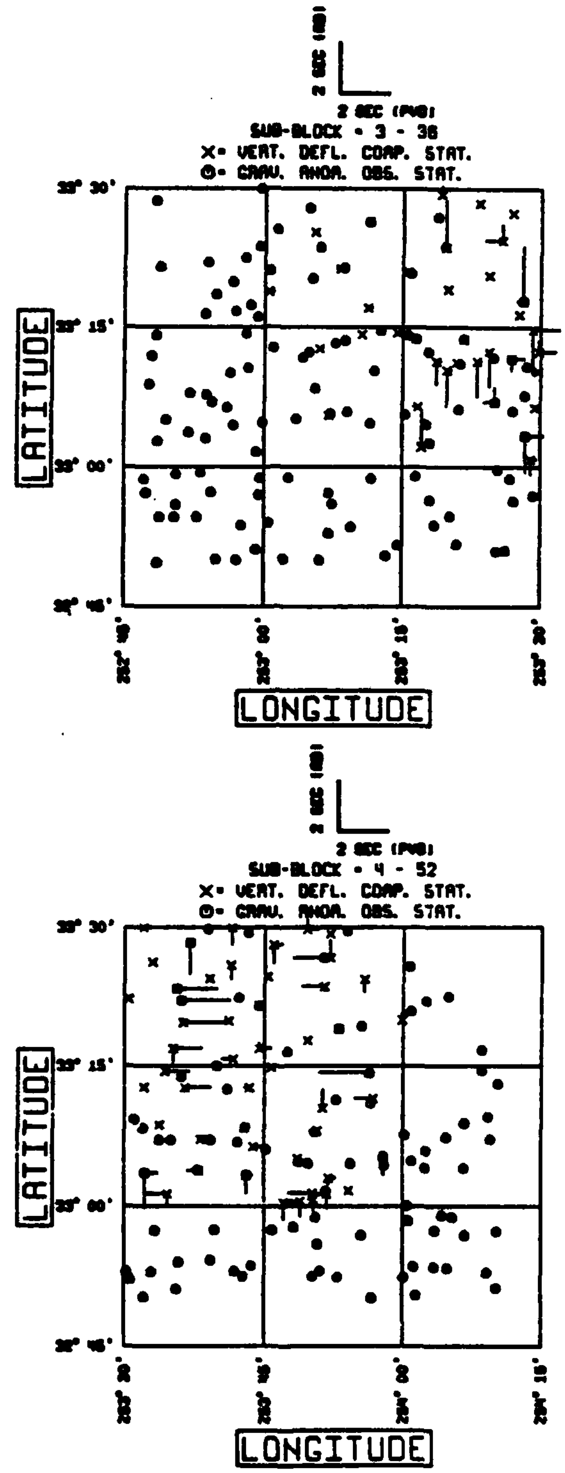

Figure 47. Comparison by Station of Control and Least Squares Collocation - Predicted Vertical Deflections at the North Block of the Test Area. Sub-blocks #3 and 4.

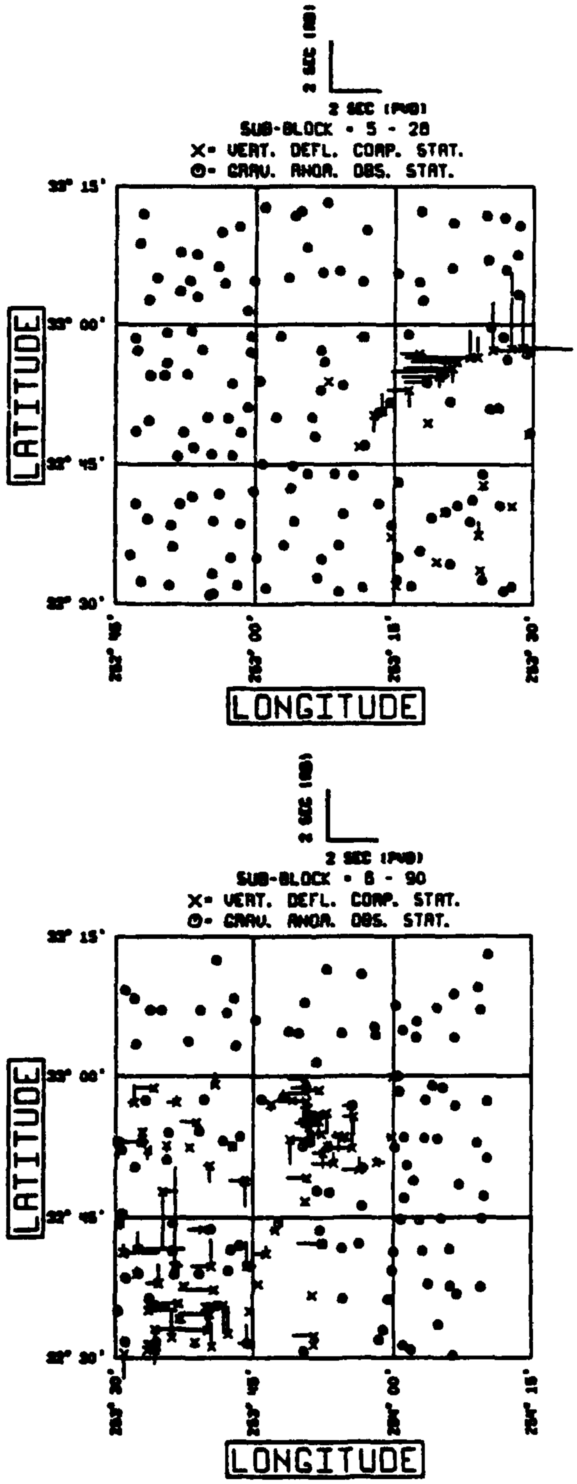

Figure 48. Comparison by Station of Control and Least Squares Collocation - Predicted Vertical Deflections at the South Block of the Test Area. Sub-blocks #5 and 6.

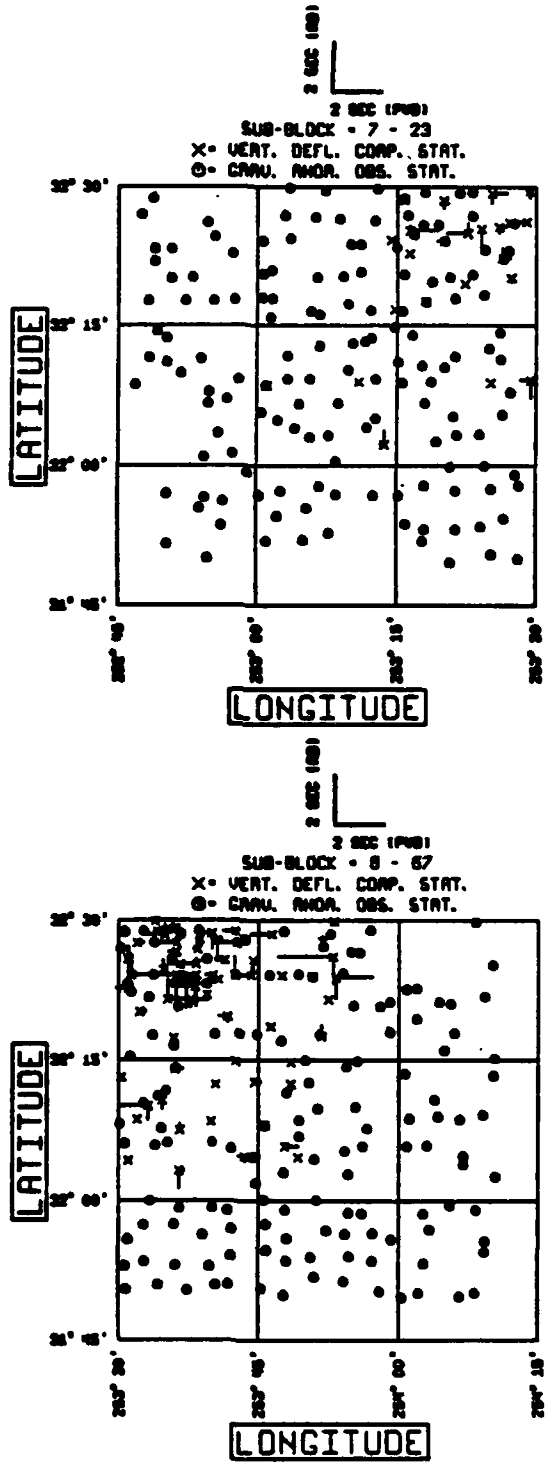

Figure 49. Comparison by Station of Control and Least Squares Collocation - Predicted Vertical Deflections at the South Block of the Test Area. Sub-blocks #7 and 8.

5.5. Comparison of the Bjerhammar and Hardy Predictors to Least-Squares Collocation

In the sequel a comparison between the Bjerhammar Method (BM), the Hardy Method (HM) and Least Squares Collocation (LSC) will be attempted. The CPU time comparison is based on times required on the IBM 3081 computer. In the event that only Δg observations are available the results from the White Sands tests are shown in Table 37.

Table 37. RMS Differences Between Predicted and Control from the Three Predictors. Only Δg Observed.

Block	Δg(mgals)			$\xi('')$			$\eta('')$			CPU Time
Sub-Block	BM	HM	LSC	BM	HM	LSC	BM	HM	LSC	(sec)
NORTH	3.08	3.13	2.84	0.90	4.93	0.76	1.00	11.36	0.92	BM
SOUTH	3.79	3.88	3.68	0.90	2.43	0.80	1.13	4.77	1.03	NB: 512
1	4.27	4.32	4.23	0.91	2.86	0.83	0.81	11.42	0.79	SB: 1440
2	2.54	2.56	2.59	0.64	6.17	0.63	0.99	3.95	0.91	HM
3	2.84	2.88	2.28	1.26	2.32	1.02	0.70	18.44	0.75	NB: 500
4	2.86	2.98	2.65	0.81	6.00	0.61	1.28	9.52	1.10	SB: 1392
5	3.43	3.73	3.01	1.27	3.93	1.00	1.36	7.24	1.25	LSC
6	6.22	5.69	6.25	0.94	1.49	0.86	1.28	4.97	1.16	NB: 638
7	3.20	3.57	3.36	0.58	1.04	0.57	0.75	4.18	0.79	SB: 1182
8	2.23	2.63	1.68	0.74	2.91	0.67	0.89	3.12	0.79	

From Table 37 and keeping in mind that both the observed and the control Δg have a standard deviation of 2 mgals one sees that all three methods can predict gravity anomalies within 3 to 4 mgals. Furthermore, the difference in the quality of the predictions introduced by each method never exceeded the observation error. Also, sub-blocks that performed well or poorly with some method behaved similarly with all methods. For instance, sub-block #6 yielded the largest RMS difference and sub-block #8 yielded the smallest RMS difference for all methods.

The picture is different for vertical deflection predictions. From Table 37 one can see immediately that the HM cannot perform to a satisfactory level. On the other hand BM and LSC performed equally well with the exception of sub-blocks #3 and 5 at which LSC outperformed BM at the ξ predictions by about $0''.25$ which is not very large keeping in mind that the standard deviations of the control deflections are $0''.3$.

In case that both Δg and (ξ,η) are utilized as observations one gets the results of Table 38.

Table 38. RMS Differences Between Predicted and Control from the Three Predictors. Both Δg and (ξ,η) Observed. Downward Continuation on a $(7' \times 7')$ Grid for Both BM and HM.

Block	Δg(mgals)			$\xi('')$			$\eta('')$			CPU Time
Sub-Block	BM	HM	LSC	BM	HM	LSC	BM	HM	LSC	(sec)
NORTH	3.56	4.50	2.93	0.65	0.81	0.58	0.65	0.77	0.56	BM
SOUTH	4.69	5.34	3.44	0.62	0.69	0.64	0.92	1.08	0.66	NB: 892
1	4.07	4.56	4.08	0.66	0.69	0.59	0.54	0.54	0.48	SB: 1140
2	3.16	3.68	2.40	0.63	0.62	0.49	0.75	0.77	0.60	HM
3	3.03	3.85	2.56	0.83	1.00	0.82	0.44	0.93	0.31	NB: 880
4	4.34	6.14	3.00	0.49	0.90	0.44	0.75	0.79	0.68	SB: 1128
5	4.30	4.77	3.37	0.57	0.76	0.89	0.89	1.18	1.06	LSC
6	4.06	5.03	4.61	0.70	0.75	0.70	0.80	0.91	0.59	NB: 861
7	6.25	7.00	3.70	0.59	0.69	0.31	1.03	1.12	0.37	SB: 1469
8	2.90	3.37	1.82	0.51	0.55	0.49	1.04	1.23	0.59	

From Table 38 one sees that all methods can predict Δg to about 3 to 5 mgals. Also, the discrepancies of the RMS differences among different methods are always smaller than the standard deviation of the Δg values. LSC is favored over both BM and HM in terms of Δg predictions.

As far as vertical deflection predictions are concerned all methods can predict ξ to about $0\overset{''}{.}6$ to $0\overset{''}{.}8$ and η to about $0\overset{''}{.}6$ to $1\overset{''}{.}0$. In the majority of the cases all methods performed equally well with the exception of sub-blocks #3 and 4 in favor of BM and LSC, #5 in favor of BM and #7 in favor of LSC for ξ and sub-block #3 in favor of BM and LSC, #5 in favor of BM and LSC and #6, 7 and 8 in favor of LSC for η. Overall, similar accuracy was obtained by all three methods.

In the event that one has (ξ,η) observations only one gets the results of Table 39.

From Table 39 one sees superiority of the LSC solution in the Δg predictions, which, however yields rather large RMS discrepancies. In terms of vertical deflection predictions one can observe LSC to perform better than both BM and HM with the exception of sub-block #5 for η. Therefore, in this case the LSC solution is preferred.

Table 39. RMS Differences Between Predicted and Control from the Three Predictors. Only (ξ,η) Observed.

Block	Δg(mgals)			ξ(")			η(")			CPU
Sub-Block	BM	HM	LSC	BM	HM	LSC	BM	HM	LSC	(sec)
NORTH	13.19	16.48	5.41	1.25	0.97	0.67	1.06	0.98	0.86	BM
SOUTH	9.19	12.61	7.36	1.08	0.91	0.72	0.99	1.01	0.86	NB: 36
1	11.98	11.68	6.02	1.06	0.87	0.65	0.91	1.16	0.87	SB: 36
2	8.15	5.93	3.75	0.76	0.74	0.52	0.74	0.77	0.66	HM
3	16.00	23.62	5.91	1.00	0.97	0.73	0.80	0.88	0.83	NB: 36
4	12.85	10.43	5.46	1.79	1.20	0.76	1.50	1.09	1.02	SB: 36
5	10.62	6.49	5.92	1.58	1.46	1.31	1.25	1.23	1.27	LSC
6	7.34	20.09	3.49	1.11	0.80	0.58	0.89	0.93	0.79	NB:130
7	10.20	10.90	10.70	1.00	0.97	0.53	1.35	1.37	0.64	SB:140
8	7.25	12.46	5.47	0.75	0.72	0.60	0.85	0.86	0.80	

A comparison of the three methods reveals that BM and LSC performed equally well in all cases, except the case of only (ξ,η) observations, in which LSC performed better than BM. The HM, however, yielded peculiar results. For example, Δg were predicted to about 3 to 4 mgals from gravity data only (Table 37). From the same solution, (ξ,η) were predicted unacceptably. From only (ξ,η) observations (Table 39), vertical deflections were predicted well, whereas Δg were predicted unacceptably. These types of results from HM come as no surprise in light of the comments in subsection 3.2.4.

The best vertical deflection predictions for all three methods were abtained when both Δg and (ξ,η) observations were used (Table 38). The downward continuation for both the BM and the HM was performed on to a (7'x7') on the geosphere. In Table 38, only the RMS differences of control minus predicted quantities are given. The corresponding average differences are about 1 mgal for Δg and for (ξ,η) they are in the order of a few tenths of an arcsecond. Furthermore, the predictions obtained from ıe three methods agree very well as seen from Figures 26 through 49. The RMS prediction differences between any two methods are 2 to 4 mgals for Δg and in the sub-second level for (ξ,η). Furthermore, the corresponding average differences are less than 0.7 mgals for Δg and for (ξ,η) they are less than two tenths of an arcsecond in absolute value. In the North Block, the best agreement is observed between the predicted both Δg and (ξ,η) from the BM and LSC and the worst agreement is observed between HM and LSC. In the South Block, the best agreement is observed between BM and HM whereas the worst one is observed between the HM and LSC. Correlation coefficients between average (ξ,η) differences (control minus predicted) among methods in each sub-block ranged from 0.2 to 0.9. The average correlation coefficient was 0.7. The corrresponding correlation coefficients from Δg predictions ranged from 0.82 to 0.99. The average value was 0.90.

Examination of the differences of control minus predicted vertical deflections at individual stations yields interesting results. For example, in Kearsley et al., [1985, p. 68] the ξ component of the vertical deflection at station 191 was reported as a suspected error in the control data. This appears to be the case from the results of this investigation also. Furthermore, stations with large differences from one method, yield large differences with all three methods (e.g. stations 376, 383, 395, 404, 286 and 305 for ξ and stations 199, 200, 202, 203, 128 and 29 for η to name only a few). On the other hand, there are some stations with small differences from one method and large differences from another (e.g. stations 378, 320 and 172 for ξ and 349, 355 and 127 for η).

As far as CPU time requirements for the three predictors, Tables 37, 38 and 39 indicate that there is no method that consistently required less time than the others. It is worth noting that 75% of the time estimates for BM and HM is needed to compute an optimal value for the radius of the geosphere.

The software for both the BM and the HM was converted to work on the CRAY X-MP/24 supercomputer. This conversion was almost effortless. However, it will take a moderate effort to modify the LSC software (GEOCOL) to work on the supercomputer. The CPU time requirements for both the BM and the HM on the CRAY X-MP/24, including an optimal r_0 computation, are shown in Table 40.

Table 40. CPU Time Requirements (in seconds) for BM and HM on the CRAY X-MP/24 Supercomputer.

Type of Observable	BM		HM	
	NB	SB	NB	SB
Δg	7.7	22.6	8.8	23.7
Δg and (ξ,η)	10.4	24.8	10.9	28.8
(ξ,η)	0.1	0.1	0.1	0.1

Comparison of Table 40 to Tables 37, 38 and 39 reveals improvement by a factor of at least 10 and as much as 90.

Lastly, in the event that an optimal $\hat{r}_0$ is required for the BM or the HM and no control data exist in an area, then the observations can be separated in two groups. The first group should be regarded as observations and the second one should be regarded as control data. These two groups can be used with the s^2-method to compute an optimal geosphere radius. Finally, the entire data set should be used as observations to perform the solution.

5.6 Comparison With the Four Methods Tested with the New Mexico Test Data

In Kearsley et al. [1985] four methods to predict deflections of the vertical from gravity anomaly data were tested and intercompared. These methods were the Fast Fourier Transform (FFT), the Combined Collocation-Integration (CINT), the Numerical Integration (RINT) and the Terrain Effect Integration and Collocation (TEIC) method. In Tables 4.5 and 4.6 of [ibid, pp. 93-94] they reported RMS discrepancies, control minus predicted vertical deflections, predicted from gravity data in the order of 1" when height data are used.

In the sequel we will compare the results of the four methods in [Kearsley et al., 1985] with the results of this investigation. The comparison will be based on Tables 4.5 and 4.6 of [ibid, pp. 93-94] and on Table 37 of this work. However, the results of our LSC will be used rather than the ones of TEIC because the results of our LSC solution are slightly better. A summary of these results appear in Table 41. In Table 41, the column designated AG shows the RMS values of the vertical deflections by sub-block.

Table 41. Comparison of the Bjerhammar and Hardy Predictors with the Four Methods Tested at New Mexico. Only Δg Observed.

	AG		BM		HM		LSC		FFT		CINT		RINT	
BLOCK	ξ	η	$\Delta\xi$	$\Delta\eta$	$\Delta\xi$	$\Delta\eta$	$\Delta\xi$	$\Delta\eta$	$\Delta\xi$	$\Delta\eta$	$\Delta\xi$	$\Delta\eta$	$\Delta\xi$	$\Delta\eta$
North	4.3	7.9	0.9	1.0	4.9	11.4	0.8	0.9	1.1	1.3	1.0	1.6	1.1	2.0
1	2.8	5.6	0.9	0.8	2.9	11.4	0.8	0.8	1.2	1.4	0.8	1.4	0.7	1.4
2	4.1	9.1	0.6	1.0	6.2	4.0	0.6	0.9	1.0	1.4	0.9	1.6	0.7	2.2
3	5.1	6.6	1.3	0.7	2.3	18.4	1.0	0.8	1.2	1.3	1.4	1.5	1.8	1.6
4	4.7	8.7	0.8	1.3	6.0	9.5	0.6	1.1	0.8	1.3	1.0	1.8	0.9	2.5
South	3.0	7.1	0.9	1.1	2.4	4.8	0.8	1.0	0.9	1.2	0.8	1.2	0.7	1.6
5	4.0	7.9	1.3	1.4	3.9	7.2	1.0	1.3	0.9	1.2	0.7	1.3	0.9	1.6
6	2.8	7.7	0.9	1.3	1.5	5.0	0.9	1.2	0.8	1.1	0.9	1.1	0.6	1.7
7	3.4	6.3	0.6	0.8	1.0	4.2	0.6	0.8	1.0	1.5	0.8	1.4	0.6	1.2
8	2.4	6.2	0.7	0.9	2.9	3.1	0.7	0.8	0.8	1.1	0.8	1.2	0.7	1.5

From Table 41 one can see that the methods that performed best were LSC and BM. Furthermore, LSC performed slightly better than BM (by about $0\overset{''}{.}1$ on the average, which is below the (ξ,η) noise level).

However, the most important conclusion drawn from Table 41 is that, when reference field and RTM effects are removed from the data and restored at the predictions, there are at least five methods that can predict vertical deflections to the sub-second level from gravity data.

CHAPTER VI

SUMMARY, CONCLUSIONS, RECOMMENDATIONS

Two deterministic methods for gravity field approximation have been investigated. The first one was the Bjerhammar Dirac Impulse method and the second one was the Hardy's biharmonic potential method.

Bjerhammar defined the discrete geodetic boundary value problem as the one at which observations are given at discrete points and it is required to find a gravity field such that all observations are satisfied. The solution is constructed such that the disturbing potential is harmonic outside a sphere fully internal to the Earth and regular at infinity. The Dirac Impulses that generate the disturbing potential are computed by a downward continuation process and they are used to perform predictions in an upward continuation scheme.

Hardy's work was initiated by the fact that the integral representation of the disturbing potential is singular at points that induce potential. Based on the non-uniqueness of the solution of the inverse problem of potential theory one can assume that the density anomaly function of the Earth together with its normal derivative is zero at the boundary. An integral representation of the disturbing potential can be derived which is non-singular at points that induce potential and which satisfies the biharmonic equation. An approximation to the fundamental integral is also derived. Operationally, the biharmonic sources are computed as the solution of a linear system and then they are used to perform predictions.

Both of the aforementioned methods can use any linear functionals of the disturbing potential as observations and/or quantities to be predicted.

Tests were performed for both methods with the White Sands Test Data. The predictions were compared to independently observed gravity anomalies and vertical deflections that served as control data. Reference field and residual terrain model effects were removed from the observations and were restored at the predicted values before any comparison to the control data was done.

A factor that influences the quality of the results with both predictors is the radius of the internal sphere. Two approaches to compute it from gravity data failed for both methods. However, a technique for optimal radius computation that yielded satisfactory results is to consider some measure of the quality of the predictions a second order polynomial in the radius.

The Bjerhammar method, *performing* the downward continuation on the nadir points of the observations and with only gravity data resulted in RMS differences of control minus predicted values in the order of 3 to 4 mgals Δg, 0."9 for ξ and 1."0 for η. When vertical deflection observations were introduced the RMS discrepancies became 3.5 to 4.5 mgals for Δg and 0."8 for ξ and η. When the gravity observations were completely removed, the RMS differences became larger than 10 mgals for Δg, and about 1" for both ξ and η. The aforementioned results pertain to both the Asymmetric and the Symmetric Kernel approach. In fact, the only difference between the AK and the SK is that the optimal radii associated with the AK are usually smaller than the ones with the SK (see Table 17).

When the downward continuation is performed onto a grid on the geosphere, the Bjerhammar method predicted Δg to 3 to 4 mgals, ξ to about 0."9 and η to about 1."1 from gravity observations alone. When vertical deflection observations were introduced, the RMS differences of control minus predicted values was the same (about 3 to 4 mgals) for Δg, whereas it became about 0."7 for ξ and 0."8 for η. On the other hand, the predictions from (ξ,η) data alone were unacceptable both for Δg and (ξ,η).

For every variation of the Bjerhammar predictor, standard deviations of the predictions were computed according to (2-57). These standard deviations cannot be considered a safe indicator of the quality of the predictions. The reason for this is that there were many well predicted quantities with large standard deviations and there were many poorly predicted quantities with small standard deviations.

The Hardy method, when the biharmonic sources were located at the nadir points of the observations, gave RMS discrepancies of control minus predicted values on the order of 3 to 4 mgals for Δg whereas the vertical deflection predictions were very poor. When vertical deflection observations were introduced, the RMS differences were larger than 10 mgals for Δg and larger than 2."5 for ξ and η. When the gravity data were completely removed, the RMS differences were *degraded further for* Δg whereas they became smaller than 1" for both ξ and η.

When the downward continuation is performed onto a grid on the geosphere, the Hardy method with only gravity data, yielded RMS discrepancies in the order of 3 to 4 mgals for Δg whereas the vertical deflections were worse than 2."7 for all grid sizes. The introduction of vertical deflection observations degraded the Δg predictions to 4.5 to 5.5 mgals whereas it upgraded the (ξ,η) predictions to the 1" level. The complete removal of Δg data rendered both the Δg and the (ξ,η)

predictions unacceptable.

For every variation of the Hardy predictor, the standard deviations σ of the predictions did not prove to be indicative of the quality of the resultss, since in many cases large σ's were associated with well predicted quantities and vice versa.

Comparison of the two predictors (BM and HM) with Least Squares Collocation (LSC) indicates that BM and LSC yield comparable results in all cases with the exception of the case where only (ξ,η) observations are utilized in which case LSC performed better than BM. On the other hand, HM performed well when it predicted Δg from Δg data or (ξ,η) from (ξ,η) data and the downward continuation was performed at the nadir points of the observations.

The most important overall result of this work is that when reference field and RTM effects are taken into account, there are at least five methods that can predict (ξ,η) from Δg to the sub-second level, even in mountainous areas. Furthermore, the improvement of the predictions should not be anticipated from a theoretical breakthrough but from data type and coverage improvement.

As far as future investigations are concerned it is recommended that undulations and/or gravity gradients be predicted from various data types with both predictors. Particularly for the Hardy method it is suggested that a low degree and order spherical biharmonic expansion (e.g. 6 to 10) be computed from the formulae given in Appendix A.5 using $10^\circ \times 10^\circ$ or $5^\circ \times 5^\circ$ global data and then be tested as to its reliability.

APPENDIX A

DERIVATIONS

1. Show that if $M_i = \frac{2b_i}{t} - \frac{\partial b_i}{\partial t}$

with $b_i = t - 3dt + \frac{2t}{d} - 5t^2\cos\omega - 3t^2\cos\omega\,\ell nu$,

then $M_i = 1 + \frac{t^2-1}{d^3} + 3t\cos\omega$

<u>Proof:</u>

Recalling equations (2-21) and (2-22) one has

$$\frac{\partial d}{\partial t} = \frac{t-\cos\omega}{d}$$

and

$$\frac{\partial u}{\partial t} = \frac{1}{2}\left(\frac{t-\cos\omega}{d} - \cos\omega\right).$$

Therefore

$$M_i = \frac{2b_i}{t} - \frac{\partial b_i}{\partial t} = 2 - 6d + \frac{4}{d} - 10t\cos\omega - 6t\cos\omega\,\ell nu -$$

$$-\left[1 - 3\frac{\partial}{\partial t}(td) + 2\frac{\partial}{\partial t}\left(\frac{t}{d}\right) - 10t\cos\omega - 6t\cos\omega\,\ell nu - 3t^2\cos\omega\,\frac{\partial}{\partial t}(\ell nu)\right] =$$

$$= 2 - 6d + \frac{4}{d} - 10t\cos\omega - 6t\cos\omega\,\ell nu - \left[1 - 3t\,\frac{t-\cos\omega}{d} - 3d + \right.$$

$$+ 2\,\frac{d - t\,\frac{t-\cos\omega}{d}}{d^2} - 10t\cos\omega - 6t\cos\omega\,\ell nu -$$

$$\left. - 3t^2\cos\omega\,\frac{1}{u}\,\frac{1}{2}\left(\frac{t-\cos\omega}{d} - \cos\omega\right)\right] =$$

$$= 2 - 6d + \frac{4}{d} - 10t\cos\omega - 6t\cos\omega\,\ell nu - 1 + \frac{3t^2}{d} - \frac{3t\cos\omega}{d} + 3d - \frac{2}{d} +$$

$$+ \frac{2t^2}{d^3} - \frac{2t\cos\omega}{d^3} + 10t\cos\omega + 6t\cos\omega\,\ln u + \frac{3t^2\cos\omega(t-\cos\omega)}{2ud} - \frac{3t^2\cos^2\omega}{2u} =$$

$$= 1 - 3d + \frac{2}{d} + \frac{3t^2}{d} - \frac{3t\cos\omega}{d} + \frac{2t^2}{d^3} - \frac{2t\cos\omega}{d^3} + \frac{3t^2\cos\omega(t-\cos\omega)}{2ud} -$$

$$- \frac{3t^2\cos^2\omega}{2u} =$$

$$= 1 - 3d + \frac{2}{d} + \frac{3t^2}{d} - \frac{6t\cos\omega}{d} + \frac{2t^2}{d^3} - \frac{2t\cos\omega}{d^3} + \frac{3t\cos\omega}{d} +$$

$$+ \frac{3t^2\cos\omega(t-\cos\omega)}{2ud} - \frac{3t^2\cos^2\omega}{2u} =$$

$$= \frac{1}{d^3}\left[d^3 - 3d^4 + 2d^2 + 3t^2d^2 - 6td^2\cos\omega + 2t^2 - 2t\cos\omega\right] +$$

$$+ \frac{3t\cos\omega}{d}\left[1 + \frac{t^2 - t\cos\omega - td\cos\omega}{2u}\right] =$$

$$= \frac{1}{d^3}\left[d^3 - 3d^4 - d^2 + 3d^2(1 + t^2 - 2t\cos\omega) + 2t^2 - 2t\cos\omega\right] +$$

$$+ \frac{3t\cos\omega}{2ud}\left[2u + t^2 - t\cos\omega - td\cos\omega\right] =$$

$$= \frac{1}{d^3}(d^3 - 3d^4 - d^2 + 3d^4 + 2t^2 - 2t\cos\omega) +$$

$$+ \frac{3t\cos\omega}{2ud}(1 - t\cos\omega + d + t^2 - t\cos\omega - td\cos\omega) =$$

$$= \frac{1}{d^3}(d^3 - d^2 + 2t^2 - 2t\cos\omega) + \frac{3t\cos\omega}{2ud}(d^2 + d - td\cos\omega) =$$

$$= \frac{1}{d^3}(d^3 - 1 - t^2 + 2t\cos\omega + 2t^2 - 2t\cos\omega) +$$

$$+ \frac{3t\cos\omega}{2ud}\, d\,(d + 1 - t\cos\omega) =$$

$$= \frac{1}{d^3}(d^3 + t^2 - 1) + \frac{3t\cos\omega}{2u}\, 2u = 1 + \frac{t^2-1}{d^3} + 3t\cos\omega \quad \text{q.e.d.}$$

2. Show that $A_1 = \frac{\partial}{\partial\omega}\left[1 - 3d + \frac{2}{d} - 5t\cos\omega - 3t\cos\omega\,\ln u\right] =$

$$= t\sin\omega\left[8 - \frac{2}{d^3} - \frac{3(d+1)^2}{2ud} + 3\ell nu\right]$$

Proof:

Recalling equations (2-16) and (2-18) one can show that

$\frac{\partial d}{\partial\omega} = \frac{t\sin\omega}{d}$ and $\frac{\partial u}{\partial\omega} = \frac{t\sin\omega}{2}\left(1 + \frac{1}{d}\right)$. Therefore:

$$A_1 = \frac{\partial}{\partial\omega}\left[1 - 3d + \frac{2}{d} - 5t\cos\omega - 3t\cos\omega\,\ell nu\right] =$$

$$= -3\frac{\partial d}{\partial\omega} + 2(-1)d^{-2}\frac{\partial d}{\partial\omega} - 5t(-\sin\omega) - 3t(-\sin\omega)\ell nu - 3t\cos\omega\,\frac{1}{u}\frac{\partial u}{\partial\omega} =$$

$$= -3\frac{t\sin\omega}{d} - \frac{2}{d^2}\frac{t\sin\omega}{d} + 5t\sin\omega + 3t\sin\omega\,\ell nu - \frac{3t\cos\omega}{u}\frac{t\sin\omega}{2}\left(1 + \frac{1}{d}\right) =$$

$$= t\sin\omega\left[-\frac{3}{d} - \frac{2}{d^3} + 5 + 3\ell nu - \frac{3t\cos\omega}{2u} - \frac{3t\cos\omega}{2ud}\right] =$$

$$= t\sin\omega\left[8 - \frac{2}{d^3} + 3\ell nu - \frac{3}{2ud}(2ud + 2u + td\cos\omega + t\cos\omega)\right] =$$

$$= t\sin\omega\left[8 - \frac{2}{d^3} + 3\ell nu - \frac{3}{2ud}((1 - t\cos\omega + d)d + (1 - t\cos\omega + d) + \right.$$

$$\left. + td\cos\omega + t\cos\omega)\right] =$$

$$= t\sin\omega\left[8 - \frac{2}{d^3} + 3\ell nu - \frac{3}{2ud}(d - dt\cos\omega + d^2 + 1 - t\cos\omega + \right.$$

$$\left. + d + td\cos\omega + t\cos\omega)\right] =$$

$$= t\sin\omega\left[8 - \frac{2}{d^3} + 3\ell nu - \frac{3}{2ud}(d^2 + 2d + 1)\right] =$$

$$= t\sin\omega\left[8 - \frac{2}{d^3} - \frac{3(d+1)^2}{2ud} + 3\ell nu\right] \quad \text{q.e.d.}$$

3. Show that if $g_{ij}^{\Delta g} = \frac{t^2(1-t^2)}{d^3} - 3t^3\cos\omega - t^2$,

with $d^2 = 1 + t^2 - 2t\cos\omega$ and $t = \frac{r_0}{r}$,

then $\frac{\partial g_{ij}^{\Delta g}}{\partial r_0} = \frac{t^2}{r_0}\left[\frac{2}{d^3}(1 - 2t^2) - \frac{3t(1-t^2)(t-\cos\omega)}{d^5} - 9t\cos\omega - 2\right]$

<u>Proof:</u>

Firstly: $t = \frac{r_0}{r} \Rightarrow \frac{\partial}{\partial r_0}(t^n) = nt^{n-1}\frac{\partial t}{\partial r_0} = nt^{n-1}\frac{1}{r} = \frac{nt^n}{r_0}$

Secondly: $\frac{\partial d}{\partial r_0} = \frac{\partial}{\partial r_0}[(1 + t^2 - 2t\cos\omega)^{1/2}] =$

$$= \frac{1}{(1+t^2-2t\cos\omega)^{1/2}}(2t-2\cos\omega)\frac{\partial t}{\partial r_0} = \frac{t(t-\cos\omega)}{r_0 d}$$

Hence:

$$\frac{\partial g_{ij}^{\Delta g}}{\partial r_0} = \frac{\left[(1-t^2)\frac{\partial(t^2)}{\partial r_0} + t^2\frac{\partial(1-t^2)}{\partial r_0}\right]d^3 - t^2(1-t^2)\frac{\partial(d^3)}{\partial r_0}}{d^6} -$$

$$- 3\cos\omega\frac{\partial(t^3)}{\partial r_0} - \frac{\partial(t^2)}{\partial r_0} =$$

$$= \frac{1}{d^3}\left[(1-t^2)\frac{2t^2}{r_0} + t^2\left(-\frac{2t^2}{r_0}\right)\right] - \frac{t^2(1-t^2)}{d^6}3d^2\frac{t(t-\cos\omega)}{r_0 d} -$$

$$- 3\cos\omega\frac{3t^3}{r_0} - \frac{2t^2}{r_0} =$$

$$= \frac{2t^2}{r_0 d^3}(1 - 2t^2) - \frac{3t^3(1-t^2)(t-\cos\omega)}{r_0 d^5} - 9t^3\frac{\cos\omega}{r_0} - \frac{2t^2}{r_0}\text{, or}$$

$$\frac{\partial g_{ij}^{\Delta g}}{\partial r_0} = \frac{t^2}{r_0}\left[\frac{2}{d^3}(1 - 2t^2) - \frac{3t(1-t^2)(t-\cos\omega)}{d^5} - 9t\cos\omega - 2\right] \quad \text{q.e.d.}$$

4. Show that if $\begin{Bmatrix} g^{\xi}_{ij} \\ g^{\eta}_{ij} \end{Bmatrix} = \frac{\sin\omega}{\gamma}\begin{Bmatrix}\cos\alpha \\ \sin\alpha\end{Bmatrix} L$,

with $L = 8t^3 - \frac{2t^3}{d^3} - \frac{3t^3(d+1)^2}{2ud} + 3t^3\ell nu$,

$u = \frac{1}{2}(1 - t\cos\omega + d)$ and ℓ and t as in A.3, then,

$$\begin{pmatrix} \frac{\partial g^{\xi}_{ij}}{\partial r_0} \\ \frac{\partial g^{\eta}_{ij}}{\partial r_0} \end{pmatrix} = \frac{3t^3\sin\omega}{r_0\gamma}\left[8 - \frac{2}{d^3} - \frac{3(d+1)^2}{2ud} + 3\ell nu + \right.$$

$$\left. + \frac{t(t-\cos\omega)}{d^2}\left(\frac{2}{d^3} + \frac{(d+1)^2}{4u^2} + \frac{1}{2ud}\right) - \frac{t\cos\omega}{2u}\left[\frac{(d+1)^2}{2ud} + 1\right]\right]\begin{Bmatrix}\cos\alpha \\ \sin\alpha\end{Bmatrix}$$

Proof:

Firstly: $$\frac{\partial u}{\partial r_o} = \frac{1}{2}\left[-\frac{\partial t}{\partial r_o}\cos\omega + \frac{\partial d}{\partial r_o}\right] =$$

$$= \frac{1}{2}\left[-\frac{t}{r_o}\cos\omega + \frac{t(t-\cos\omega)}{r_o d}\right] = \frac{t}{2r_o}\left[\frac{t-\cos\omega}{d} - \cos\omega\right]$$

Then:

(a) $$\frac{\partial}{\partial r_o}\left[\frac{t^3}{d^3}\right] = \frac{d^3\frac{\partial(t^3)}{\partial r_o} - t^3\frac{\partial(d^3)}{\partial r_o}}{d^6} = \frac{3t^3}{r_o d^3} - \frac{t^3\cdot 3d^2}{r_o d^6}\,\frac{t(t-\cos\omega)}{r_o d}$$, or

$$\frac{\partial}{\partial r_o}\left[\frac{t^3}{d^3}\right] = \frac{3t^3}{r_o d^3} - \frac{3t^4(t-\cos\omega)}{r_o d^5}$$

(b) $$\frac{\partial}{\partial r_o}[t^3(d+1)^2] = (d+1)^2\frac{\partial(t^3)}{\partial r_o} + t^3\frac{\partial}{\partial r_o}[(d+1)^2] =$$

$$= (d+1)^2\frac{3t^3}{r_o} + t^3\cdot 2(d+1)\frac{\partial d}{\partial r_o} =$$

$$= \frac{t^3(d+1)}{r_o}\left[3(d+1) + \frac{2t(t-\cos\omega)}{d}\right]$$

$$\frac{\partial}{\partial r_o}(ud) = d\frac{\partial u}{\partial r_o} + u\frac{\partial d}{\partial r_o} = d\frac{t}{2r_o}\left[\frac{t-\cos\omega}{d} - \cos\omega\right] + u\frac{t(t-\cos\omega)}{r_o d},$$ thus

$$\frac{\partial}{\partial r_o}\left[\frac{t^3(d+1)^2}{ud}\right] = \frac{ud\frac{\partial}{\partial r_o}[t^3(d+1)^2] - t^3(d+1)^2\frac{\partial}{\partial r_o}(ud)}{u^2d^2} =$$

$$= \frac{t^3(d+1)}{r_o ud}\left[3(d+1) + \frac{2t(t-\cos\omega)}{d}\right] -$$

$$- \frac{t^3(d+1)^2}{u^2d^2}\left[\frac{td}{2r_o}\left[\frac{t-\cos\omega}{d} - \cos\omega\right] + \frac{ut(t-\cos\omega)}{r_o d}\right]$$

(c) $$\frac{\partial}{\partial r_o}[t^3\ln u] = \ln u\frac{\partial(t^3)}{\partial r_o} + t^3\frac{\partial}{\partial r_o}(\ln u) =$$

$$= \frac{3t^3}{r_o}\ln u + \frac{t^3}{u}\,\frac{t}{2r_o}\left[\frac{t-\cos\omega}{d} - \cos\omega\right],$$ therefore:

$$\frac{\partial L}{\partial r_o} = 8\,\frac{\partial(t^3)}{\partial r_o} - 2\,\frac{\partial}{\partial r_o}\left(\frac{t^3}{d^3}\right) - \frac{3}{2}\,\frac{\partial}{\partial r_o}\left[\frac{t^3(d+1)^2}{ud}\right] + 3\,\frac{\partial}{\partial r_o}\,(t^3\ell nu) =$$

$$= 8\,\frac{3t^3}{r_o} - 2\left[\frac{3t^3}{r_o d^3} - \frac{3t^4(t-\cos\omega)}{r_o d^5}\right] - \frac{3}{2}\left[\frac{3t^3(d+1)^3}{r_o ud} + \right.$$

$$+ \frac{2t^4(d+1)(t-\cos\omega)}{r_o ud^2} - \frac{t^4(d+1)^2}{2r_o u^2 d^2}\,(t - \cos\omega - d\cos\omega) -$$

$$\left. - \frac{t^4(d+1)^2(t-\cos\omega)}{r_o ud^3}\right] + \frac{9t^3}{r_o}\,\ell nu + \frac{3t^4(t-\cos\omega)}{2r_o ud} - \frac{3t^4\cos\omega}{2r_o u} =$$

$$= \frac{3}{r_o}\left(8t^3 - \frac{2t^3}{d^3} - \frac{3t^3(d+1)^3}{2ud} + 3t^3\ell nu\right) + \frac{6t^4(t-\cos\omega)}{r_o d^5} -$$

$$- \frac{3t^4(d+1)(t-\cos\omega)}{r_o ud^2} + \frac{3t^4(d+1)^2(t-\cos\omega-d\cos\omega)}{4r_o u^2 d^2} +$$

$$+ \frac{3t^4(d+1)^2(t-\cos\omega)}{2r_o ud^3} + \frac{3t^4(t-\cos\omega)}{2r_o ud} - \frac{3t^4\cos\omega}{2r_o u} =$$

$$= \frac{3}{r_o}\,L + \frac{3t^4(t-\cos\omega)}{r_o d^2}\left[\frac{2}{d^3} + \frac{(d+1)^2}{4u^2}\right] - \frac{3t^4\cos\omega}{2ur_o}\left[\frac{(d+1)^2}{2ud} + 1\right] +$$

$$+ \frac{3t^4(t-\cos\omega)}{2r_o ud}\left[\left(\frac{d+1}{d}\right)^2 - 2\left(\frac{d+1}{d}\right) + 1\right], \text{ thus:}$$

$$\begin{pmatrix} \dfrac{\partial g^{\xi}_{\downarrow}}{\partial r_o} \\[2ex] \dfrac{\partial g^{\eta}_{\downarrow}}{\partial r_o} \end{pmatrix} = \frac{3t^3\sin\omega}{r_o\gamma}\left[8 - \frac{2}{d^3} - \frac{3(d+1)^2}{2ud} + 3\ell nu + \right.$$

$$\left. + \frac{t(t-\cos\omega)}{d^2}\left(\frac{2}{d^3} + \frac{(d+1)^2}{4u^2} + \frac{1}{2ud}\right) - \frac{t\cos\omega}{2u}\left[\frac{(d+1)^2}{2ud} + 1\right]\right]\begin{Bmatrix}\cos\alpha\\ \sin\alpha\end{Bmatrix}$$

q.e.d.

5. **The biharmonic equation is $\Delta^2 V = 0$. Find its solutions.**

Solution:

Let the Cartesian rectangular coordinates x, y, z be expressed as:

$$x = x(q_1,\ q_2,\ q_3),\ y = y(q_1,\ q_2,\ q_3),\ z = z(q_1,\ q_2,\ q_3)$$

such that x, y, z are continuously differentiable functions and also solvable for q_1, q_2, q_3, i.e., the Jacobian of the transformation does not vanish.

For orthogonal coordinate systems $\left(\frac{\partial x}{\partial q_i}\frac{\partial x}{\partial q_j} + \frac{\partial y}{\partial q_i}\frac{\partial y}{\partial q_j} + \frac{\partial z}{\partial q_i}\frac{\partial z}{\partial q_j} = 0,\ i \neq j\right)$, the Laplacian is [Kellogg, 1929; p. 183], [Heiskanen and Moritz, 1967; p. 19]:

$$\Delta V = \frac{1}{h_1 h_2 h_3}\left[\frac{\partial}{\partial q_1}\left(\frac{h_2 h_3}{h_1}\frac{\partial V}{\partial q_1}\right) + \frac{\partial}{\partial q_2}\left(\frac{h_3 h_1}{h_2}\frac{\partial V}{\partial q_2}\right) + \frac{\partial}{\partial q_3}\left(\frac{h_1 h_2}{h_3}\frac{\partial V}{\partial q_3}\right)\right]$$

where

$$h_i = \left\{\left(\frac{\partial x}{\partial q_i}\right)^2 + \left(\frac{\partial y}{\partial q_i}\right)^2 + \left(\frac{\partial z}{\partial q_i}\right)^2\right\}^{1/2}$$

and $h_1 h_2 h_3 = \left|\frac{\partial(x,y,z)}{\partial(q_1,q_2,q_3)}\right| = |J|$ and J is the Jacobian of the transformation.

In the usual spherical coordinates which satisfy:

$$\begin{pmatrix} x = r\sin\theta\cos\lambda \\ y = r\sin\theta\sin\lambda \\ z = r\cos\theta \end{pmatrix}$$

one has

$$\frac{\partial x}{\partial r} = \sin\theta\cos\lambda; \quad \frac{\partial x}{\partial \theta} = r\cos\theta\cos\lambda; \quad \frac{\partial x}{\partial \lambda} = -\,r\sin\theta\sin\lambda$$

$$\frac{\partial y}{\partial r} = \sin\theta\sin\lambda; \quad \frac{\partial y}{\partial \theta} = r\cos\theta\sin\lambda; \quad \frac{\partial y}{\partial \lambda} = r\sin\theta\cos\lambda$$

$$\frac{\partial z}{\partial r} = \cos\theta; \quad \frac{\partial z}{\partial \theta} = -\,r\sin\theta; \quad \frac{\partial z}{\partial \lambda} = 0 \text{ , hence}$$

$h_1 = 1$; $h_2 = r$; $h_3 = r\sin\theta$.

With these values for q_i, h_i, i = 1, 2, 3, ΔV becomes after differentiation [Heiskanen and Moritz, 1967; p. 19]:

$$\Delta V = \frac{\partial^2 V}{\partial r^2} + \frac{2}{r}\frac{\partial V}{\partial r} + \frac{1}{r^2}\frac{\partial^2 V}{\partial \theta^2} + \frac{\cot\theta}{r^2}\frac{\partial V}{\partial \theta} + \frac{1}{r^2\sin^2\theta}\frac{\partial^2 V}{\partial \lambda^2}$$

Now

$$\Delta^2 V = \Delta(\Delta V) = \frac{1}{r^2\sin\theta}\left[\frac{\partial}{\partial r}\left(r^2\sin\theta\,\frac{\partial(\Delta V)}{\partial r}\right) + \frac{\partial}{\partial \theta}\left(\sin\theta\,\frac{\partial(\Delta V)}{\partial \theta}\right) + \right.$$

$$\left. + \frac{\partial}{\partial \lambda}\left(\frac{1}{\sin\theta}\frac{\partial(\Delta V)}{\partial \lambda}\right)\right] = \frac{1}{r^2\sin\theta}\left[\frac{\partial A}{\partial r} + \frac{\partial B}{\partial \theta} + \frac{\partial \Gamma}{\partial \lambda}\right]$$

Computing A, B, Γ yields:

$$A = r^2\sin\theta \frac{\partial}{\partial r}(\Delta V) = r^2\sin\theta \frac{\partial^3 V}{\partial r^3} - 2\sin\theta \frac{\partial V}{\partial r} + 2r\sin\theta \frac{\partial^2 V}{\partial r^2} -$$

$$- \frac{2\sin\theta}{r} \frac{\partial^2 V}{\partial \theta^2} + \sin\theta \frac{\partial^3 V}{\partial r \partial \theta^2} - \frac{2\cos\theta}{r} \frac{\partial V}{\partial \theta} + \cos\theta \frac{\partial^2 V}{\partial r \partial \theta} -$$

$$- \frac{2}{r\sin\theta} \frac{\partial^2 V}{\partial \lambda^2} + \frac{1}{\sin\theta} \frac{\partial^3 V}{\partial r \partial \lambda^2}$$

$$B = \sin\theta \frac{\partial}{\partial \theta}(\Delta V) = \sin\theta \frac{\partial^3 V}{\partial \theta \partial r^2} + \frac{2\sin\theta}{r} \frac{\partial^2 V}{\partial \theta \partial r} + \frac{\sin\theta}{r^2} \frac{\partial^3 V}{\partial \theta^3} -$$

$$- \frac{1}{r^2\sin^2\theta} \frac{\partial V}{\partial \theta} + \frac{\cos\theta}{r^2} \frac{\partial^2 V}{\partial \theta^2} - \frac{2\cos\theta}{r^2\sin^2\theta} \frac{\partial^2 V}{\partial \lambda^2} + \frac{1}{r^2\sin\theta} \frac{\partial^3 V}{\partial \theta \partial \lambda^2}$$

$$\Gamma = \frac{1}{\sin\theta} \frac{\partial}{\partial \lambda}(\Delta V) = \frac{1}{\sin\theta} \frac{\partial^3 V}{\partial \lambda \partial r^2} + \frac{2}{r\sin\theta} \frac{\partial^2 V}{\partial \lambda \partial r} + \frac{1}{r^2\sin\theta} \frac{\partial^3 V}{\partial \lambda \partial \theta^2} +$$

$$+ \frac{\cos\theta}{r^2\sin^2\theta} \frac{\partial^2 V}{\partial \lambda \partial \theta} + \frac{1}{r^2\sin^3\theta} \frac{\partial^3 V}{\partial \lambda^3} \text{, therefore:}$$

$$\Delta^2 V = \left\{\frac{\partial^4 V}{\partial r^4} + \frac{1}{r^4} \frac{\partial^4 V}{\partial \theta^4} + \frac{1}{r^4\sin^4\theta} \frac{\partial^4 V}{\partial \lambda^4} + \frac{2}{r^2} \frac{\partial^4 V}{\partial r^2 \partial \theta^2} + \frac{2}{r^2\sin^2\theta} \frac{\partial^4 V}{\partial r^2 \partial \lambda^2} +\right.$$

$$+ \frac{2}{r^4\sin^2\theta} \frac{\partial^4 V}{\partial \theta^2 \partial \lambda^2} + \frac{4}{r} \frac{\partial^3 V}{\partial r^3} + \frac{2\cot\theta}{r^2} \frac{\partial^3 V}{\partial r^2 \partial \theta} - \frac{2\cot\theta}{r^4\sin^2\theta} \frac{\partial^3 V}{\partial \theta \partial \lambda^2} +$$

$$\left. + \frac{2\cot\theta}{r^4} \frac{\partial^3 V}{\partial \theta^3} - \frac{\cot^2\theta}{r^4} \frac{\partial^2 V}{\partial \theta^2} + \frac{4}{r^4\sin^4\theta} \frac{\partial^2 V}{\partial \lambda^2} + \frac{\cot\theta(1+2\sin^2\theta)}{r^4\sin^2\theta} \frac{\partial V}{\partial \theta}\right\}$$

Assuming $V(r, \theta, \lambda) = f(r)\cdot Y(\theta, \lambda)$ with $Y(\theta, \lambda) = g(\theta)\cdot h(\lambda)$ we get

$$\Delta^2 V = f^{(4)} Y + \frac{1}{r^4} \frac{\partial^4 Y}{\partial \theta^4} f + \frac{1}{r^4\sin^4\theta} f \frac{\partial^4 Y}{\partial \lambda^4} + \frac{2}{r^2} f'' \frac{\partial^2 Y}{\partial \theta^2} +$$

$$+ \frac{2}{r^2\sin^2\theta} f'' \frac{\partial^2 Y}{\partial \lambda^2} + \frac{2}{r^4\sin^2\theta} f \frac{\partial^4 Y}{\partial \theta^2 \partial \lambda^2} + \frac{4}{r} f^{(3)} Y +$$

$$+ \frac{2\cot\theta}{r^2} f'' \frac{\partial Y}{\partial \theta} - \frac{2\cot\theta}{r^4\sin^2\theta} f \frac{\partial^3 Y}{\partial \theta \partial \lambda^2} +$$

$$+ \frac{2\cot\theta}{r^4} \frac{\partial^3 Y}{\partial \theta^3} f - \frac{\cot^2\theta}{r^4} f \frac{\partial^2 Y}{\partial \theta^2} + \frac{4}{r^4\sin^4\theta} f \frac{\partial^2 Y}{\partial \lambda^2} +$$

$$+ \frac{\cot\theta(1+2\sin^2\theta)}{r^4\sin^2\theta} f \frac{\partial Y}{\partial \theta}$$

where the derivatives of f are with respect to r.

Now $\Delta^2 V = 0 \iff \frac{r^4}{fY}\Delta^2 V = 0 \iff$

$$\iff \frac{r^4 f^{(4)}}{f} + \frac{1}{Y}\frac{\partial^4 Y}{\partial\theta^4} + \frac{1}{Y\sin^4\theta}\frac{\partial^4 Y}{\partial\lambda^4} + \frac{2r^2 f''}{f}\frac{1}{Y}\frac{\partial^2 Y}{\partial\theta^2} + \frac{2f''r^2}{f}\frac{1}{Y\sin^2\theta}\frac{\partial^2 Y}{\partial\lambda^2}$$

$$+ \frac{2}{Y\sin^2\theta}\frac{\partial^4 Y}{\partial\theta^2\partial\lambda^2} + \frac{4r^3 f^{(3)}}{f} + \frac{2r^2 f''}{f}\frac{\cot\theta}{Y}\frac{\partial Y}{\partial\theta} - \frac{2\cot\theta}{Y\sin^2\theta}\frac{\partial^3 Y}{\partial\theta\partial\lambda^2} +$$

$$+ \frac{2\cot\theta}{Y}\frac{\partial^3 Y}{\partial\theta^3} - \frac{\cot^2\theta}{Y}\frac{\partial^2 Y}{\partial\theta^2} + \frac{4}{Y\sin^4\theta}\frac{\partial^2 Y}{\partial\lambda^2} + \frac{\cot\theta(1+2\sin^2\theta)}{Y\sin^2\theta}\frac{\partial Y}{\partial\theta} = 0 \quad (1)$$

Let Z, Δ_1 be defined as

$$Z = \Delta_1 Y = \left(\frac{\partial^2}{\partial\theta^2} + \cot\theta\frac{\partial}{\partial\theta} + \frac{1}{\sin^2\theta}\frac{\partial^2}{\partial\lambda^2}\right) Y =$$

$$= \frac{\partial^2 Y}{\partial\theta^2} + \cot\theta\frac{\partial Y}{\partial\theta} + \frac{1}{\sin^2\theta}\frac{\partial^2 Y}{\partial\lambda^2}$$

Also, let

$$L = \frac{\partial^4 Y}{\partial\theta^4} + \frac{1}{\sin^4\theta}\frac{\partial^4 Y}{\partial\lambda^4} + \frac{2}{\sin^2\theta}\frac{\partial^4 Y}{\partial\theta^2\partial\lambda^2} - \frac{2\cot\theta}{\sin^2\theta}\frac{\partial^3 Y}{\partial\theta\partial\lambda^2} + 2\cot\theta\frac{\partial^3 Y}{\partial\theta^3} -$$

$$- \cot^2\theta\frac{\partial^2 Y}{\partial\theta^2} + \frac{4}{\sin^4\theta}\frac{\partial^2 Y}{\partial\lambda^2} + \frac{\cot\theta(1+2\sin^2\theta)}{\sin^2\theta}\frac{\partial Y}{\partial\theta}$$

$$M = \frac{r^4 f^{(4)}}{f} + \frac{4r^3 f^{(3)}}{f}$$

On the other hand:

$$\frac{\partial Z}{\partial\theta} = \frac{\partial}{\partial\theta}\left(\frac{\partial^2 Y}{\partial\theta^2} + \cot\theta\frac{\partial Y}{\partial\theta} + \frac{1}{\sin^2\theta}\frac{\partial^2 Y}{\partial\lambda^2}\right) =$$

$$= \frac{\partial^3 Y}{\partial\theta^3} + \cot\theta\frac{\partial^2 Y}{\partial\theta^2} - \frac{1}{\sin^2\theta}\frac{\partial Y}{\partial\theta} + \frac{1}{\sin^2\theta}\frac{\partial^3 Y}{\partial\theta\partial\lambda^2} - \frac{2\cos\theta}{\sin^3\theta}\frac{\partial^2 Y}{\partial\lambda^2}, \text{ and:}$$

$$\frac{\partial^2 Z}{\partial\theta^2} = \frac{\partial}{\partial\theta}\left(\frac{\partial^3 Y}{\partial\theta^3} + \cot\theta\frac{\partial^2 Y}{\partial\theta^2} - \frac{1}{\sin^2\theta}\frac{\partial Y}{\partial\theta} + \frac{1}{\sin^2\theta}\frac{\partial^3 Y}{\partial\theta\partial\lambda^2} - \frac{2\cos\theta}{\sin^3\theta}\frac{\partial^2 Y}{\partial\lambda^2}\right) =$$

$$= \frac{\partial^4 Y}{\partial\theta^4} - \frac{1}{\sin^2\theta}\frac{\partial^2 Y}{\partial\theta^2} + \cot\theta\frac{\partial^3 Y}{\partial\theta^3} + \frac{2\cos\theta}{\sin^3\theta}\frac{\partial Y}{\partial\theta} - \frac{1}{\sin^2\theta}\frac{\partial^2 Y}{\partial\theta^2} -$$

$$- \frac{2\cos\theta}{\sin^3\theta}\frac{\partial^3 Y}{\partial\theta\partial\lambda^2} + \frac{1}{\sin^2\theta}\frac{\partial^4 Y}{\partial\theta^2\partial\lambda^2}\ \frac{2(1+2\cos^2\theta)}{\sin^4\theta}\frac{\partial^2 Y}{\partial\lambda^2} - \frac{2\cos\theta}{\sin^3\theta}\frac{\partial^3 Y}{\partial\theta\partial\lambda^2}$$

$$\frac{\partial Z}{\partial\lambda} = \frac{\partial^3 Y}{\partial\lambda\partial\theta^2} + \cot\theta\,\frac{\partial^2 Y}{\partial\lambda\partial\theta} + \frac{1}{\sin^2\theta}\,\frac{\partial^3 Y}{\partial\lambda^3}\ , \text{ and}$$

$$\frac{\partial^2 Z}{\partial\lambda^2} = \frac{\partial^4 Y}{\partial\theta^2\partial\lambda^2} + \cot\theta\,\frac{\partial^3 Y}{\partial\theta\partial\lambda^2} + \frac{1}{\sin^2\theta}\,\frac{\partial^4 Y}{\partial\lambda^4}\ , \text{ hence:}$$

$$\begin{aligned}
\Delta_1 Z + 2Z &= \frac{\partial^2 Z}{\partial\theta^2} + \cot\theta\,\frac{\partial Z}{\partial\theta} + \frac{1}{\sin^2\theta}\,\frac{\partial^2 Z}{\partial\lambda^2} = \\
&= \frac{\partial^4 Y}{\partial\theta^4} - \frac{1}{\sin^2\theta}\,\frac{\partial^2 Y}{\partial\theta^2} + \cot\theta\,\frac{\partial^3 Y}{\partial\theta^3} + \frac{2\cos\theta}{\sin^3\theta}\,\frac{\partial Y}{\partial\theta} - \frac{1}{\sin^2\theta}\,\frac{\partial^2 Y}{\partial\theta^2} - \\
&\quad - \frac{2\cos\theta}{\sin^3\theta}\,\frac{\partial^3 Y}{\partial\theta\partial\lambda^2} + \frac{1}{\sin^2\theta}\,\frac{\partial^4 Y}{\partial\theta^2\partial\lambda^2} + \frac{2(1+2\cos^2\theta)}{\sin^4\theta}\,\frac{\partial^2 Y}{\partial\lambda^2} - \\
&\quad - \frac{2\cos\theta}{\sin^3\theta}\,\frac{\partial^3 Y}{\partial\theta\partial\lambda^2} + \cot\theta\left(\frac{\partial^3 Y}{\partial\theta^3} + \cot\theta\,\frac{\partial^2 Y}{\partial\theta^2} - \frac{1}{\sin^2\theta}\,\frac{\partial Y}{\partial\theta} + \right. \\
&\quad \left. + \frac{1}{\sin^2\theta}\,\frac{\partial^3 Y}{\partial\theta\partial\lambda^2} - \frac{2\cos\theta}{\sin^3\theta}\,\frac{\partial^2 Y}{\partial\lambda^2}\right) + \frac{1}{\sin^2\theta}\left(\frac{\partial^4 Y}{\partial\theta^2\partial\lambda^2} + \cot\theta\,\frac{\partial^3 Y}{\partial\theta\partial\lambda^2} + \right. \\
&\quad \left. + \frac{1}{\sin^2\theta}\,\frac{\partial^4 Y}{\partial\lambda^4}\right) + 2\,\frac{\partial^2 Y}{\partial\theta^2} + 2\cot\theta\,\frac{\partial Y}{\partial\theta} + \frac{2}{\sin^2\theta}\,\frac{\partial^2 Y}{\partial\lambda^2} = \\
&= \frac{\partial^4 Y}{\partial\theta^4} + \frac{1}{\sin^4\theta}\,\frac{\partial^4 Y}{\partial\lambda^4} + \frac{2}{\sin^2\theta}\,\frac{\partial^4 Y}{\partial\theta^2\partial\lambda^2} + 2\cot\theta\,\frac{\partial^3 Y}{\partial\theta^3} - \frac{2\cot\theta}{\sin^2\theta}\,\frac{\partial^3 Y}{\partial\theta\partial\lambda^2} + \\
&\quad + \left(\cot^2\theta - \frac{2}{\sin^2\theta} + 2\right)\frac{\partial^2 Y}{\partial\theta^2} + \left(\frac{2+4\cos^2\theta}{\sin^4\theta} - \frac{2\cos^2\theta}{\sin^4\theta} + \frac{2}{\sin^2\theta}\right)\frac{\partial^2 Y}{\partial\lambda^2} + \\
&\quad + \left(\frac{\cos\theta}{\sin^3\theta} + \frac{2\cos\theta}{\sin\theta}\right)\frac{\partial Y}{\partial\theta} = \\
&= \frac{\partial^4 Y}{\partial\theta^4} + \frac{1}{\sin^4\theta}\,\frac{\partial^4 Y}{\partial\lambda^4} + \frac{2}{\sin^2\theta}\,\frac{\partial^4 Y}{\partial\theta^2\partial\lambda^2} + 2\cot\theta\,\frac{\partial^3 Y}{\partial\theta^3} - \frac{2\cot\theta}{\sin^2\theta}\,\frac{\partial^3 Y}{\partial\theta\partial\lambda^2} - \\
&\quad - \cot^2\theta\,\frac{\partial^2 Y}{\partial\theta^2} + \frac{4}{\sin^4\theta}\,\frac{\partial^2 Y}{\partial\lambda^2} + \frac{\cot\theta(1+2\sin^2\theta)}{\sin^2\theta}\,\frac{\partial Y}{\partial\theta} = L
\end{aligned}$$

therefore $\Delta_1 Z + 2Z = L$

Now (1) becomes:

$$M + \frac{L}{Y} + \frac{2r^2 f''}{f}\,\frac{1}{Y}\,Z = 0 \iff$$

$$\iff M + \frac{1}{Y}\,(\Delta_1 Z + 2Z) + \frac{2r^2 f''}{f}\,\frac{Z}{Y} = 0 \iff$$

$$\iff M + \frac{1}{Y}\,(\Delta_1^2 Y + 2\Delta_1 Y) + \frac{2r^2 f''}{f}\,\frac{\Delta_1 Y}{Y} = 0 \qquad (2)$$

If one assumes $\Delta_1 Y = cY$ (3)

with c a constant one gets

$$\Delta_1^2 Y = \Delta_1(\Delta_1 Y) = \Delta_1(cY) = c\Delta_1 Y \qquad (4)$$

Substituting (4) in (2) one obtains

$$M + \frac{1}{Y}(c\Delta_1 Y + 2\Delta_1 Y) + \frac{2r^2 f''}{f}\frac{\Delta_1 Y}{Y} = 0 \quad \text{which using (3) becomes:}$$

$$M + \frac{1}{Y}(c^2 Y + 2cY) + \frac{2r^2 f''}{f} c = 0 \quad \Leftrightarrow$$

$$\Leftrightarrow \frac{r^4 f^{(4)}}{f} + \frac{4r^3 f^{(3)}}{f} + \frac{2r^2 f''}{f} c + c^2 + 2c = 0 \qquad (5)$$

Selecting the constant $c = -n(n+1)$, equation (5) yields

$$\frac{\partial^4 f}{\partial r^4} + \frac{4}{r}\frac{\partial^3 f}{\partial r^3} - \frac{2n(n+1)}{r^2}\frac{\partial^2 f}{\partial r^2} + \frac{n(n-1)(n+1)(n+2)}{r^4} f = 0 \qquad (6)$$

The solutions of (6) are r^n, $r^{-(n+1)}$, r^{n+2} and $r^{-(n-1)}$ as can be verified by substitution. On the other hand (3) becomes:

$$\frac{\partial^2 Y}{\partial \theta^2} + \cot\theta\frac{\partial Y}{\partial \theta} + \frac{1}{\sin^2\theta}\frac{\partial^2 Y}{\partial \lambda^2} + n(n+1)Y = 0$$

the solutions of which are [Heiskanen and Moritz, 1967; p. 21] the surface spherical harmonics

$P_{nm}(\cos\theta)\cos m\lambda$ and $P_{nm}(\cos\theta)\sin m\lambda$

and $P_{nm}(\cos\theta)$ are the Legendre's functions [ibid, p. 21]. Therefore, the biharmonic functions (solutions of $\Delta^2 V = 0$) can be represented as:

$$V_i(r,\theta,\lambda) = \sum_{n=0}^{\infty} r^n \sum_{m=0}^{n} [(a_{nm} + r^2 c_{nm})\cos m\lambda + (b_{nm} + r^2 d_{nm})\sin m\lambda] P_{nm}(\cos\theta)$$

$$V_e(r,\theta,\lambda) = \sum_{n=0}^{\infty} \frac{1}{r^{n+1}} \sum_{m=0}^{n} [(a_{nm} + r^2 c_{nm})\cos m\lambda + (b_{nm} + r^2 d_{nm})\sin m\lambda] P_{nm}(\cos\theta),$$

where a_{nm}, b_{nm}, c_{nm}, and d_{nm} are arbitrary constants.

REFERENCES

Arfken, G., Mathematical Methods for Physicists, 3rd ed., Academic Press, New York, 1985.

Aseltine, J.A., Transform Method in Linear System Analysis, McGraw-Hill, New York, 1958.

Berezin, I.S., N.P. Zhidkov, Computing Methods, Vol. I, (translated), Pergamon Press, Oxford, 1965.

Bjerhammar, A., "Gravimetric Geodesy Free of Density Estimates Through Analysis of Discrete Gravity Data", U.S. Department of Commerce, AD430002, Fort Belvoir, VA, 1963.

Bjerhammar, A., "A New Theory of Geodetic Gravity", Division of Geodesy, The Royal Institute of Technology, Stokholm, No. 243, 1964.

Bjerhammar, A., "On the Discrete Boundary Value Problem", extract from Proceedings of Symposium on Earth's Gravitational Field and Secular Variations in Position, The School of Surveying, The University of New South Wales, Sydney, Australia, 1973.

Bjerhammar, A., "A Solution of the Boundary Value Problem Without Gravity Reduction", Division of Geodesy, The Royal Institute of Technology, Stokholm, 1974.

Bjerhammar, A., "Reflexive Prediction", Sixth Symposium on Mathematical Geodesy, Siena, Italy, April 1975a.

Bjerhammar, A., "Discrete Approaches to the Solution of the Boundary Value Problem in Physical Geodesy", Bolletino di Geodesia e Scienze Affini, No. 2, 1975b.

Bjerhammar, A., "A Dirac Approach to Physical Geodesy", Zeitschrift Fur Vermessungwesen, No. 2, 1976.

Bjerhammar, A., "A Review of Discrete Methods in Physical Geodesy", Second International Summer School in the Mountains, Ramsau, Austria, 1977.

Bjerhammar, A., "Collocation-Reflexive Prediction in Physical Geodesy", Division of Geodesy, The Royal Institute of Technology, Stokholm, 1979.

Bjerhammar, A., "The Geodetic Boundary Value Problem for a Fixed Boundary Surface", Division of Geodesy, The Royal Institute of Technology, Stokholm, 1982.

Bjerhammar, A., "Harmonic Embedding in Physical Geodesy", preprint, Dept. of Geodetic Science and Surveying, The Ohio State University, June 1986.

Bjerhammar, A., L. Svensson, "The Convergence of Harmonic Reduction to an Internal Sphere", Division of Geodesy, The Royal Institute of Technology, Stokholm, 1978.

Boullion, T.L., P.L. Odell, Generalized Inverse Matrices, John Wiley & Sons, New York, 1971.

Brown, B.M., The Mathematical Theory of Linear Systems, John Wiley & Sons, New York, 1961.

Cristescu, R., G. Marinescu, Applications of the Theory of Distributions, (translated), John Wiley & Sons, London, 1973.

Cruz, J.Y., "Disturbance Vector in Space From Surface Gravity Anomalies Using Complementary Models", Report No. 366, Dept. of Geodetic Science and Surveying, The Ohio State University, August 1985, AFGL-TR-85-0209, ADA155730.

Dermanis, A., Linear Algebra and Theory of Matrices, (in Greek), Zetes, Thessaloniki, 1985.

Dirac, P.A.M., The Principles of Quantum Mechanics, Clarenton Press, Oxford, 1947.

Forsberg, R., "A Study of Terrain Reductions, Density Anomalies and Geophysical Inversion Methods in Gravity Field Modelling", Report No. 355, Dept. of Geodetic Science and Surveying, The Ohio State University, April 1984, AFGL-TR-84-0174, ADA150788.

Forsberg, R., C.C. Tscherning, "The Use of Height Data in Gravity Field Approximation by Collocation", Journal of Geophysical Research, Vol. 86, No. B9, pp. 7843-7854, September 1981.

Forsberg, R., Private Communication, Dept. of Geodetic Science and Surveying, The Ohio State University, 1988.

Gel'fand, I.M., G.E. Shilov, Generalised Functions, Vols. 1 and 2, (translated), Academic Press, New York, 1968.

Hardy, R.L., "Least Squares Prediction", Photogrammetric Engineering and Remote Sensing, Vol. 43, No. 4, April 1977.

Hardy, R.L., "The Application of Multiquadric Equations and Point Mass Anomaly Models to Crustal Movement Studies", NOAA Technical Report NOS76 NGS11, U.S. Department of Commerce, Rockville, Maryland, 1978.

Hardy, R.L., "Biharmonic Potential Models for Use in Geodesy and Geophysics", preprint, Engineering Research Institute, Iowa State University, 1983a.

Hardy, R.L., "The Biharmonic Potential and Its Geodetic Applications", Technical Papers, 43rd Annual Meeting, ACSM, Washington, D.C., 1983b.

Hardy, R.L., W.M. Gopfert, "Least Squares Prediction of Gravity Anomalies, Geoidal Undulations and Deflections of the Vertical with Multiquadric Harmonic Functions", Engineering Research Institute, Iowa State University, 1975.

Hardy, R.L., S.A. Nelson, "A Multiquadric-Biharmonic Representation and Approximation of Disturbing Potential", Geophysical Research Letters, Vol. 13, No. 1, January 1986.

Heiskanen, W.A., H. Moritz, Physical Geodesy, W.H. Freeman and Co., San Francisco, 1967.

Hoskins, R.F., Generalised Functions, John Wiley & Sons, New York, 1979.

Jacobs, K., Measure and Integral, Academic Press, New York, 1978.

Jones, D.S., The Theory of Generalised Functions, Cambridge University Press, Cambridge, 1966.

Katsambalos, K.E., "Simulation Studies on the Computation of the Gravity Vector in Space From Surface Data Considering the Topography of the Earth", Report No. 314, Dept. of Geodetic Science and Surveying, The Ohio State University, June 1981, AFGL-TR-81-0187, AD-A109856/5.

Kearsley, A.H.W., M.G. Sideris, J. Krynski, R. Forsberg, K.P. Schwarz, "White Sands Revisited-A Comparison of Techniques to Predict Deflections of the Vertical", Publication 30007, Division of Surveying Engineering, The University of Calgary, 1985.

Kellogg, O.D., Foundations of Potential Theory, Frederick Ungar Publishing Co., New York, 1929.

Krarup, T., "A Contribution to the Mathematical Foundation of Physical Geodesy", Meddelelse No. 44, Geodetisk Institut, Copenhagen, 1969.

Lanczos, C., Linear Differential Operators, D. Van Nostrand Co. Ltd., London, 1961.

Lavrent'ev, M.M., V.G. Romanov, S.P. Shishat·skii, Ill-Posed Problems of Mathematical Physics and Analysis, (translated), American Mathematical Society, Providence, Rhode Island, 1986.

MacMillan, W.D., The Theory of the Potential, McGraw-Hill Book Co., New York, 1930.

Moritz, H., Advanced Physical Geodesy, Herbert Wichmann Verlag, Karlsruhe, 1980.

Pick, M., J. Picha, V. Vyskocil, Theory of the Earth's Gravity Field, Elsevier Scientific Publishing Co., New York, 1973.

Rapp, R.H., "Geometric Geodesy", Vol. 2, (class notes of GS760), Dept. of Geodetic Science and Surveying, The Ohio State University, 1981.

Rapp, R.H., "Gravimetric Geodesy", (class notes of GS776), Dept. of Geodetic Science and Surveying, The Ohio State University, 1982a.

Rapp, R.H., "A FORTRAN Program for the Computation of Gravimetric Quantities From High Degree Spherical Harmonic Expansions", Report No. 334, Dept. of Geodetic Science and Surveying, The Ohio State University, September 1982b, AFGL-TR-82-0272, ADA123406.

Rapp, R.H., "Advanced Gravimetric Geodesy", (class notes of GS871), Dept. of Geodetic Science and Surveying, The Ohio State University, 1983.

Rapp, R.H., "Geometric Geodesy", Vol. 1, (class notes of GS658), Dept. of Geodetic Science and Surveying, The Ohio State University, 1984.

Rapp, R.H. and J.Y. Cruz, "Spherical Harmonic Expansions of the Earth's Gravitational Potential to Degree 360 Using 30′ Mean Anomalies", Report No. 376, Dept. of Geodetic Science and Surveying, The Ohio State University, December 1986, NASA, Grant NGR36-008-161, OSURF Project No. 783210.

Rektorys, K. (ed), Survey of Applicable Mathematics, (translated), M.I.T. Press, Cambridge, Massachusetts, 1969.

Sanso', F., "Recent Advances in the Theory of the Geodetic Boundary Value Problem", in Advances in Geodesy, Selected Papers from Reviews of Geophysics and Space Physics, 1984.

Scheik, J.E., Private Communication, Dept. of Mathematics, The Ohio State University, 1987.

Schwarz, K.P. (ed), "Techniques to Predict Gravity Anomalies and Deflections of the Vertical in Mountainous Areas", Publication 30004, Division of Surveying Engineering, The University of Calgary, 1983.

Sigl, R. Introduction to Potential Theory, (translated), Abacus Press, Cambridge, Massachusetts, 1985.

Sjöberg, L., "A Comparison of Bjerhammar's Methods and Collocation in Physical Geodesy", Report No. 273, Dept. of Geodetic Science and Surveying, The Ohio State University, December 1981, AFGL-TR-82-0084, AD-A115216/4.

Sünkel, H., "A General Surface Representation Module Designed for Geodesy", Report No. 292, Dept. of Geodetic Science and Surveying, The Ohio State University, October 1979, AFGL-TR-79-0245, AD-A092918/2.

Tscherning, C.C., Documentation of the GEOCOL Fortran program, Release 4.0, Danish Geodetic Institute, 1987.

Torge, W., Geodesy, (translated), Walter de Gruyter, Berlin, 1980.

Tretter, S.A., Introduction to Discrete-Time Signal Processing, John Wiley & Sons, New York, 1976.

Uotila, U.A., "Adjustment Computations", Vol. 2, (class notes of GS651), Dept. of Geodetic Science and Surveying, The Ohio State University, 1982a.

Uotila, U.A., "Advanced Adjustment Computations", (class notes of GS762) Dept. of Geodetic Science and Surveying, The Ohio State University, 1982b.

Uotila, U.A., "Adjustment Computations", Vol. 1, (class notes of GS650), Dept. of Geodetic Science and Surveying, The Ohio State University, 1985.

Volynskii, B.A., V. Ye. Bukhman, Analogues for the Solution of Boundary-Value Problems, (translated), Pergamon Press, New York, 1965.

Wichiencharoen, C., "Fortran Programs for Computing Geoid Undulations From Potential Coefficients and Gravity Anomalies", Internal Report, Dept. of Geodetic Science and Surveying, The Ohio State University, September 1982.